People's Democratic Republic of Algeria

Ministry of Higher Education and Scientific Research

University of Amar Thelidji – Laghouat

Faculty of Science and Technology
Mechanical Department
Specialty: Energetics
2nd Year Master LMD

Theme

Numerical study of key parameters for improving cooling efficiency in a regenerative cooled nozzle

Jury Members:

Mr. HAMDI Nacer eddine

Mr. Lakhdar Hachani

Mr. BENSAYAH Khaled

prepared by:

TAOUTI med abderrahmane

MERAD hadj azize

Academic year 2022– 2023

ACKNOWLEDGEMENTS

الحمد لله الذي تتم بنعمته الصـــالحات الحمد لله على جميع النعم حمدا يليق بجلاله وعظيم ســـلطانه، اللهم أتمم عليهم نعمك التي لاتحصى

First, we express our profound gratitude to Mr. **BENSAYAH Khaled**, our supervisor. We are incredibly thankful for his unwavering support, guidance, assistance, advice, and patience throughout the duration of this project.

We would also like to acknowledge all those who directly or indirectly contributed to the successful completion of this endeavor. Their contributions have been invaluable, and we are deeply grateful for their assistance.

Furthermore, we sincerely thank our beloved parents for their unwavering support, both morally and materially, during the realization of this project. Their encouragement and belief in us have been instrumental in our achievements. We also extend our appreciation to our brothers and sisters for their continuous support.

In conclusion, we would like to express our heartfelt gratitude to everyone involved in making this project a reality. Their contributions and support have been invaluable, and we are truly thankful for their assistance throughout this journey.

Dedication

I dedicate this humble work to my beloved parents, who have always been my pillars of support, encouraging me to strive for success in my studies. Their unwavering belief in me has been a driving force throughout my academic journey.

I also extend my gratitude to my brother Hamza, , and my sisters, who have been there for me with their love and support. Their presence in my life has brought me immense joy and strength.

Today, I want to express my heartfelt appreciation to my grandmother and uncles for their guidance and wisdom. Their presence has enriched my life in countless ways.

To the entire **Merad** and **Bouazize** family, I am deeply thankful for your continuous support and encouragement. Your presence in my life has been a source of inspiration.

I would like to acknowledge the invaluable role played by all the teachers who have contributed to my growth and progress. Special thanks to **Bensnouci**, **Bensayah**, **Hamdi**, and many others who have imparted their knowledge and shaped my educational journey.

To the dedicated teachers in the mechanics department, I am grateful for your expertise and guidance, which has allowed me to reach this level of accomplishment.

I want to express my gratitude to my partner, **Med Abderrhmane Taouti,** for their unwavering support and collaboration throughout this endeavor.

Lastly, I want to thank all my friends, whose friendship and support have brought joy and camaraderie into my life.

To all these remarkable individuals, I offer my sincere thanks and dedication for their unwavering support and belief in me.

MERAD HADJ AZIZE.

This modest work is dedicated:

To the dearest people in my life, my father and my mother who were the candles lighting my way to success; who gave me everything their loves, their sacrifices so that I can follow my studies in good conditions and who do not stop encouraging me and watching for my good

Supervised teacher: **Khaled bensayah**

Partner in memo : **hadj azize merad**

To my dear **Mother** and my dear **Father** who supported and encouraged me during these years of study.

To my brothers: **Abdelkader** and **Abdellatif**

To my sisters: **Khadija** and **Fatima** and **saida**

All my **friends**

Also, I will not fail to express my sincere thanks to the members of the Board of Directors You agreed, without any reservation, to value this thesis at its fair value, and to share it with me Their notes are certainly relevant, Don will contribute Any doubt your person, to improve this work.

TAOUTI MED ABDERRAHMANE.

Abstract (English)

We have known since the development of the liquid rocket engine began, there was a need to predict maximum heat flow and its problems it affects the engine material, which reduces its efficiency and thus controls the thermal behaviour of the rocket engine wall. to prevent

Due to thermal failure, the engine is generally cooled by coolant flowing into the passages that line and pass through the ducts, the hottest part of the engine (i.e. the combustion chamber and the nozzle wall). This is a liquid cooling system. If the refrigerant is a propellant that, once it has passed through the refrigerant circuit, can be injected into

Combustion chamber or can be thrown into the sea. The first case is referred to as regenerative cooling system while the latter as a vacuum cooling system. In the case of a high-performance rocket engine (eg as engines LO2 / hydrogen and LO2 / methane) the working pressure of the coolant is supercritical and therefore It behaves far from an ideal liquid or gas. Liquid cooling system (often referred to as regenerative cooling

Due to the limited application of vacuum cooling (vacuum cooling) of cryogenic rocket engines and there are several hypotheses in order to prevent the rocket engine from melting and bypass the problem, the technology The background of this master's thesis.

Résumé (Français)

Nous savons depuis le début du développement du moteur-fusée à liquide qu'il était nécessaire de prévoir le flux de chaleur maximal et ses problèmes, il affecte le matériau du moteur, ce qui réduit son efficacité et contrôle ainsi le comportement thermique de la paroi du moteur-fusée. Pour prévenir

En raison d'une panne thermique, le moteur est généralement refroidi par du liquide de refroidissement circulant dans les passages qui bordent et traversent les conduits, la partie la plus chaude du moteur (c'est-à-dire la chambre de combustion et la paroi de la tuyère). Il s'agit d'un système de refroidissement liquide. Si le fluide frigorigène est un propulseur qui, une fois passé dans le circuit frigorifique, peut être injecté dans

Chambre de combustion ou peut être jeté à la mer. Le premier cas est appelé système de refroidissement régénératif tandis que le second est un système de refroidissement sous vide. Dans le cas d'un moteur-fusée à hautes performances (par exemple, comme les moteurs LO2 / hydrogène et LO2 / méthane) la pression de travail du liquide de refroidissement est supercritique et donc Il se comporte loin d'être un liquide ou un gaz idéal. Système de refroidissement liquide (souvent appelé refroidissement régénératif En raison de l'application limitée du refroidissement sous vide (refroidissement sous vide) des moteur-fusée cryogéniques et il existe plusieurs hypothèses afin d'empêcher le moteur-fusée de fondre et de contourner le problème, la technologie L'arrière-plan de cette thèse de maîtrise.

Symbol	Description
α	Speed of sound alsoc
a	Kinetic energy of the average quantities
c*	Speed of turbulent sound
C_p	Specific heat at constant pressure
C_v	Specific heat at constant volume
C_f	friction coefficient
δ	Thickness of the boundary layer
ΔU	Explicit increase in vector U
δU	Implicit increase of the vector U
$U_{I,j}$	Kronecker symbol
Δt	Time increase
e	Internal energy per unit of mass
e_t	Total energy per unit mass
ε	Rate of dissipation of turbulent kinetic energy
ε^*	Isotropic dissipation rat
F	Eulerian flow in the direction x
F_v	Viscous flow in the direction x
F_ξ	Eulerian flow in the direction ξ
$F_{v\xi}$	Viscous flow in the direction ξ
G	Eulerian flow in the direction $\mathcal{Y}$
G_v	Viscous flow in the direction $\mathcal{Y}$
$G\eta$	Eulerian flow in the direction η
$Gv\eta$	Viscous flow in the direction η
γ	Specific Heat Report ($\gamma = \frac{c_p}{c_v}$)
h	Heat transfer coefficient
h_t	Total enthalpy per unit mass
k	Kinetic energy of turbulent
ω	Specific dissipation rate
l	Spatial scale of turbulence
l_m	Mixing length
λ_c	coefficient of thermal conductivity
M_e	Number of Mach outside the boundary layer (also M_∞)
M_t	Turbulent Mach number ($M_t = \sqrt{2K}/c$)
$\mathcal{E}_{\mathcal{NS}}(u_i)$	Naiver-Stokes operator
q_j	Heat flow per unit area and unit time in the direction x_j
q_w	Parietal heat flow

NOMENCLATURE

μ	Molecular viscosity
v	Kinematic viscosity
μ_t	Turbulent viscosity
μ_{ef}	Effective diffusion coefficient of momentum
μ_{kef}	Effective diffusion coefficient of k
$\mu_{\omega ef}$	Effective diffusion coefficient of ω
Pr	Prandtl number
Pr_t	Prandtl turbulent number
p	hydrostatic pressure
p^*	Effective pressure p*=p+2/3ρk
p_0	Generator or chamber pressure (also p c)
p_w	Static wall pressure
Re	Reynolds number
Re_t	Reynolds turbulent number
ρ	density
S_0	Vector of source terms
$\vec{s}_{i+\frac{1}{2}}$	Vector surface between meshes (I,j) et (i+1,j)
$\vec{s}_{j+\frac{1}{2}}$	Vector surface between meshes (i,j) et (i,j+1)
$\begin{pmatrix} m_x \\ m_y \end{pmatrix}$	Module 1 surface vector components between (i,j) et (i+1,j)
$\begin{pmatrix} n_x \\ n_y \end{pmatrix}$	Module 1 surface vector components between (i,j) et (i,j+1)
σ_{ij}	Tenser des constraints visqueuses
t	Time
T	Temperature
T_0	Generator temperature
T_w	Parietal temperature
T_{aw}	Adiabatic temperature
τ	Kolmogorov time
η	Kolmogorov ladder
τ_w	Parietal friction
U	Vector of conservative quantities
u	speed in the direction x
u_i	speed in the direction x_i
V	Vector of non-conservative quantities
$\mathcal{V}_{I,j}$	speed in the direction $\mathcal{Y}$
$\mathcal{V}_{i,j}$	Mesh volume (i,j)
S_{ij}	Strain tensor
Ω_{ij}	Vorticity Tensor
$\bar{f}$	Overall average of quantity f

NOMENCLATURE

$f^{'}$	Fluctuation of quantity f for the overall average
$\tilde{f}$	Quantity Favre Average f
$f^{''}$	Fluctuation of quantity f for the average of Favre
(x,y)	Axes of the Cartesian landmark

Abbreviations

RANS	(Reynolds Averaged Naiver-Stokes)
SST	(Shear Stress Tensor)
JPL	(Jet Propulsion Laboratory)
CFD	(computational fluid dynamics)

List of Figures

List of Tables

Contents **page**

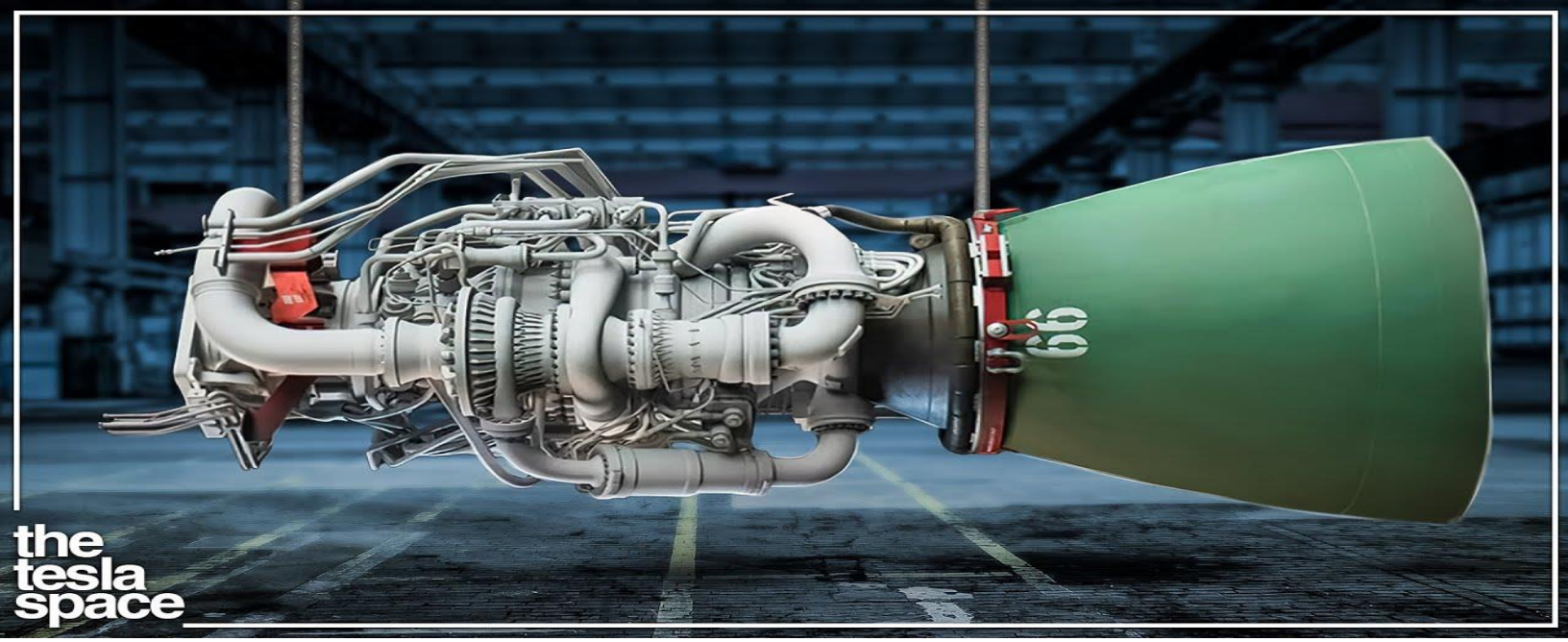

1. INTRODUCTION

Rocket engines face extreme temperatures reaching up to 3300°C (6000°F) that can easily melt most metals. To prevent the engines from melting, they employ various cooling techniques such as regenerative cooling, film cooling, and ablative cooling. Additional methods like radiative cooling and adjusting the fuel to oxidizer ratio are also used to prevent engine damage.

During a rocket launch, the visible fire, steam, and smoke observed on the Launchpad and below the nozzles represent only a fraction of the heat generated within the engine itself. The hot gases produced inside a rocket engine can reach temperatures surpassing half the surface temperature of the sun. For instance, the F1 engine of the Saturn V rocket used during the Apollo missions reached temperatures close to 3300°C (6000°F). This temperature range is comparable to modern launch vehicles like the Space Shuttle and SpaceX's Falcon 9 rocket.

These incredibly high temperatures pose a significant risk of melting metals. Aluminium, for example, melts at 660°C (1220°F), stainless steel at 1510°C (2750°F), and even titanium will melt at 1670°C (3040°F).

To ensure the combustion chamber and nozzle walls remain relatively cool and do not melt, rocket engine manufacturers employ a range of cooling techniques. These techniques involve circulating coolants through the walls, injecting coolant films along the inner surfaces, utilizing sacrificial ablative linings, promoting radiative heat transfer, and adjusting the fuel and oxidizer mixture. By combining these cooling techniques, rocket engines can effectively manage the

extreme temperatures, preventing the melting of vital components and ensuring the engines operate safely and reliably.

1-1 How Rocket Engines Stay Cool

As highlighted in the introduction, the temperatures inside the combustion chamber and nozzle of a rocket engine far exceed the melting point of most metals, necessitating active or passive cooling methods to prevent them from melting. Over the years, engineers have developed several cooling techniques to keep rocket engines cool and protect the combustion chamber walls, nozzle, and other surfaces from melting. These cooling techniques can be used individually, but often multiple methods are employed simultaneously in the same engine for effective cooling. The primary and commonly used cooling techniques in modern rockets include:

1. **Regenerative Cooling**
2. **Film Cooling *(Curtain Cooling)***
3. **Ablative Cooling**
4. **Dump Cooling**
5. **Radiative Cooling**
6. **Heatsink**
7. **Fuel/Oxidizer Ratio**

Figure.1-1:engines of a Saturn v rocket used both regenerative and film cooling to stay cool.

By employing these cooling techniques, rocket engines can effectively manage the extreme temperatures and prevent melting or structural damage, ensuring safe and

Reliable operation.

1.1.1. Regenerative Cooling

Regenerative cooling is a widely used method of active engine cooling in rocket engines. It involves pumping the rocket's fuel through a network of channels embedded within the walls of the combustion chamber and nozzle to prevent them from melting. This cooling technique has been employed since the early Apollo missions and continues to be utilized in modern rockets such as SpaceX's Falcon 9 with the Merlin engine.

The cooling system comprises a series of channels located in the walls of the combustion chamber, throat, and upper section of the nozzle. Pressurized fuel is circulated through these channels to

extract heat from the walls. The relatively cold fuel flows through the channels in the chamber and nozzle walls before returning to the combustion chamber, where it combines with the oxidizer and undergoes combustion to generate thrust for the rocket.

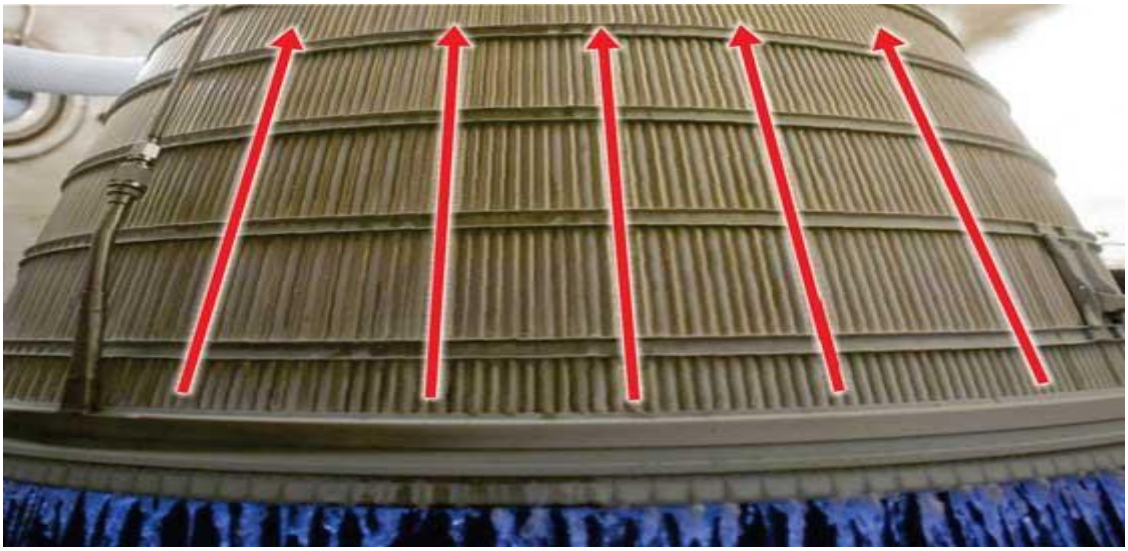

Figure 1-2: an example of a regeneratively cooled engine nozzle using liquid hydrogen as fuel. The tubes carrying the fuel through the nozzle walls are clearly visible, with arrows indicating the direction of flow.

In the past, the chamber and nozzle walls consisted of numerous steel tubes shaped to the desired profile. These tubes were combined with a binder metal and brazed together to create a single structure with hollow channels. However, advancements in technology have led to the adoption of liner and structural jacket configurations for modern chamber and nozzle walls.

The liner is typically made of a highly conductive metal like copper alloy, which efficiently conducts the lower temperatures of the circulating coolant to the inner walls and the outer

Structural jacket. The liner is initially forged using hot spin forming and then machined to attain the precise shape of the combustion chamber and nozzle. Channels are subsequently cut into its outer surface.

Figure1-3: a cross-section of a modern combustion chamber wall with the slotted liner, made from copper alloy, visible at the top with the structural jacket consisting of Inconel at the bottom.

To complete the cooling system, a structural jacket is fitted to the slotted outer wall of the liner, and the two metals are bonded together using advanced techniques such as electro-plating, welding, and brazing. Inconel, a strong and heat-resistant metal, is commonly used as the jacket material to withstand the high temperatures within the rocket engine. However, in certain cases, other heat-resistant metals like stainless steel may also be utilized.

Similar to the traditional tube-based walls, the fuel is pumped through the channels in the liner to extract heat from the walls before being returned to the combustion chamber for further combustion.

1.1.2. Film Cooling (Curtain Cooling)

Film cooling is an active engine cooling technique where fuel, in its liquid or gaseous form, is injected along the inside walls of the combustion chamber and nozzle to create a protective boundary layer. This layer partially insulates the walls of the rocket engine from the hot gases, helping to keep them cool. Film cooling is commonly used alongside regenerative cooling and is often employed simultaneously in the same engine to optimize cooling efficiency.

In film, cooling, additional fuel is pumped through holes in the outer perimeter of the fuel/oxidizer injector, close to the chamber walls of the combustion chamber. This fuel does not react with the oxidizer and gets trapped between the inside walls and the combusted gases flowing

through the chamber. As a result, a thin film coating of relatively cool fuel is formed, which flows along the inside walls of the chamber, throat, and upper section of the nozzle.

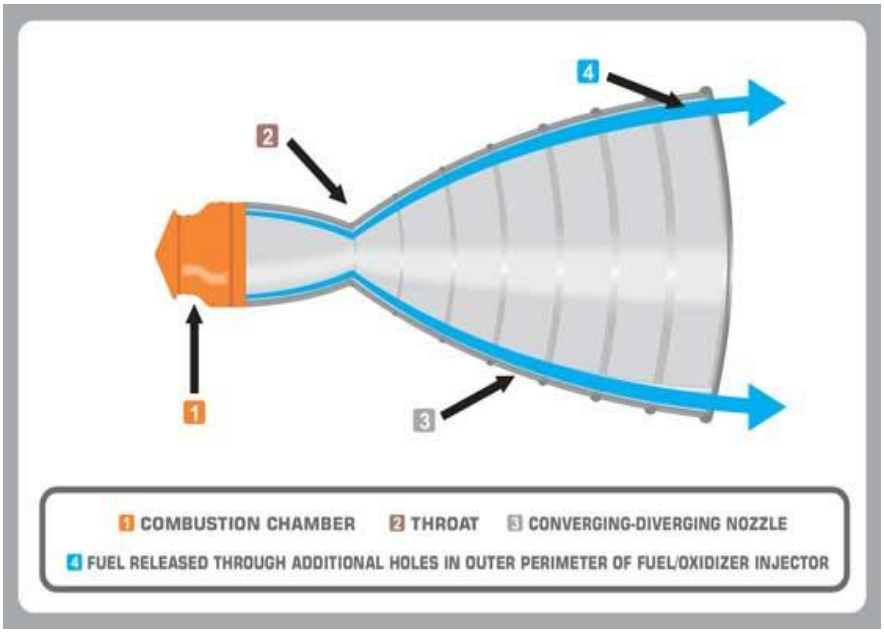

Figure1-4: Simplified diagram illustrating how film cooling works by pumping fuel through holes in the outer perimeter of the fuel injector in the combustion chamber to provide a protective layer between the hot gases and chamber walls.

The thin fuel coating acts as a protective layer, helping to keep the engine walls cool. The fuel continues to flow along the channel walls until it starts mixing with the oxidizer or oxygen in the atmosphere as it exits the nozzle, where combustion occurs.

To provide additional film cooling in regions with more severe heat buildup, such as the throat of the nozzle where temperatures and pressures are at their peak, fuel can also bleed through holes created in the chamber walls. This ensures enhanced protection for critical areas.

Exhaust gases from the engine's gas generator, which powers the turbopumps responsible for fuel and oxidizer delivery, can also be utilized for film cooling. Normally.

These gases are expelled overboard. However, in some cases, the exhaust gas can be redirected through the gas generator's exhaust manifold to exit through holes near the nozzle extension. This creates a layer of gas that acts as additional insulation, protecting the nozzle walls.

By combining regenerative cooling with film cooling techniques and potentially utilizing exhaust gases, rocket engines can effectively manage and dissipate heat, preventing the melting of engine components and ensuring optimal performance.

1.1.3. Ablative Cooling

Ablative cooling is a technique used for engine cooling in which the inner walls of the combustion chamber and nozzle are coated with a layer of material that erodes and burns away as it is exposed to high temperatures. This process carries away the excess heat along with the eroded material as it exits the nozzle alongside the hot gases.

While regenerative and film-cooling methods are highly effective in keeping a rocket engine cool, they come with added complexity and weight due to the necessary components and processes involved. Ablative cooling offers a simpler and more cost-effective alternative for mitigating the intense heat buildup.

Figure.1-5: the hydrogen-fueled Delta IV Heavy (left) supposedly transparent exhaust gases display an orange tint as a result of the material burnt away from its ablative nozzle.

Ablative cooling was also used in the nozzles of the Apollo Command Module (center and right) to maneuver in space where only short bursts of thrust were required at a time.

To implement ablative cooling, a layer of strong and heat-resistant materials such as carbon composites, silica, or graphite is applied to the inner walls of the combustion chamber and nozzle. As the hot gases flow over these walls, they heat the ablative material, causing it to erode and be expelled out of the nozzle along with the exhaust gases, carrying away the heat in the process.

However, ablative cooling does have some drawbacks. As the ablative material burns away, the volume inside the combustion chamber and nozzle expands, which can impact engine efficiency.

The precise measurements and design of the chamber and nozzle's throat are crucial for achieving optimal pressures and temperatures, and as more material erodes, the efficiency decreases.

Additionally, ablative cooling is not suitable for engines intended for long-duration burns. The amount of ablative material available is limited, and adding enough material for extended burns would result in excessive engine weight. Furthermore, it is not ideal for engines intended for reuse, as refurbishing such an engine would require extensive overhaul and rebuild processes, which can be costly and time-consuming, negating the benefits of engine reusability.

1.1.4. Dump Cooling

Dump cooling is a type of engine cooling that is similar to regenerative cooling, but with a key difference. Instead of circulating the fuel back to the combustion chamber after it has passed through the channels in the chamber walls, it is simply discharged or "dumped" overboard at the aft end of the nozzle.

During the launch of a rocket, the majority of its mass is made up of fuel, as the energy required to reach orbit is significant. Therefore, fuel efficiency is crucial in rocket design, and any unnecessary wastage of propellant is undesirable.

Dump cooling, in theory, offers a solution to cool rocket engines. However, in practical applications, it has very limited if any use. The concept involves directly releasing the fuel that has been used for cooling, which can lead to inefficient use of propellant and compromise the overall performance of the rocket engine.

Due to the high value placed on fuel efficiency and the need to optimize every aspect of rocket design, dump cooling is not commonly employed in actual rocket engines. Other cooling techniques such as regenerative cooling and film cooling are preferred, as they provide more efficient and controlled methods of dissipating heat while conserving propellant.

1.1.5. Radiative Cooling

Radiative cooling is a method of engine cooling commonly employed by rocket engine nozzles optimized for operation in a vacuum. It involves using the nozzle's surface to radiate heat away from the engine into space. Typically, a metal with a high melting point and excellent thermal conductivity is chosen for manufacturing the nozzle extensions.

In the present era, spectators have the convenience of witnessing major rocket launches from the comfort of their homes. When observing the deployment of a launch vehicle's upper stage, one can often notice the distinctive red glow emanating from its engine nozzles. This glow is a result of the intense heat generated by the hot exhaust gases, causing the nozzle to become red hot.

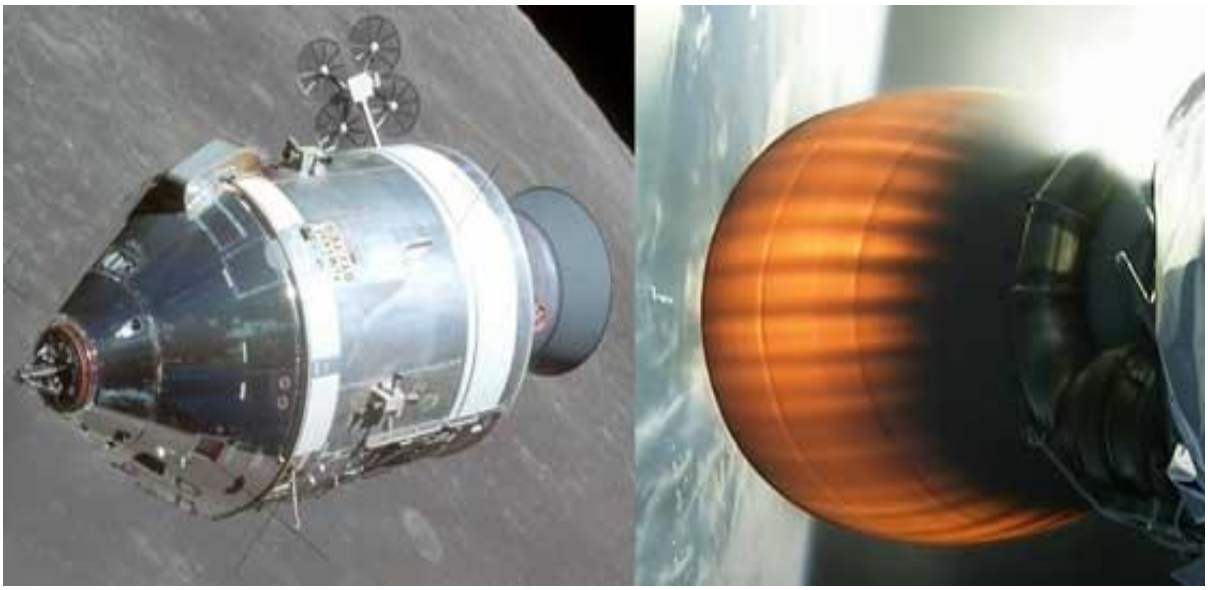

Figure.1-6 :both the nozzle extensions of the Apollo Service Module (left) and the Falcon 9 Vacuum optimized Merlin engine (right) are made from Niobium and use radiative cooling to keep the nozzle temperatures down.

In the vacuum environment of space, where there is no air to facilitate heat conduction, the engine nozzle takes advantage of its surroundings by utilizing radiative cooling. The nozzle's surface emits thermal radiation, allowing the heat to dissipate into space.

To effectively employ radiative cooling, nozzle extensions are typically fabricated from materials such as Niobium alloy. These materials possess desirable characteristics for this cooling method, including a high melting point, efficient thermal conductivity, and resistance to thermal shocks. Using such materials, helps maintain the structural integrity of the nozzle while effectively dissipating heat through radiative cooling.

1.1.6. Heatsink

The concept proposed for using a "heatsink" approach to cool rocket engine chamber and nozzle walls involves using a thicker metal that would take longer to heat up to the point of melting. The idea is that a thicker wall would require a larger area to be heated, thus prolonging the time it takes to reach the melting point and effectively acting as a heatsink.

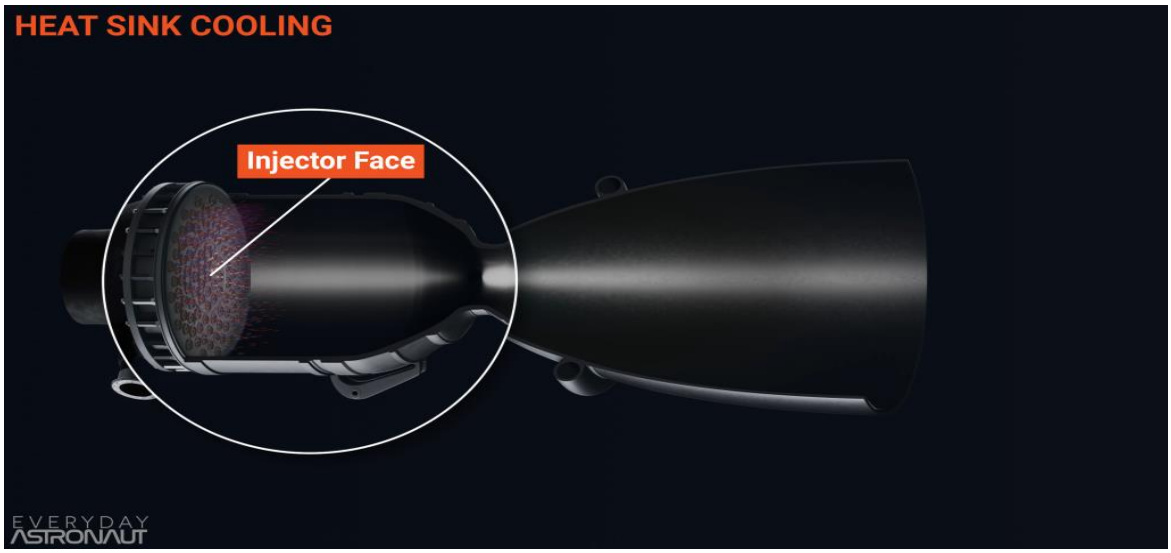

Figure.1-7 :A render of aninjector face of anengine. Here propellants mix and combustin the main combustion chamber releasing incrediblea mounts of heat energy.

However, there are significant drawbacks that render this cooling method impractical. Firstly, adding the necessary weight to achieve effective cooling through a thicker metal would make the rocket engine too heavy for practical use. Weight reduction is a critical consideration in rocket design.

Secondly, even if weight were not a major concern, the extremely high temperatures of 6,000° Celsius (3,300° Fahrenheit) experienced in rocket engines would pose challenges for maintaining structural integrity over the typical burn period. Despite the increased bulk, even the most heat-resistant metals would struggle to remain structurally sound under such extreme conditions.

1.1.7. Fuel/Oxidizer Rati

Changing the fuel to oxidizer ratio in a rocket engine is a sometimes-overlooked method of cooling the engine. By adjusting the mixing ratio of the propellants to run either fuel-rich or oxidizer-rich, the temperature generated inside the engine can be reduced.

The ideal fuel to oxidizer ratio, where maximum efficiency is achieved and all the fuel is burned, also results in the highest energy release and the highest temperatures. However, these temperatures can often exceed the capabilities of the engine components.

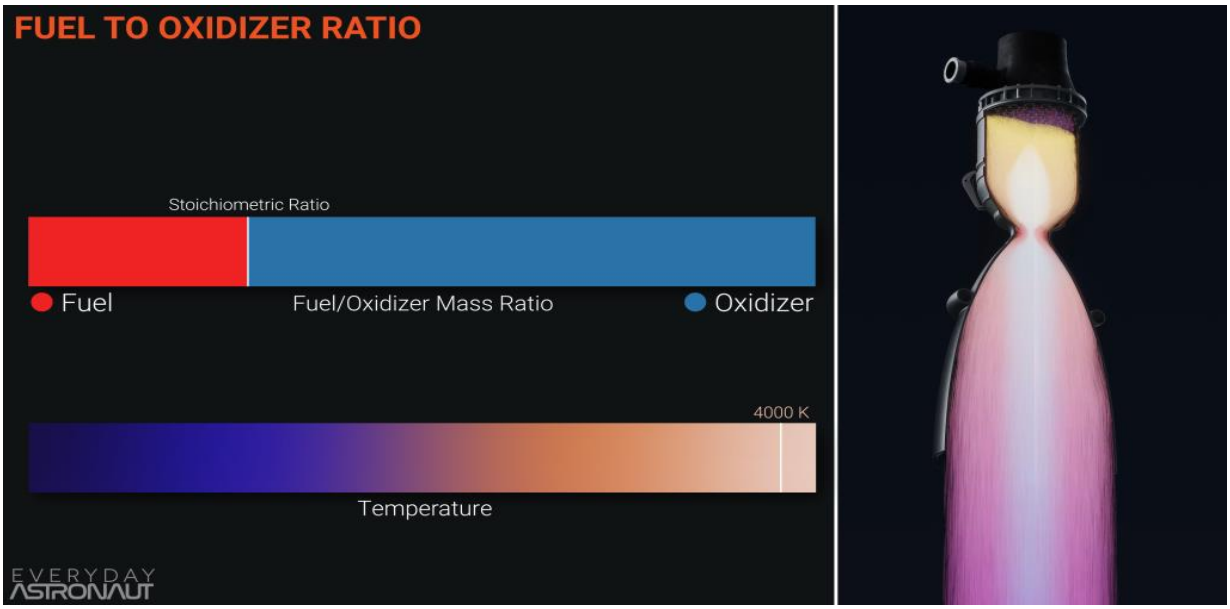

Figure.1.8:agraphic of the fuel to oxidizer mass ratio if fuel and oxidizer would be burnt at the stoichiometric ratio. Resulting in extremely high temperatures that would destroy an engine

To mitigate this, many launch vehicles employ a propellant mix in their combustion chambers that is either fuel-rich or oxidizer-rich, which lowers the temperatures generated during combustion.

This form of cooling is particularly beneficial for the engine's gas generator or preburner, which is responsible for creating the hot gases that drive the engine's turbopumps. Other cooling methods may not be suitable for keeping the spinning turbine cool in these areas.

1.2. Rocket& Principles properties

1.2.1. Propellants

The characteristics of combustion products have a significant influence on heat transfer and the selection of cooling methods. Factors such as propellant flow rates, temperature, weight, viscosity, and specific heat determine the suitability of cooling techniques such as regenerative cooling, transpiration cooling, dump cooling, or film cooling. Therefore, when designing a chamber cooling system, careful consideration is given to the properties of the propellants used.**[2]**

1.2.2. Chamber pressure

In general, increasing chamber pressure results in higher heat flux in a nozzle due to higher combustion-gas density and mass flow rates per unit area. To meet the demands of high-pressure applications, a combination of regenerative and film-cooling methods is typically used. **[1]**

1.2.3. Propellant feed system

In most cases, when the chamber pressure of a rocket engine is increased, it leads to a higher heat flux in the nozzle. This is primarily due to the increased density of the combustion gases and the higher mass flow rates per unit area. To effectively manage and dissipate this increased heat, a combination of regenerative cooling and film cooling methods is commonly employed. This combination of cooling techniques helps to meet the requirements of high-pressure applications and maintain the structural integrity of the engine. **[2]**

1.2.4. Thrust-chamber construction material

The design of a rocket engine's cooling system is heavily influenced by the properties of the materials used in the thrust chamber. The strength of the material at high temperatures and its thermal conductivity are important factors that determine whether a particular material is suitable for regenerative cooling. For film-cooled chambers, materials with higher allowable working temperatures are preferred to maintain lower film-coolant flow rates. Radiation cooling, on the other hand, relies on the availability of materials capable of withstanding high temperatures of 2000 K or more. The success of ablative cooling also depends on the availability of suitable materials.

It is important to note that the design of the thrust-chamber cooling system cannot be considered in isolation; it must be integrated with the rest of the engine design. For example, the optimization of a high-performance engine's chamber pressure may be limited by the capacity and efficiency of the chamber-cooling system. Chamber pressure also affects other design parameters, including the nozzle expansion ratio, propellant feed pressure, and overall weight. Therefore, a complete analysis of chamber-cooling systems requires expertise in heat transfer, fluid mechanics, thermodynamics, materials science, and structure.

Rocket engines consist of a combustion chamber and a supersonic nozzle. The nozzle includes a converging section that narrows down to the throat, the nozzle's most narrow cross-section, and a diverging section that expands outwards towards the exit. The combustion products generate high temperatures and pressures, resulting in the conversion of the gas into high-velocity exhaust gas. In supersonic flow, most of the enthalpy is converted into kinetic energy, producing thrust. Newton's third law of physics, the conservation of momentum, is responsible for the thrust force. The pressure force on the wall is balanced by the equal and opposite reaction force by the walls,

except for the pressure force at the exit. The high velocity gas exiting the nozzle propels the rocket in the opposite direction.**[3]**

The nozzle geometry produces high velocities by choking the high-pressure combustion gas through the throat. The geometrical convergence causes the pressure to decrease and the velocity to increase from subsonic in the combustion chamber to Mach 1 at the throat. The subsequent rapid thermodynamic expansion of the gas into the diverging section causes the velocity to become supersonic. The Mach number is the ratio of the velocity of the moving body to the velocity of sound in the same medium. A Mach number of one indicates that the body is moving at the speed of sound in the given medium. Mach numbers less than one are subsonic, while Mach numbers greater than one are supersonic. Local Mach numbers in rocket engines refer to the velocity of the exhaust flow. The local Mach number is

Calculated at a particular location within the nozzle by the equation .

$$M_x = v_x / \sqrt{\gamma R T_x}$$

Where the $x$subscript indicates a specific location in the nozzle.

M Is the Mach number.

v Is the velocity.

γ Is the specific heat ratio.

R Is the gas constant for the particular gas.

T Is the absolute temperature in Kelvin.

The expansion area ratio of the exit to the throat, combined with the chemical kinetics of the fuel, determines the achievable Mach numbers and the exit pressure. Rocket engines are considered perfectly expanded and most efficient when the outlet pressure is equal to the ambient pressure. However, because of the rapidly changing atmospheric pressure during flight, a dynamic expansion area ratio that adjusts with altitude would be ideal. Unfortunately, current rocket technology only allows for a fixed expansion area ratio. Therefore, the nozzle must be designed with an area ratio that is efficient at the target ambient pressure and operational over a wide range of altitude

2.1.Introduction

In order to simulate the flow within solid propellant engines, specifically within the combustion chamber and nozzle, it is necessary to utilize a compressible formulation of the equations of fluid mechanics. This requires specialized treatments such as appropriate mesh selection and boundary conditions. The primary aim of chapter 2 is to offer a comprehensive overview of all the formulations that have been developed for this particular work.

2.2. Equations of fluid mechanics

At present, the direct simulation approach for solving the Naiver-Stokes equations is only applicable to flows of relatively low Reynolds numbers and for simple or overly simplified geometries that are not representative of real-world industrial applications. Consequently, when seeking to simulate realistic flows, it becomes necessary to focus on mean quantities and derive a set of equations that describe these quantities. This is typically accomplished by applying Favre decomposition to the unknowns in the problem, resulting in a new set of equations known as the averaging equations.

2.2.1. Reminder of instantaneous equations

The fundamental equations that describe fluid mechanics are composed of three separate equations that correspond to the conservation of mass, momentum, and energy, respectively.

$$\frac{\partial}{\partial t}\rho + \frac{\partial}{\partial x_j}\rho u_j = 0 \qquad (2.1)$$

$$\frac{\partial}{\partial t}\rho u_i + \frac{\partial}{\partial x_j}\left(\rho u_i u_j + p\delta_{ij}\right) = \frac{\partial}{\partial x_j}\sigma_{ij} \qquad (2.2)$$

$$\frac{\partial}{\partial t}\rho e_t + \frac{\partial}{\partial x_j}\left[u_j(\rho e_t + p)\right] = \frac{\partial}{\partial x_j}\sigma_{ij}u_i - \frac{\partial}{\partial x_j}q_j \qquad (2.3)$$

Where u_i are the velocity components, p the pressure, ρ the density, σ_{ij} is the viscous stress tensor, e_t is the total energy and q_j is the heat flow. To close these equations, we add the thermodynamic relationships that link pressure, temperature and density. The heat flux intensity by conduction q_j is, by designating by λ the coefficient of thermal conduction of the fluid, proportional, according to the law de Fourier, with temperature gradient

$$q_j = -\lambda_c \frac{\partial T}{\partial x_j} \qquad (2.4)$$

The choice of the e_t total energy variable to write energy conservation is one form among others. Indeed the total energy conservation equation can be written as a function of the internal energy e = c_vT, for a perfect gas this relation is given by:

$$e_t = e + \frac{1}{2}u_k u_k \qquad (2.5)$$

$$\frac{\partial}{\partial t}\rho e_t + \frac{\partial}{\partial x_j}\rho h_t u_j = \frac{\partial}{\partial x_j}\sigma_{ij}u_i - \frac{\partial}{\partial x_j}q_j \qquad (2.6)$$

With mass enthalpy 1: $h = e + \frac{p}{\rho}$, the equation 2.3 can be written

Where $h\,t = h + \frac{1}{2}u_k u_k$ is the total enthalpy per unit mass. For compressible flows, the viscous stress tensor σ_{ij} depends on the second viscosity coefficient λ (which represents the resistance that the viscous forces oppose to the compression of an elementary volume of fluid) in addition to the molecular viscosityμ. The law of behavior, which links the tensor of viscous stresses to the tensor of average deformation rate, is, for a Newtonian fluid

$$\sigma_{ij} = 2\mu S_{ij} + \lambda \frac{\partial u_k}{\partial x_k}\delta_{ij} \qquad (2.7)$$

Where $S_{ij} = \frac{1}{2}\left(\frac{\partial u_i}{\partial x_j} + \frac{\partial u_j}{\partial x_i}\right)$is the symmetric portion of the velocity tensor and δ_{ij} is the symbol of Kroenke$\left(\delta_{ij} = 1 \text{ if } i = j, 0, \text{ otherwise}\right)$. With $2\,\mu + 3\,\lambda = 0$, because the changes in volume are

made without viscosity (hypothesis of Stokes) we consider the perfect gas state law, which links pressure, temperature and density:

$$p = \rho r T = \rho(\gamma - 1)c \qquad (2.8)$$

Where r is the perfect gas constant equal to the universal gas constant divided by the molecular mass of the fluid We can also rewrite the heat flow by showing the number of **Prandtl** laminar, Pr :

$$q_j = -\lambda_c \frac{\partial \Gamma}{\partial x_j} = -\frac{\gamma \mu}{\Pr} \frac{\partial e}{\partial x_j} (2.9)$$

2: with $\Pr = \frac{\mu c_p}{\lambda_c} = \gamma \frac{\mu c_v}{\lambda_c}$

The viscosity of a fluid varies according to its temperature, the law of Sutherland, which connects viscosity, and temperature, this law is given by:

$$\mu(T) = \mu_0 \sqrt{\frac{T}{T_0} \frac{1 + \frac{S}{T_i}}{1 + \frac{S}{T}}}$$

Where S = 110.4K, T_0 = 273.15 K and μ_0 = 1.711.10^5 Pa.s

2.3 The averaged Naiver-Stokes equations

The technique of combining two averages is used to simplify the Naiver-Stokes equations, which are used to describe fluid dynamics. This technique involves decomposing pressure and density into an average centered on the value of **(3)**, and decomposing other quantities such as speed, temperature, and energy into an average that is weighted by density using equation **(4)**. By assuming negligible fluctuations in viscosity and thermal conductivity, the statistical average of the open-form Naiver-Stokes equations can be simplified, and the focus can be shifted away from Reynolds decomposition. This simplified form of the equations can be used to study the statistical behavior of fluids in fields such as fluid mechanics and aerodynamics.

$$3: \phi = \bar{\phi} + \phi', \bar{\phi'} = 0 \ (2.10)$$

$$4:\begin{cases}\phi = \bar{\phi} + \phi' & \text{moyenne selon} \quad \text{Reynolds} \\ \phi = \tilde{\phi} + \phi'' & \text{moyenne selon} \quad \text{Favre} \\ & \rho = \bar{\rho} + \rho'\end{cases} \qquad (2.11)$$

2.3.1. Average mass conservation equation

Using a weighted average for speed, the mass conservation equation becomes:

$$\frac{\partial \bar{\rho}}{\partial t} + \frac{\partial}{\partial x_i}\left(\bar{\rho}\tilde{v}_j\right) = 0 \qquad (2.12)$$

The density fluctuation equation is obtained by subtracting the mean equation (2.12) from the instantaneous equation (2.3):

$$\frac{\partial \rho'}{\partial t} + \frac{\partial}{\partial x_j}\left(\rho'\tilde{u}_j\right) + \frac{\partial}{\partial x_j}\left(\rho u_j''\right) = 0 \qquad (2.13)$$

2.3.2. Conservation equation of the mean momentum

Using a technique similar to that of the continuity equation, the equation of the momentum takes the form of

$$\frac{\partial}{\partial t}\bar{\rho}\tilde{u_\iota} + \frac{\partial}{\partial x_j}\bar{\rho}\bar{u}_i\bar{u}_i = -\frac{\partial \bar{p}}{\partial x_i} + \frac{\partial}{\partial x_j}\left(\bar{\sigma}_{ij} - \bar{\sigma_{ij}''}\right) - \frac{\partial}{\partial x_j}\bar{\rho}\widetilde{u_\iota'' u_\iota''} \qquad (2.14)$$

The equation of the momentum for the fluctuating component of the velocity is obtained by subtracting the mean equation (2.14) from the instantaneous equation of the momentum:

$$\frac{\partial}{\partial t}\left(\rho'\tilde{u}_i + \rho u_i''\right) + \frac{\partial}{\partial x_j}\left(\rho'\tilde{u}_j\tilde{u}_i + \rho\tilde{u}_i u_i'' + \rho u_i''\tilde{u}_j + \rho u_i'' u_j'' - \overline{\rho u_\iota'' u_\iota''}\right) = -\frac{\partial p'}{\partial x_i} + \frac{\partial}{\partial x_i}\left(\sigma_{ij}'' - \overline{\sigma_{\iota j}''}\right) \qquad (2.15)$$

In addition to the conventional terms that already exist in the instantaneous equation, we have shown a new term; $\left(-\frac{\partial}{\partial x_j}\bar{\rho}\widetilde{u_i'' u_j''}\right)$, Which has a dimension of a constraint and whose existence is

the basis of the closure problem. The decomposition of the viscous stress tensor σ_{ij} , shows not only an average value of type $\tilde{\sigma}_{ij}$, but also a nonzero term 1:

$$\overline{\sigma_{ij}''} = \bar{\mu}\left(\frac{\partial \overline{u_i''}}{\partial x_j} + \frac{\partial \overline{u_j''}}{\partial x_i}\right) - \frac{2}{3}\bar{\mu}\frac{\partial \overline{u_k''}}{\partial x_k} \qquad (2.16)$$

this term can be overlooked by assuming that all terms involving fluctuations other than Reynolds tensions are negligible .The equation of the momentum averaged is written:

$$\frac{\partial}{\partial t}\bar{\rho}\tilde{u}_i + \frac{\partial}{\partial x_j}\bar{\rho}\tilde{u}_i\tilde{u}_j = -\frac{\partial \bar{p}}{\partial x_i} + \frac{\partial}{\partial x_j}\left(\bar{\mu}\left(\frac{\partial \tilde{u}_i}{\partial x_j} + \frac{\partial \tilde{u}_j}{\partial x_i} - \frac{2}{3}\delta_{ij}\frac{\partial \tilde{u}_k}{\partial x_k}\right) - \bar{\rho}\widetilde{u_i''u_j''}\right) \qquad (2.17)$$

2.3.3. Average energy conservation equation

The transport equation of energy, when it applies formalism of Favre, becomes:

$$\begin{aligned}
&\frac{\partial}{\partial t}\left(\bar{\rho}\left(\tilde{e} + \frac{\tilde{u}_i\tilde{u}_i}{2}\right) + \frac{\overline{\rho u_i'' u_i''}}{2}\right) + \frac{\partial}{\partial x_j}\left(\bar{\rho}\tilde{u}_j\left(\tilde{e} + \frac{\tilde{u}_i\tilde{u}_i}{2}\right) + \tilde{u}_j\bar{p} + \tilde{u}_j\overline{\rho u_i'' u_j''}\right) \\
&= -\frac{\partial}{\partial x_j}\left(\overline{\rho u_j'' e''} + \bar{p}\overline{u_j''} + \overline{p' u_j''} + \tilde{u}_i\overline{\rho u_j'' u_i''} + \frac{1}{2}\overline{\rho u_j'' u_i'' u_i''}\right) \qquad (2.18) \\
&+ \frac{\partial}{\partial x_j}\left(\tilde{\sigma}_{ij}\tilde{u}_i + \tilde{o}_{ij}\overline{u_i''} + \overline{o_{ij}''}\tilde{u}_i + \overline{\sigma_{ij}'' u_i''}\right) - \frac{\partial}{\partial x_j}\left(\tilde{q}_i + \overline{q_j''}\right)
\end{aligned}$$

5: $\frac{1}{2}\overline{\rho u_i'' u_i''}$: Kinetic energy of turbulent fluctuations per unit of volume, noted $\bar{\rho}k$ where:

$$k = \frac{1}{2}\widetilde{u_i'' u_i''} \qquad (2.19)$$

$\frac{1}{2}\bar{\rho}\tilde{u}_i\tilde{u}_i$ kinetic energy of average motion per unit volume

$\overline{\rho u_j'' e''}$: turbulent transport of heat

$\frac{1}{2}\overline{\rho u_j'' u_i'' u_i''}$: turbulent transport of turbulent energy

$\overline{\sigma_{ij} u_i''} = \left(\tilde{\sigma}_{ij}\overline{u_i''} + \overline{\sigma_{ij}'' u_i''}\right)$: Molecular diffusion of turbulent energy

As for the equation of momentum, new terms appear 5 Subtracting the mean equation (2.18) from the instantaneous equation (2.3). The energy fluctuation equation can be derived:

$$\begin{gathered}\frac{\partial}{\partial t}\rho\left(e''+\tilde{u}_i u_i''+\frac{1}{2}u_i''u_i''\right)-\frac{\partial}{\partial t}\frac{1}{2}\overline{\rho u_i''u_i''}+\frac{\partial}{\partial t}\rho'\left(z+\frac{1}{2}\tilde{u}_i\tilde{u}_i\right)+\\ \frac{\partial}{\partial x_j}\rho\tilde{u}_j\left(e''+\tilde{u}_i u_i''+\frac{1}{2}u_i''u_i''\right)+\frac{\partial}{\partial x_j}\rho'\tilde{u}_i\left(\tilde{e}+\frac{1}{2}\tilde{i}_i\tilde{u}_i\right)+\\ \frac{\partial}{\partial x_i}\rho u_i''\left(\ddot{e}+e''+\frac{1}{2}\tilde{u}_i\tilde{u}_i+\tilde{u}_i u_i''+\frac{1}{2}u_i''u_i''\right)-\\ \frac{\partial}{\partial x_j}\left(\frac{1}{2}\tilde{u}_j\overline{\rho u_i''u_i''}+\overline{\rho u_i''e''}+\tilde{u}_i\overline{\rho u_i''u_j''}+\frac{1}{2}\overline{\rho u_i''u_i''u_i''}\right)+\\ \frac{\partial}{\partial x_j}\left(\bar{u}_j p'+u_j''\bar{p}+u_j''p'\right)-\frac{\partial}{\partial x_j}\left(\bar{u_j''}\bar{p}+\overline{u_j''p'}\right)=\\ \frac{\partial}{\partial x_j}\left(\delta_{ij}u_i''+\sigma_{ij}''\tilde{u}_i+\sigma_{ij}''u_i''\right)-\frac{\partial}{\partial x_j}\left(\tilde{\sigma}_{ij}\overline{u_i''}+\overline{\sigma_{ij}''}\tilde{u}_i+\overline{\sigma_{ij}''u_i''}\right)-\frac{\partial}{\partial x_j}\left(q_j''-\overline{q_j''}\right)\end{gathered} \tag{2.20}$$

The velocity-temperature correlation can be expressed by:

$$\overline{\rho u_j''e''}=c_v\overline{\rho u_j''T''} \tag{2.21}$$

The pressure-velocity correlation:

$$\begin{gathered}\bar{p}\overline{u_j''}+\overline{p'u_j''}=\overline{pu_j''}=(\gamma-1)\overline{\rho e u_j''}\\ =(\gamma-1)\overline{\rho e''u_j''}\\ =c_v(\gamma-1)\overline{\rho T''u_j''}\end{gathered} \tag{2.22}$$

With:

$$\overline{\rho u_j''e''}+\overline{pu_j''}=\gamma c_v\overline{\rho u_j''T''} \tag{2.23}$$

(2.23) is the overall expression of (2.21) and (2.22) the correlation of viscous stress and velocity fluctuations is given by:

$$\overline{\sigma_{ij}u_i''}=\tilde{\sigma}_{ij}\overline{u_i''}+\overline{\sigma_{ij}''u_i''} \tag{2.24}$$

For the analysis of terms$(\tilde{\sigma}_{ij}\overline{u_i''})$ and $(\overline{\sigma_{ij}''u_i''})$, the speed fluctuation$u_i''$ needs to be expressed in other known terms, while keeping the conventional average for ρ and$p$,, and that of

Favre for the speed, the temperature, etc. . . . Vendome **[4]** proposes two possible approaches:

1. Knowing that the total temperature T_t is constant in vortices . In this case, the temperature fluctuation $T''$is expressed in a function of the mean value of the speed fluctuation.

$$\begin{aligned} T_t &= T + \frac{1}{2c_p} u_i u_i = c_0 \\ T_t &= \tilde{T} + \frac{1}{2c_p}\left(\tilde{u}_i \tilde{u}_i + \widetilde{u_i'' u_i''}\right) \\ T'' &= -\frac{\tilde{u}_i u_i''}{c_p} - \frac{1}{2c_p}\left(u_i'' u_i'' - \widetilde{u_i'' u_i''}\right) \end{aligned} \qquad (2.25)$$

Where c_0 is a constant In the case of a unidirectional flow, we can write:

$$T'' = -\frac{\tilde{u}_i u_i''}{c_p} \qquad (2.26)$$

Introducing the hypothesis of Rubes in, for a behavior polytrophic turbulence:

$$\frac{p'}{\bar{p}} = n\frac{\rho'}{\bar{\rho}} = \frac{n}{n-1}\frac{\rho T''}{\bar{\rho}\tilde{T}} \qquad (2.27)$$

Where n is the polytrophic exponent, we obtain an expression giving fluctuation in density :

$$\rho' = -\frac{\rho \tilde{u}_i u_i''}{(n-1)c_p \tilde{T}} \qquad (2.28)$$

Using the relations between conventional and weighted by mass taking into account the expression of fluctuation ofρ, we obtain:

$$\bar{u_i''} = -\frac{\overline{\rho' u_i''}}{\bar{\rho}} = \frac{\tilde{u}_j \widetilde{u_i'' u_j''}}{(n-1)c_p \tilde{T}} \qquad (2.29)$$

2. This approach uses the polytrophic relationship (2.27), we obtain:

$$\overline{u_i''} = -\frac{\overline{\rho' u_i''}}{\bar{\rho}} = \frac{\widetilde{u_i'' T''}}{(n-1)\tilde{T}} \ldots\ldots\ldots (2.30)$$

It appears in this expression the correlation speed-temperature, which takes into account the case of a heat flux or temperature imposed as conditions on limits, as opposed to the expression (2.29)

The term ($\widetilde{\sigma_{ij}''u_i''}$) can be expressed either from (2.29) or (2.30), its role isnegligible .for Mach values below 5 **[9]-[6].** The term ($\overline{\sigma_{ij}''u_i''}$) is modeled

.

$$\overline{\sigma_{ij}''u_i''} = \overline{\mu u_i''\left(\frac{\partial u_i''}{\partial x_j} + \frac{\partial u_j}{\partial x_i} - \frac{2}{3}\delta_{ij}\frac{\partial u_k'}{\partial x_k}\right)}$$
$$= \bar{\mu}\left(\frac{\partial}{\partial x_j}\frac{\overline{u_i''u_i''}}{2} + \overline{u_i''\frac{\partial u_j''}{\partial x_i}} - \frac{2}{3}\delta_{ij}u_i''\frac{\partial u_k''}{\partial x_k}\right) \qquad (2.31)$$

The terms $\overline{\sigma_{ij}''}\widetilde{u_i''}\overline{q_j''}$ET $-\frac{1}{2}\rho u_j''\bar{u}_i''u_i''$being neglected, for we hold only correlations involving Reynolds stress are accounted for. Equation (2.18) can be written as follows:

$$\frac{\partial}{\partial t}\bar{\rho}\left(\tilde{e} + \frac{\tilde{u}_i\tilde{u}_i}{2} + k\right) + \frac{\partial}{\partial x_j}\left(\bar{\rho}\tilde{u}_j\left(\tilde{e} + \frac{\tilde{u}_i\tilde{u}_i}{2} + k\right) + \tilde{u}_j\bar{p}\right) =$$
$$\frac{\partial}{\partial x_j}\tilde{u}_i\left(\bar{\mu}\left(\frac{\partial\tilde{u}_i}{\partial x_j} + \frac{\partial\tilde{u}_j}{\partial x_i} - \frac{2}{3}\delta_{ij}\frac{\partial\tilde{u}_k}{\partial x_k}\right) - \overline{\rho u_i''u_j''}\right) - \qquad (2.32)$$
$$\frac{\partial}{\partial x_j}\left(-\lambda_c\frac{\partial\tilde{T}}{\partial x_j} + \overline{\gamma c_v\rho T''u_j''}\right)$$

In addition, the averaging equation is taken into account:

$$\bar{p} = \bar{\rho}(c_p - c_v)\tilde{T} = (\gamma - 1)\bar{\rho}\tilde{e} \quad (2.33)$$

We can also write an equation giving the pressure fluctuation:

$$p' = (\gamma - 1)(\rho'\tilde{e} + \rho e'') \qquad 2.34)$$

The state equation can still be put in the form:

$$\frac{p'}{\bar{p}} = \frac{T''}{\tilde{T}} + \frac{\rho'}{\bar{\rho}} + \frac{\rho'T''}{\bar{\rho}\tilde{T}} \qquad (2.35)$$

2.4. Closing of equations

The establishment of the system of previously written equations testifies to the appearance of additional terms which are expressed in the form of correlations, which reflect the effect of turbulence on the movement of the middle field and which make the system of equations open. The problem of closure then arises in establishing the link between the correlations and the mean field.

The search for algebraic equations or relationships to close the equation system constitutes the modelling procedure that must be based on experimental validation. The Reynolds tension is the main correlation as it largely determines the behavior of the mean velocity field. In the closure of the first order, the double correlations are expressed as a function of the gradient of the mean field and a viscosity of the turbulence through a hypothesis of Boussinesq **[7]**. The closure of the second order is based on the balance equations for the components of the double velocity correlation, the third order approach of the triple correlations **[8]** simple at present very complex.
For turbulent heat flow, the closure can be carried to different levels upto the transport model by a partial differential balance equation **[9]**. The question arises: at what level should the closure of the thermal correlation be carried out in relation to the closure of the kinematic correlation. The answer depends on the nature of the flows that are being considered andis at the same time a compromise between the complexity of the model and its performance. Very schematically, we can consider that obtaining system close of equations can be done from the system opened by:

*Reduction of unknown numbers
*Addition of additional equations
* Combinations of the two previous procedures.

2.5.The Turbulent Kinetic Energy Transport Equation

A differential equation for turbulent kinetic energy k can be obtainedby:
1. Considering the instantaneous equation of the momentum written in primitive variables, a Naiver-Stokes equation can be written as:

$$\mathcal{E}_{NS}(u_i) = \rho \frac{\partial u_i}{\partial t} + \rho u_j \frac{\partial u_i}{\partial x_j} + \frac{\partial p}{\partial x_i} - \frac{\partial \sigma_{ij}}{\partial x_j} \qquad (2.36)$$

In this case, the equation of the momentum is obtained by:

$$\mathcal{E}_{\mathcal{NS}}(u_i) = 0 \qquad (2.37)$$

2. We multiply the previous equation by u_i'' and we average in time:

$$\overline{u_\iota'' \mathcal{E}_{NS}(u_\iota) = 0} \qquad (2.38)$$

$$\overline{u_\iota'' \rho \frac{\partial u_\iota}{\partial t}} + \overline{u_\iota'' \rho u_\jmath \frac{\partial u_\iota}{\partial x_\jmath}} + \overline{u_\iota'' \frac{\partial p}{\partial x_\iota}} - \overline{u_\iota'' \frac{\partial \sigma_{\iota\jmath}}{\partial x_\jmath}} = 0 \quad (2.39)$$

With

a)
$$\overline{u_\iota'' \rho \frac{\partial u_\iota}{\partial t}} = \overline{u_\iota'' \rho \frac{\partial u_\iota''}{\partial x_\jmath}} = \frac{\partial}{\partial t}\frac{1}{2}\overline{\rho u_\iota'' u_\iota''} - \frac{1}{2}\overline{u_\iota'' u_\iota'' \frac{\partial \rho}{\partial t}}$$

b)
$$\overline{u_\iota'' \rho u_\jmath \frac{\partial u_\iota}{\partial x_\jmath}} = \overline{\tilde{u}_\jmath \rho \frac{\partial}{\partial x_\jmath}\frac{1}{2}u_\iota'' u_\iota''} + \overline{\rho u_\jmath'' \frac{\partial}{\partial x_\jmath}\frac{1}{2}u_\iota'' u_\iota''} + \overline{\rho u_\jmath'' u_\iota''}\frac{\partial \tilde{u}_i}{\partial x_j}$$
$$= \overline{\rho u_\jmath'' u_\iota''}\frac{\partial \tilde{u}_i}{\partial x_j} + \frac{\partial}{\partial x_j}\tilde{u}_j \frac{1}{2}\overline{\rho u_\iota'' u_\iota''} - \frac{1}{2}\overline{\rho u_\iota'' u_\iota'' \frac{\partial}{\partial x_\jmath}\rho \tilde{u}_\jmath}$$
$$+ \frac{\partial}{\partial x_j}\frac{1}{2}\overline{\rho u_\jmath'' u_\iota'' u_\iota''} - \frac{1}{2}\overline{u_\iota'' u_\iota'' \frac{\partial}{\partial x_\jmath}\rho u_\jmath''}$$

c)
$$\overline{u_\iota'' \frac{\partial p}{\partial x_\iota}} = \overline{u_\iota''}\overline{\frac{\partial p}{\partial x_\iota}} + \frac{\partial}{\partial x_i}\overline{u_\iota'' p'} - \overline{p' \frac{\partial u_\iota''}{\partial x_\iota}}$$

d)
$$-\overline{u_\iota'' \frac{\partial \sigma_{\iota\jmath}}{\partial x_\jmath}} = \overline{\sigma_{\iota\jmath}\frac{\partial u_\iota''}{\partial x_\jmath}} - \frac{\partial}{\partial x_j}\overline{u_\iota'' \sigma_{\iota\jmath}}$$

From the continuity equation, the following can be deduced:

$$\frac{1}{2}\overline{u_\iota'' u_\iota'' \frac{\partial \rho}{\partial t}} + \frac{1}{2}\overline{\rho u_\iota'' u_\iota'' \frac{\partial}{\partial x_\jmath}\rho \tilde{u}_\jmath} + \frac{1}{2}\overline{u_\iota'' u_\iota'' \frac{\partial}{\partial x_\jmath}\rho u_\jmath''} = 0 \qquad (2.40)$$

We obtain the following scalar equation:

$$\underbrace{\frac{\partial}{\partial t}\frac{1}{2}\overline{\rho u_i'' u_i''} + \frac{\partial}{\partial x_j}\tilde{u}_j\frac{1}{2}\overline{\rho u_i'' u_i''}}_{1} = \underbrace{-\overline{\rho u_j'' u_i''}\frac{\partial \tilde{u}_i}{\partial x_j}}_{2} \quad (2.41)$$

$$\underbrace{-\frac{\partial}{\partial x_j}\left(\frac{1}{2}\overline{\rho u_j'' u_i'' u_i''} + \overline{u_j'' p'} - \overline{u_i'' \sigma_{ij}}\right.}_{3}$$

$$\underbrace{-\overline{u_i''}\frac{\partial \bar{p}}{\partial x_i}}_{4} + \underbrace{\overline{p'\frac{\partial u_i''}{\partial x_i}}}_{5} - \underbrace{\overline{\sigma_{ij}\frac{\partial u_i''}{\partial x_j}}}_{6}$$

The terms represent respectively:

1. Temporal variation of k and its convection by the mean velocity field

2. Represents the production of turbulence kinetic energy by mean motion

3. Represent respectively

a) Diffusion by turbulent movements: $\frac{1}{2}\overline{\rho u_j'' u_i'' u_i''}$

b) diffusion by pressure fluctuations: $\overline{u_j'' p'}$

c) molecular motion diffusion: $\overline{u_i'' \sigma_{ij}}$

4. The interaction of the medium pressurized field with velocity fluctuations

5. Correlation between fluctuation of pressure and divergence of fluctuating velocities

6. Corresponds to the destruction of turbulence kinetic energy by the effect of viscosity

2.6. Reynolds Stress Transport Equation

This equation plays an important role in the closure to the second order with transport equations or in its simple form in the closure to the first order, which is presented as an equation of the kinetic energy of turbulence. Consider the products $\mathcal{E}_{\mathcal{N}\delta}$ (u_i by the speed fluctuation u_j'') and ENS (u_j by u_i'').The statistical average of the sum of the two products gives:

$$\overline{u_j''\mathcal{E}_{N\delta}(u_\iota) + u_\iota''\mathcal{E}_{\mathcal{N}}(u_j)} = 0 \quad (2.42)$$

$$\begin{cases} \mathcal{E}_{\mathcal{N}\delta}(u_i) = \rho\frac{\partial u_i}{\partial t} + \rho u_k\frac{\partial u_i}{\partial x_k} + \frac{\partial p}{\partial x_i} - \frac{\partial \sigma_{ik}}{\partial x_k} \\ \mathcal{E}_{\mathcal{N}\delta}(u_j) = \rho\frac{\partial u_j}{\partial t} + \rho u_k\frac{\partial u_j}{\partial x_k} + \frac{\partial p}{\partial x_j} - \frac{\partial \sigma_{jk}}{\partial x_k} \end{cases} \quad (2.43)$$

We start with the development of unsteady terms:

$$\overline{u_j''\rho\frac{\partial u_\iota}{\partial t}} + \overline{u_\iota''\rho\frac{\partial u_J}{\partial t}} = \frac{\partial}{\partial t}\overline{\rho u_\iota'' u_j''} - \overline{u_\iota'' u_j''\frac{\partial \rho}{\partial t}} \quad (2.44)$$

The convective term is written:

$$\overline{u_j''\rho u_k\frac{\partial u_\iota}{\partial x_k}} + \overline{u_\iota''\rho u_k\frac{\partial u_J}{\partial x_k}} = \frac{\partial}{\partial x_k}\tilde{u}_k\overline{\rho u_\iota'' u_j''} - \overline{u_\iota'' u_j''\frac{\partial \rho\tilde{u}_k}{\partial x_k}} + \frac{\partial}{\partial x_k}\overline{\rho u_k'' u_\iota'' u_j''} - \overline{u_\iota'' u_j''\frac{\partial \rho u_k''}{\partial x_k}} + \overline{\rho u_k'' u_\iota''}\frac{\partial \tilde{u}_j}{\partial x_k} + \overline{\rho u_k'' u_j''}\frac{\partial \tilde{u}_i}{\partial x_k} \quad (2.45)$$

The term of the pressure gradient:

$$\overline{u_\iota''\frac{\partial p}{\partial x_J}} + \overline{u_J''\frac{\partial p}{\partial x_\iota}} = \overline{u_\iota''}\overline{\frac{\partial p}{\partial x_J}} + \overline{u_J''}\overline{\frac{\partial p}{\partial x_\iota}} + \overline{u_\iota''\frac{\partial p'}{\partial x_J}} + \overline{u_J''\frac{\partial p'}{\partial x_\iota}} \quad (2.46)$$

$$= \overline{u_\iota''}\overline{\frac{\partial p}{\partial x_J}} + \overline{u_J''}\frac{\widetilde{\partial p}}{\partial x_i} + \frac{\partial}{\partial x_j}\overline{u_\iota'' p'} + \frac{\partial}{\partial x_i}\overline{u_J'' p'} - p'\left(\frac{\overline{\partial u_\iota''}}{\partial x_J} + \frac{\partial u_J''}{\partial x_\iota}\right)$$

The viscous term:

$$-\overline{u_J''\frac{\partial \sigma_{\iota k}}{\partial x_k}} - \overline{u_\iota''\frac{\partial \sigma_{Jk}}{\partial x_k}} = -\frac{\partial}{\partial x_k}\overline{u_J''\sigma_{\iota k}} + \overline{\sigma_{\iota k}\frac{\partial u_J''}{\partial x_k}} - \frac{\partial}{\partial x_k}\overline{u_\iota''\sigma_{Jk}} + \overline{\sigma_{Jk}\frac{\partial u_\iota''}{\partial x_k}} \quad (2.47)$$

Using equation (2.40), we obtain the transport equation for the Reynolds stresses:

$$\begin{aligned}&\frac{\partial}{\partial t}\overline{\rho u_i'' u_j''} + \frac{\partial}{\partial x_k}\tilde{u}_k\overline{\rho u_i'' u_j''} = -\overline{\rho u_k'' u_i''}\frac{\partial \tilde{u}_j}{\partial x_k} - \rho u_k'' u_j''\frac{\partial \tilde{u}_i}{\partial x_k}\\ &-\frac{\partial}{\partial x_k}\left(\overline{\rho u_k'' u_i'' u_j''} + \overline{u_i'' p'}\delta_{jk} + \overline{u_j'' p'}\delta_{ik} - \overline{u_j''\sigma_{ik}} - u_i''\sigma_{jk}\right)\\ &-\overline{u_i''}\frac{\partial \tilde{p}}{\partial x_j} - \overline{u_j''}\frac{\partial \tilde{p}}{\partial x_i} + \overline{p'\left(\frac{\partial u_i''}{\partial x_j} + \frac{\partial u_j''}{\partial x_i}\right)} - \overline{\sigma_{ik}\frac{\partial u_j''}{\partial x_k}} - \overline{\sigma_{jk}\frac{\partial u_i''}{\partial x_k}}\end{aligned} \quad (2.48)$$

This transport equation is used as an alternative to Reynolds $-\rho u_i'' u_j''$,tensor modeling, it contains triple correlation terms, which will need to be modeled

2.7.The transport equation of turbulent dissipation

Dissipation equation requires much more effort; dissipation is given from the following expression:

$$\bar{\rho}\varepsilon = \overline{\sigma_{ik}\frac{\partial u_j''}{\partial x_k}} = \bar{\mu}\overline{\left(\frac{\partial u_i}{\partial x_k} + \frac{\partial u_k}{\partial x_i} - \frac{2}{3}\delta_{ik}\frac{\partial u_n}{\partial x_n}\right)\frac{\partial u_i''}{\partial x_k}} \quad (2.49)$$

We can express an equation for viscous stress σ_{ik} using expressions (2.36) and (2.37). By adding kinematic viscosity to have a dimension of a constraint.

$$v\left(\frac{\partial}{\partial x_k}\mathcal{E}_{NS}(u_i) + \frac{\partial}{\partial x_i}\mathcal{E}_{NS}(u_k) - \frac{2}{3}\delta_{ik}\frac{\partial}{\partial x_n}\mathcal{E}_{NS}(u_n)\right) \quad (2.50)$$

The terms of equation (2.48) are given respectively by:

$$\begin{aligned}&\frac{\partial}{\partial x_k}\mathcal{E}_{N\delta}(u_i) = \rho\frac{\partial}{\partial t}\left(\frac{\partial u_i}{\partial x_k}\right) + \rho u_l\frac{\partial}{\partial x_l}\left(\frac{\partial u_i}{\partial x_k}\right) + \frac{\partial \rho}{\partial x_k}\frac{\partial u_i}{\partial t} + \frac{\partial \rho u_l}{\partial x_k}\frac{\partial u_i}{\partial x_l}\\ &-\frac{\partial^2}{\partial x_k \partial x_l}\mu\left(\frac{\partial u_i}{\partial x_l} + \frac{\partial u_l}{\partial x_i} - \frac{2}{3}\delta_{il}\frac{\partial u_j}{\partial x_j}\right) + \frac{\partial^2 p}{\partial x_k \partial x_i} = 0\end{aligned} \quad (2.51)$$

$$\begin{aligned}&\frac{\partial}{\partial x_i}\mathcal{E}_{NS}(u_k) = \rho\frac{\partial}{\partial t}\left(\frac{\partial u_k}{\partial x_i}\right) + \rho u_l\frac{\partial}{\partial x_l}\left(\frac{\partial u_k}{\partial x_i}\right) + \frac{\partial \rho}{\partial x_i}\frac{\partial u_k}{\partial t} + \frac{\partial \rho u_l}{\partial x_i}\frac{\partial u_k}{\partial x_l}\\ &-\frac{\partial^2}{\partial x_i \partial x_l}\mu\left(\frac{\partial u_k}{\partial x_l} + \frac{\partial u_l}{\partial x_k} - \frac{2}{3}\delta_{kl}\frac{\partial u_j}{\partial x_j}\right) + \frac{\partial^2 p}{\partial x_k \partial x_i} = 0\end{aligned} \quad (2.52)$$

$$-\frac{2}{3}\delta_{ik}\frac{\partial}{\partial x_n}\mathcal{E}_{NS}(u_n) = -\frac{2}{3}\delta_{ik}\left\{\rho u_l\frac{\partial}{\partial x_l}\left(\frac{\partial u_n}{\partial x_n}\right)+\rho\frac{\partial}{\partial t}\left(\frac{\partial u_n}{\partial x_n}\right)+\frac{\partial \rho u_l}{\partial x_n}\frac{\partial u_n}{\partial x_l}\right.$$
$$\left.-\frac{\partial^2}{\partial x_n\partial x_l}\mu\left(\frac{\partial u_n}{\partial x_l}+\frac{\partial u_l}{\partial x_n}-\frac{2}{3}\delta_{nl}\frac{\partial u_j}{\partial x_j}\right)+\frac{\partial^2 p}{\partial x_n\partial x_n}+\frac{\partial \rho}{\partial x_n}\frac{\partial u_n}{\partial t}\right\} \quad (2.53)$$

Equation (2.50) can take the form:

$$v\rho\left(\frac{\partial}{\partial t}\left(\frac{\partial u_i}{\partial x_k}+\frac{\partial u_k}{\partial x_i}-\frac{2}{3}\delta_{ik}\frac{\partial u_n}{\partial x_n}\right)+u_l\frac{\partial}{\partial x_l}\left(\frac{\partial u_i}{\partial x_k}+\frac{\partial u_k}{\partial x_i}-\frac{2}{3}\delta_{ik}\frac{\partial u_n}{\partial x_n}\right)\right)=$$
$$+v\frac{\partial^2}{\partial x_k\partial x_l}\mu\left(\frac{\partial u_i}{\partial x_l}+\frac{\partial u_l}{\partial x_i}-\frac{2}{3}\delta_{il}\frac{\partial u_j}{\partial x_j}\right)+\frac{2}{3}\delta_{ik}v\frac{\partial^2 p}{\partial x_n\partial x_n}-2v\frac{\partial^2 p}{\partial x_k\partial x_i}-$$
$$\frac{2}{3}\delta_{ik}v\frac{\partial^2}{\partial x_n\partial x_l}\mu\left(\frac{\partial u_n}{\partial x_l}+\frac{\partial u_l}{\partial x_n}-\frac{2}{3}\delta_{nl}\frac{\partial u_j}{\partial x_j}\right)+v\frac{\partial^2}{\partial x_i\partial x_l}\mu\left(\frac{\partial u_k}{\partial x_l}+\frac{\partial u_l}{\partial x_k}-\frac{2}{3}\delta_{kl}\frac{\partial u_j}{\partial x_j}\right)- \quad (2.54)$$
$$v\frac{\partial \rho}{\partial x_i}\frac{\partial u_k}{\partial t}-v\frac{\partial \rho u_l}{\partial x_i}\frac{\partial u_k}{\partial x_l}-v\frac{\partial \rho}{\partial x_k}\frac{\partial u_i}{\partial t}-v\frac{\partial \rho u_l}{\partial x_k}\frac{\partial u_i}{\partial x_k}+\frac{2}{3}\delta_{ik}v\frac{\partial \rho}{\partial x_n}\frac{\partial u_n}{\partial t}+\frac{2}{3}\delta_{ik}v\frac{\partial \rho u_l}{\partial x_n}\frac{\partial u_n}{\partial x_l}$$

Deriving from $x_k$the equation for the speed fluctuation, u_i''we get:

$$\rho\frac{\partial}{\partial t}\left(\frac{\partial u_i''}{\partial x_k}\right)+\rho u_l\frac{\partial}{\partial x_l}\left(\frac{\partial u_i''}{\partial x_k}\right)=-\frac{\partial \rho'}{\partial x_k}\frac{\partial \tilde{u}_i}{\partial t}-\rho'\frac{\partial^2 \tilde{u}_i}{\partial t\,\partial x_k}-\frac{\partial \rho}{\partial x_k}\frac{\partial u_i''}{\partial t}-\frac{\partial \rho' \tilde{u}_l}{\partial x_k}\frac{\partial \tilde{u}_i}{\partial x_l}$$
$$-\rho'\tilde{u}_l\frac{\partial^2 \tilde{u}_i}{\partial x_l\partial x_k}-\frac{\partial \rho u_l}{\partial x_k}\frac{\partial u_i''}{\partial x_l}-\frac{\partial \rho u_l''}{\partial x_k}\frac{\partial \tilde{u}_i}{\partial x_l}-\rho u_l''\frac{\partial^2 \tilde{u}_i}{\partial x_l\partial x_k}-\frac{\partial^2 p'}{\partial x_i\partial x_k}+\frac{\partial^2}{\partial x_l\partial x_k}\rho\overline{u_i''u_l''}+ \quad (2.55)$$
$$\frac{\partial^2}{\partial x_l\partial x_k}\mu\left(\frac{\partial u_i''}{\partial x_l}+\frac{\partial u_l''}{\partial x_i}-\frac{2}{3}\delta_{il}\frac{\partial u_j''}{\partial x_j}\right)-\frac{\partial^2}{\partial x_l\partial x_k}\mu\left(\frac{\partial u_i''}{\partial x_l}+\frac{\partial u_l''}{\partial x_i}-\frac{2}{3}\delta_{il}\frac{\partial u_j''}{\partial x_j}\right)$$

By multiplying the equations (2.54) and (2.55) respectively by $\left(\left(\frac{\partial u_i^*}{\partial x_k}\right)\right)$ and $((v\sigma_{ik}^*))$, where:

$$\sigma_{ik}^* = \frac{\partial u_i}{\partial x_k}+\frac{\partial u_k}{\partial x_i}-\frac{2}{3}\delta_{ik}\frac{\partial u_n}{\partial x_n} \quad (2.56)$$

The sum of two resulting equations gives a transport equation $\left(\frac{\partial u_i''}{\partial x_k}\mu\sigma_{ik}^*\right)$

$$v\rho\left(\frac{\partial u_i''}{\partial x_k}\frac{\partial \sigma_{ik}^*}{\partial t}+\frac{\partial u_i''}{\partial x_k}u_l\frac{\partial \sigma_{ik}^*}{\partial x_l}+\sigma_{ik}^*\frac{\partial}{\partial t}\left(\frac{\partial u_i''}{\partial x_k}\right)+\sigma_{ik}^*u_l\frac{\partial}{\partial x_l}\left(\frac{\partial u_i''}{\partial x_k}\right)\right)=$$

$$+\frac{2}{3}\delta_{ik}v\frac{\partial u_i''}{\partial x_k}\frac{\partial^2 p}{\partial x_n\partial x_n}-2v\frac{\partial u_i''}{\partial x_k}\frac{\partial^2 p}{\partial x_k\partial x_i}+v\frac{\partial u_i''}{\partial x_k}\frac{\partial^2}{\partial x_k\partial x_l}\mu\left(\frac{\partial u_i}{\partial x_l}+\frac{\partial u_l}{\partial x_i}-\frac{2}{3}\delta_{il}\frac{\partial u_j}{\partial x_j}\right)-$$

$$v\frac{\partial u_i''}{\partial x_k}\frac{\partial \rho}{\partial x_i}\frac{\partial u_k}{\partial t}-v\frac{\partial u_i''}{\partial x_k}\frac{\partial \rho u_l}{\partial x_i}\frac{\partial u_k}{\partial x_l}-v\frac{\partial u_i''}{\partial x_k}\frac{\partial \rho}{\partial x_k}\frac{\partial u_i}{\partial t}-v\frac{\partial u_i''}{\partial x_k}\frac{\partial \rho u_l}{\partial x_k}\frac{\partial u_i}{\partial x_l}$$

$$+\frac{2}{3}\delta_{ik}v\frac{\partial u_i''}{\partial x_k}\frac{\partial \rho}{\partial x_n}\frac{\partial u_n}{\partial t}+\frac{2}{3}\delta_{ik}v\frac{\partial u_i''}{\partial x_k}\frac{\partial \rho u_l}{\partial x_n}\frac{\partial u_n}{\partial x_l}$$

$$-v\sigma_{ik}^*\rho'\tilde{u}_l\frac{\partial^2\tilde{u}_i}{\partial x_l\partial x_k}-v\sigma_{ik}^*\frac{\partial \rho'\tilde{u}_l}{\partial x_k}\frac{\partial\tilde{u}_i}{\partial x_l}-v\sigma_{ik}^*\frac{\partial \rho}{\partial x_k}\frac{\partial u_i''}{\partial t}-v\sigma_{ik}^*\rho'\frac{\partial^2\tilde{u}_i}{\partial t\,\partial x_k} \qquad (2.57)$$

$$-v\sigma_{ik}^*\frac{\partial \rho'}{\partial x_k}\frac{\partial\tilde{u}_i}{\partial t}-v\sigma_{ik}^*\frac{\partial \rho u_l''}{\partial x_k}\frac{\partial\tilde{u}_i}{\partial x_l}-v\sigma_{ik}^*\frac{\partial^2 p'}{\partial x_i\partial x_k}-v\sigma_{ik}^*\frac{\partial \rho u_l}{\partial x_k}\frac{\partial u_i''}{\partial x_l}-v\sigma_{ik}^*\rho u_l''\frac{\partial^2\tilde{u}_i}{\partial x_l\partial x_k}+$$

$$v\sigma_{ik}^*\frac{\partial^2}{\partial x_l\partial x_k}\overline{\rho u_l''u_l''}+v\sigma_{ik}^*\frac{\partial^2}{\partial x_l\partial x_k}\mu\left(\frac{\partial u_i''}{\partial x_l}+\frac{\partial u_l''}{\partial x_i}-\frac{2}{3}\delta_{il}\frac{\partial u_j''}{\partial x_j}\right)$$

$$-v\sigma_{ik}^*\frac{\partial^2}{\partial x_l\partial x_k}\mu\left(\overline{\frac{\partial u_l''}{\partial x_l}+\frac{\partial u_l''}{\partial x_\iota}-\frac{2}{3}\delta_{\iota l}\frac{\partial u_j''}{\partial x_j}}\right)$$

The first line of equation (2.57), taking into account the equation of

Continuity, after the passage to the temporal mean, we obtain:

$$\frac{\partial}{\partial t}\overline{\left(v\rho\sigma_{\iota k}^*\frac{\partial u_l''}{\partial x_k}\right)}+\frac{\partial}{\partial x_l}\overline{\left(v\rho u_l\sigma_{\iota k}^*\frac{\partial u_l''}{\partial x_k}\right)}=\frac{\partial}{\partial t}\bar{\rho}\varepsilon+\frac{\partial}{\partial x_l}\tilde{u}_l\bar{\rho}\varepsilon+\frac{\partial}{\partial x_l}\overline{\left(u_l''v\rho\sigma_{\iota k}^*\frac{\partial u_l''}{\partial x_k}\right)}$$

2.8. Closing models of the Naiver Stokes equations

2.8.1. Models with turbulent viscosity

to avoid solving transport equations of components tensor of turbulent stresses, a hypothesis can be established to model the term$-\rho\widetilde{u_i''u_j''}$. The hypothesis of closure is that of the Boussinesq **[10],** and similarly for the closure of the energy equation.

$$-\rho\widetilde{u_i''u_j''}=2\mu_t\left(\tilde{S}_{ij}-\frac{1}{3}\tilde{u}_{k,k}\delta_{ij}\right)-\frac{2}{3}\rho k\delta_{ij} \qquad (2.58)$$

The term $-\frac{2}{3}\mu_t \tilde{u}_{k,k}\delta_{ij}$presents the volume expansion used in the case of compressible flows.

2.8.1.1. Zero equation models

The zero equation models used to model the Reynolds constraints in motion quantity equations use an algebraic turbulent viscosity or mixing length. It was Ludwig Brandt who proposed a relationship linking turbulent viscosity to the gradient of average velocity by introducing a length lm called mixing length l_m , for flows of the boundary layer type:

$$\mu_t = \rho l_m^2 \left|\frac{\partial u}{\partial y}\right| \quad (2.59)$$

This relationship reflects the state of equilibrium between the medium field and the fluctuating field. To determine l_m , Von **Karman [11]**, **Klebanoff [12]** and **Michel** and al **[13]** al proposed different models depending on wall distance, boundary layer thickness and mean velocity gradient. To take into account the effect of the wall, and Driest [14] proposed a damping function F in relationμ_t

$$\mu_t = \rho F^2 l_m^2 \left|\frac{\partial u}{\partial y}\right|$$
$$F = 1 - \exp\left(-\frac{y^+}{26}\right) \quad (2.60)$$
$$y^+ = \frac{u_\tau y}{v_p}, u_\tau = \sqrt{\tau_p/\rho}, \tau_p = \left(\mu \frac{\partial u}{\partial y}\right)_p$$

Other models have been developed by **Cebeci-Smith** [15], **Alber**[16] and the known **Baldwin-Lomax**[17] model . The advantage of this type of model is its simplicity of implementation, but the disadvantages are diverse, a lot of empiricism, absence of the history of turbulence.

2.8.1.2. Single Equation Models

Among the different models in this group, we consider only the Spalart and Allmaras (SA) model, which, unlike the Cebeci-Smith model which uses algebraic expressions for turbulent viscosity ((v_t)), the model (SA) uses a transport equation.

The Spalart-Allmaras **[17] [18] [19]** model is a viscosity model relatively recent turbulent based on a transport equation for turbulent viscosity. An old model developed by Baldwin and Barth **[20]** inspired this model. Its formulation and coefficients have been defined using dimensional analysis, and empirical results selected. The empirical results used in its development were for two-dimensional (2-D) type, mixing layers, wake, and boundary layer flow on a flat plate.

The aim of this model is to improve the predictions obtained with the algebraic models of mixing length to develop a model local for complex flows, and provide an alternative more simple to two-equation turbulence models

.The model uses the distance closest to the wall in its formulation, and provides a smooth transition from laminar to turbulent; providethat the transition start position be given. It does not require a very fine mesh in the case of flows with walls as in two-equation turbulence models, and it shows good convergence in simple flows.

The model does not give good predictions in jet flow, but gives enough good predictions in the 2-D flow of mixing layers, wake, and flat plate boundary layers and shows improved flow forecasting with adverse pressure gradients relative to models $k-\varepsilon$ and $k-\omega$, but not as much as the SST model.

Model equation:

The function of turbulent viscosity is defined as a function of a variable viscosity, $\tilde{v}$, and a wall function, , f_{v_1}, as follows:

$$v_t = \tilde{v} f_{v_1} \quad (2.61)$$

In remote wall areas, function, f_{v_1} is equal to one and ET $v_t = \tilde{v}$.

The convective transport equation of turbulent viscosity is given by:

$$\frac{\partial \rho \tilde{v}}{\partial t} + \frac{\partial}{\partial x_j}\left(\rho \tilde{v} u_j\right) = c_{b_1}(1-f_{t_2})\rho \tilde{S}\tilde{v} + \frac{1}{\sigma}\left(\frac{\partial}{\partial x_j}\left(\rho(v+\tilde{v})\frac{\partial \tilde{v}}{\partial x_j}\right) + c_{b_2}\rho \frac{\partial \tilde{v}}{\partial x_j}\frac{\partial \tilde{v}}{\partial x_j}\right) - \left(c_{w_1} f_w - \frac{c_{b_1}}{\kappa^2} f_{t_2}\right)\rho\left(\frac{\tilde{v}}{d}\right)^2 + f_{t_1}\rho \Delta U^2 \quad (2.62)$$

Where the right-hand terms represent, turbulent viscosity production, preservation of diffusion, non-conservative diffusion, dissipation turbulence near the wall, transition damping, and source of turbulence transition. The index b means "basic", w for "wall", v means "viscous", and t means "trip". Model constants and auxiliary functions are defined in terms of basic model for free sheared flows, the wall for boundary layers, the viscous model of integration with the wall, and transition model for laminar-turbulent transition.

Basic model constants for free sheared flows to control the production and diffusion of turbulent viscosity are:

$$c_{b_1} = 0.1355 \quad c_{b_2} = 0.622 \quad \sigma = 2/3$$

These auxiliary functions allow the model to predict the layer logarithmic, although the particular balance of the shear stress Reynolds is not in quantitative agreement with the experimental data. Modeling functions and constants for regions close to the wall are given by :

$$c_{w_1} = \frac{c_{b_1}}{k^2} + \frac{(1 + c_{b_2})}{a} \quad r = \frac{\varphi}{3x^2 d^2}$$
$$c_{w_2} = 0.3 \quad g = r + c_{w_2}(r^6 - r)$$
$$c_{w_3} = 2 \quad f_w = g\left(\frac{1 + c_{m_3}^6}{g^6 + c_{w_3}^{k_3}}\right)^{1/6}$$

These auxiliary functions allow the model to predict the layer logarithmic, although the particular balance of the shear stress Reynolds is not in quantitative agreement with the experimental data. Modeling functions and constants for regions close to the wall are given by :

$$\tilde{S} = S + \frac{\bar{v}}{(xd)^2} f_{v_2} \quad S = \sqrt{2S_{ij}S_{ij}} \quad x = \frac{\nu}{v}$$
$$f_{v_1} = \frac{x^3}{x^3 + c_{v_1}^3} \quad f_{v_2} = 1 - \frac{\chi}{1 + x f_{v_1}} \quad c_{v_1} = 7.1$$

Auxiliary functions and constants of the model to control the laminar region of the shear layers and the transition to the turbulence are defined with a source term controlled with the f_{t_1} and a reduction in production controlled by the function f_{t_2}

$$f_{t_1} = c_{t_1} g_t e^{\left(-c_{t_2}\frac{x_t^2}{\mathrm{md}^2}(d^2 + (g_t d_t)^2)\right)}$$
$$f_{l_2} = c_{l_3} e^{(-c_{t_4} x^2)}$$
$$g_t = \min\left(0.1, \frac{\mathrm{MU}}{\mathrm{wi}_t \Lambda I_t}\right)$$
$$c_{t_1} = 1 c_{t_2} = 2 c_{t_3} = 1.2 c_{t_4} = 0.5$$

where w_t is the vorticity at the point of disjunction of the boundary layer, ΔU is the standard of the difference between the velocity at the flow point and speed at trigger point, Λx_t is the spacing of the mesh along the wall at the trip point, and d_t is the distance from the wall. Despite the existence of too many empiricism, many constants and damping functions, the **Spalart-Allmaras** model is considered as a compromise between algebraic approaches and two equation models.

Boundary conditions:

The ideal value for turbulent viscosity in free flow regions is zero. Some solvers have problems with zero $\tilde{v}$ values in free flow, and lower $\frac{\tilde{v}}{2}$ values have been recommended. Small values are

recommended for free sheared flows, otherwise solutions show dependence on regions outside the boundary layer in velocity profiles and decay rates. On the walls, the turbulent viscosity is zero.

2.8.2. Models with two equations

A Although the models of an equation have found little success, except for the SA model, and where the transport of turbulence characteristics is important as in the case of flows of strong adverse gradients or separate flows, Two-equation models have found wide use. Different two-equation models were proposed and more details were given, for example in **[18],[21].** Three famous models based on this approach are the, k − ε model, the Wilcox$k-w$ model, and the Menter SST model **[18],[21],** which groups the two models, k − ε in the outer region and $k-w$ in the wall region.

2.8.2.1.$k-w$ Model(Wilcox):

k − w (**[18]** and **[22]**) is a well-known and widely tested turbulence viscosity model of two equations. Wilcox gives the main reference for this model, and its formulation is used here. The roots of this model can be attributed to Kolmogorov, Prandtl, Saffman, and Wilcox, in collaboration with other scientists. This model was developed at the same time and in parallel with the k − ε model as an alternative to define a turbulent viscosity function. Convective transport equations are solved for turbulent kinetic energy and its specific rate of dissipation, k and $\boldsymbol{\omega = \varepsilon/\beta^{*}k}$ respectively. Obtaining a transport equation for the frequency ω is just as delicate as for pseudo-dissipation and therefore an analogous strategy is implemented by considering a prototype equation form inspired by the equation k.

The k − w model by Wilcox is proved to be superior numerical stability model k − ε mainly in the viscous underlayment near the wall. This model does not require any damping functions as in the two-equation model k − ε and others due to the large values of ω in the wall region. Wall boundary conditions require specification of the distance between the wall and the first point of the mesh. In the logarithmic region, the model gives good agreement with the experimental results for flows with a moderate gradient of adverse pressure. In the free shear layer and the adverse pressure gradient boundary layer flows, the results of the k − wmodel are sensitive to low values of w outside the boundary layer (references **[22]** and **[23]**). In calculating complex flows, it is difficult to exercise enough control over the turbulence of the external region to avoid small values of w in the free flow and still avoid ambiguities in the results.

Models equation:

Reynolds stress are modelled in terms of turbulent viscosity as follows:

$$\tau_{t_{ij}} = 2\mu_t\left(S_{ij} - S_{nA}\delta_{ij}/3\right) - 2pk\delta_{ij}/3 \quad (2.63)$$

Where μ_t is turbulent viscosity,S_{ij} is the deformation tensor of the average velocity. ρ Is fluid density,k is turbulent kinetic energy,δ_{ij} and is kronecker symbol. Turbulent viscosity is defined as a function of turbulent kinetic energy, and specific dissipation rate, ε

$$\mu_1 = c_\mu f_\mu \rho^\mu \frac{k^2}{2} \quad (2.64)$$

The two transport equations for k and w are defined below by:

$$\frac{\partial \beta k}{\partial t} + \frac{\partial}{\partial x_j}\left(\rho\mu_j k - (\mu + o^*\mu_i)\frac{\partial k}{\partial x_j}\right) = \tau_{i_i} S_{ij} - \beta^*\rho\omega k \quad (2.65)$$

And

$$\frac{\partial \rho\omega}{\partial t} + \frac{\partial}{\partial x_j}\left(\rho u_j \omega z - (\mu + \sigma\mu_i)\frac{\partial \omega_\Delta}{\partial x_j}\right) = \alpha\frac{\Delta z}{k}\tau_{t_{ij}} S_{ij} - \beta\rho\omega_i^2 \quad (2.66)$$

With

$$a = \frac{5}{9} \quad \beta = \frac{9}{40} \quad \beta^* = \frac{9}{100}$$
$$\sigma = 0.5 \quad \sigma^* = 0.5$$

Boundary conditions

the selection of recommended external values for boundary layer flows is:

$$\omega_\infty > \lambda\frac{U_\infty}{L}\mu_{4\infty 0} < 10^{-2}\mu_{4\max}k_\infty = \frac{\mu_{t\infty}}{p_\infty}\omega_\infty$$

Where $L$the approximate length of the computation is range, and $U_\infty$is the characteristic speed. A proportionality factor $\lambda = 10$ was recommended. Free shear layers are more sensitive to low w_∞free flow values and higher de λ values are needed. Following a self-similarity analysis, a value of λ can be determined, from which a value of at least $\lambda = 10$ for mixing layers, increased to $\lambda = 80$ for round jets. Wall boundary conditions are given by the following relationships.

$$k = 0 \text{ et } a = 10\frac{6\mu}{\beta p(y_1)^2}$$

Where y_1 is the distance from the first point to the wall and $y^+ < 1$, zero gradient conditions are applied to the symmetry limits.

2.8.2.2.The $k-w$BSL (Menter model):

The **k − w** models generally do not require additional damping functions and therefore appear to exhibit a more universal behavior in the near- wall region than the k e "low-Reynolds" models. Taking into account this remark and the fact that the k w models are, contrary to the **k − ε** models, sensitive to the definition of the conditions of the distant flow, Menter proposes to define a mixed model with two equations, Having the characteristics of a closure The **k − w** near the walls and those of a model k − ε in remote areas. To develop this combination, Menter first considers the Wilcox **k − w**

Formulation, the transport equations of k and w are given respectively by:

$$\frac{\partial \rho k}{\partial t}+\frac{\partial}{\partial x_j}\left(\rho u_j k-\left(\mu+\sigma_{k_1}\mu_t\right)\frac{\partial k}{\partial x_j}\right)=\tau_{t_{ij}}S_{ij}-\beta^*\rho\omega k \quad (2.67)$$

$$\frac{\partial \rho \omega)}{\partial t}+\frac{\partial}{\partial x_j}\left(\rho u_j \omega-\left(\mu+\sigma_{\omega_1}\mu_t\right)\frac{\partial \omega}{\partial x_j}\right)=\rho\frac{\gamma_1}{\mu_t}\tau_{tt_{ij}}S_{ij}-\beta\rho\omega^2 \quad (2.68)$$

Considering that $f_2=1$to exclude aspects of base Reynolds, the equation of pseudo-dissipation:

$$\frac{\partial \rho \varepsilon}{\partial t}+\frac{\partial}{\partial x_j}\left(\rho u_j \varepsilon-\left(\mu+\frac{\mu_t}{\sigma_\varepsilon}\right)\frac{\partial \varepsilon}{\partial x_j}\right)=c_{z1}\frac{\varepsilon}{k}\tau_{t_{ij}}S_{ij}-c_{z2}f_2\rho\varepsilon\frac{\varepsilon}{k}+\phi_\varepsilon \quad (2.69)$$

is modified to take into account the relation between ε and ω given by:

$$\omega=\frac{\varepsilon}{c_\mu k} \quad (2.70)$$

We obtain the following transport equations:

$$\frac{\partial \rho k}{\partial t}+\frac{\partial}{\partial x_j}\left(\rho u_j k-(\mu+\sigma_{k2}\mu_t)\frac{\partial k}{\partial x_j}\right)=\tau_{t_{ij}}S_{ij}-\beta^*\rho\omega k \quad (2.71)$$

$$\frac{\partial \rho \omega}{\partial t}+\frac{\partial}{\partial x_j}\left(\rho u_j \omega-\left(\mu+\sigma_{\omega_2}\mu_t\right)\frac{\partial \omega}{\partial x_j}\right)=\rho\frac{\gamma_2}{\mu_t}\tau_{t_{ij}}S_{ij}-\beta\rho\omega^2 +2\rho\sigma_{aa_2}\frac{1}{\omega}\frac{\partial k}{\partial x_j}\frac{\partial \omega}{\partial x_j} \quad (2.72)$$

The transport equation for turbulent kinetic energy k remains unchanged with changes in the coefficients. For the equation of ω, a new term appeared following the passage of the equation of ε to the equation of a, called the term of cross diffusion.

To take advantage of the two models $k-\varepsilon$far from the boundary layer and $k-\omega$near the wall, Menter has introduced an F_1 function that allows switching between the two models. Now equation, equation (2.67) and equation (2.68) are multiplied by F_1 and equation (2.71) and equation (2.72) are multiplied by ($(1-F_1)$) and the corresponding equations of each set are summed to give the new model:

$$\frac{\partial \rho k}{\partial t}+\frac{\partial}{\partial x_j}\left(\rho u_j k-(\mu+\sigma_k \mu_t)\frac{\partial k}{\partial x_j}\right)=\tau_{tij}S_{ij}-\beta^*\rho\omega k \quad (2.73)$$

$$\frac{\partial \rho \omega}{\partial t}+\frac{\partial}{\partial x_j}\left(\rho u_j \omega-(\mu+\sigma_\omega \mu_t)\frac{\partial \omega}{\partial x_j}\right)=\rho\frac{\gamma}{\mu_t}\tau_{t_{ij}}S_{ij}-\beta\rho\omega^2 +2\rho(1-F_1)\sigma_{\omega 2}\frac{1}{\omega}\frac{\partial k}{\partial x_j}\frac{\partial \omega}{\partial x_j} \quad (2.74)$$

Turbulence viscosity is given by:

$$\mu_{\mathrm{t}}=\frac{\rho k}{\omega} \quad (2.75)$$

The F_1function allows you to select the Wilcox $(k-\omega)$model in the viscous under layer and logarithmic region and gradually switch to the $\mathbf{k}-\boldsymbol{\varepsilon}$ model as you move away from the wall. This allows us to benefit from the robustness of w in the near wall area and the insensitivity of e in the free flow. The function of Menter $F_1$is written

$$F_1=\tanh(\mathrm{ar}\, g_1^4) \quad (2.76)$$

With

$$\mathrm{arg}_1=\min\left(\max\left(\frac{\sqrt{k}}{0.09\omega y},\frac{500v}{\omega y^2}\right),\frac{4\rho k\sigma_{\omega_2}}{CD_{k\omega}y^2}\right)$$

Where y is the normal distance to the wall and

$$CD_{kat}=\max\left(2\rho\sigma_{\omega\omega_2}\frac{1}{\omega}\frac{\partial k}{\partial x_j}\frac{\partial \omega}{\partial x_j},10^{-20}\right)$$

With

The term $\sqrt{k}/0.09\omega\gamma$ is a scale of turbulent length, enlarged by the distance to the wall, occurs mainly in the logarithmic zone, then decreases further away from the boundary layer. The term $500\mathrm{v}/ay^2$ ensures the activation of the $k-\omega$ model in the viscous sub-layer, and tends to zero the further away from the wall.

The term $4\rho k\sigma_{\omega_2}/CD_{k\omega}, y^2$ is to prevent the degeneration of the solution for small values of w in the external flow. Let $\phi_1$represent the constants in the original model (σ_{k1} ...), $\phi_2$the constants in the transformed model $k-\omega$ (σ_{k2}...) and ϕ_1 the corresponding constants of the new model (σ_k ...), then the relationship between them is:

$$\phi = F_1\phi_1 + (1-F_1)\phi_2 \qquad (2.77)$$
$$\phi = \{\sigma_k, \sigma_{a,}\beta, \gamma\}$$

The following two groups of constants will be used: Group 1 (Wilcox):

$$\sigma_{\xi_1} = 0.5, \sigma_{\omega_1} = 0.5, \beta_1 = 0.075$$
$$\beta^* = 0.09, x = 0.41, \gamma_1 = \beta_1/\beta^* - \sigma_{\omega_1}\kappa^2/\sqrt{\beta^*}$$

Group 2 (Jones-Launder):

$$\sigma_{k_2} = 1.0, \quad \sigma_{\omega 1_2} = 0.856, \quad \beta_2 = 0.0828$$
$$\beta^* = 0.09, \quad \kappa = 0.41, \quad \gamma_2 = \beta_2/\beta^* - \sigma_{\omega_2}\mathrm{k}^2/\sqrt{\beta^*}$$

2.8.2.3. Second order closure model (SSG/LRR-RSM-w2012)

This model was developed within the framework of the European project FLOMANIA for application to aeronautical flow problems. It uses a mixture of two different pressure-strain models (the LRR part is based on an earlier version of the WilcoxRSM-W2006 **[24].** The main references of this model are those of Cecora and al **[25],** Eisfeld **[26]**, Eisfeld and al **[27],** Elis Feld **[28].**

Unlike turbulent viscosity models, the Reynolds Stress Model (RSM) considers Reynolds tensor terms as unknowns. The purpose of this model is to remove the hypothesis introduced by the gradient transport approximation. Experiments show that correlations still do not follow a change of sign with the gradients that connect them with a turbulence viscosity. According to the motion quantity equation, a transport equation for the Reynolds stress can be derived:

$$\frac{\partial}{\partial t}\left(\bar{\rho}\tilde{R}_{ij}\right) + \frac{\partial}{\partial x_k}\left(\bar{\rho}\tilde{u}_{\mathbf{k}}\tilde{R}_{ij}\right) = \bar{\rho}P_{ij} + \bar{\rho}\mathrm{I}_{ij} - \bar{\rho}\varepsilon_{ij} + \bar{\rho}D_{ij} + \bar{\rho}M_{ij} \qquad (2.78)$$

With

$$\bar{\rho}\tilde{R}_{ij} = -\tau_{ij} = \overline{\rho u_i^n u_j^{nJ}}$$

In this equation, the term production P_{ij} is correct, while the other termson the right side need modeling

$$\bar{\rho}P_{ij} = \bar{\rho}\tilde{R}_{ik}\frac{\partial\tilde{u}_j}{\partial x_k} - \bar{\rho}\tilde{R}_{jk}\frac{\partial\tilde{u}_i}{\partial x_k} \qquad (2.79)$$

In the European project FLOMANIA **[33]** the SSG/LRR-w model **[26],[27]** was developed, transferring Menter's SST model ideas **[34]** into the framework of differential Reynolds stress models. In particular, the term redistribution has been harmonized between the Launder-Reece-Rodi model (LRR) **[35]** near the walls, omitting the terms of so-called wall reflection as suggested by Wilcox [36] and the Speziale-Sarkar-Gatski model (SSG) **[37]** to the far field. The resulting redistribution term can be written in the following unified notation**:**

$$\begin{aligned}\bar{\rho}\Pi I_{ij} = &-\left(C_1\bar{\rho}\varepsilon + \tfrac{1}{2}C_1^*\bar{\rho}P_{kk}\right)\tilde{b}_{ij} + C_2\bar{\rho}\varepsilon\left(\tilde{b}_{ik}\tilde{b}_{kj} - \tfrac{1}{3}\tilde{b}_{mn}\tilde{b}_{mn}\delta_{ij}\right)\\ &+\left(C_3 - C_3^*\sqrt{II}\right)\bar{\rho}\tilde{S}_{ij}^* + C_4\bar{\rho}\tilde{k}\left(\tilde{b}_{ik}\tilde{S}_{jk} + \tilde{b}_{jk}\tilde{S}_{ik}^* - \tfrac{2}{3}\tilde{b}_{m\mathrm{H}}\tilde{S}_{mn}^*\delta_{ij}\right)\\ &+C_5\bar{\rho}\tilde{k}\left(\tilde{b}_{ik}\bar{W}_{jk} + \tilde{b}_{jk}\bar{W}_{ik}\right)\end{aligned} \qquad (2.80)$$

Which is formally identical to the SSG model and $\tilde{b}_{ij} = \tilde{R}_{ij}/(2\hbar) - \delta_{ij}/3$ is the anisotropy tensor with its second invariant $II = \tilde{b}_{ij}\tilde{b}_{ij}$

Note that the specific turbulence kinetic energy is equivalent to half of the specific Reynolds stress trace, that is $\tilde{k} = \tilde{R}_{ii}/2$ in addition, $\bar{W}_{ij} = 1/2\left(\partial\tilde{u}_i/\partial x_j - \partial\tilde{u}_j/\partial x_i\right)$ is the mean rotation tensor. With:

$$\tilde{S}_{ij}^* = \frac{1}{2}\left(\frac{\partial\tilde{u}_i}{\partial x_j} + \frac{\partial\tilde{u}_j}{\partial x_i}\right) - \frac{1}{3}\frac{\partial\tilde{u}_k}{\partial x_k}\delta_{ij}$$

Finally,$\varepsilon = C_\mu\tilde{k}\omega$where $C_\mu = 0.09$,and ω is provided by the BSL Menter [34] equation given below. The dissipation term is modelled by an isotropic tensor according to Rotta **[38]**.

$$\bar{\rho}\varepsilon_{ij} = \tfrac{2}{3}C_\mu\bar{\rho}\tilde{k}\omega\delta_{ij} \qquad (2.81)$$

A single gradient or generalized gradient diffusion models can be used alternatively. According to **[39],** we can write:

$$\bar{\rho}D_{ij} = \frac{\partial}{\partial x_k}\left[\left(\bar{\mu}\delta_{kl} + \hat{D}\frac{\bar{\rho}}{\omega}\tilde{R}_{kl}\right)\frac{\partial \tilde{R}_{ij}}{\partial x_l}\right] \qquad (2.82)$$

The contribution due to mass fluctuations, $\bar{\rho}M_{ij}$, is neglected, as it is a common practice for transonic flows. The turbulence model is closed by the equation of *w* of the model BSL de Menter [34].

$$\frac{\partial(\bar{\rho}\omega)}{\partial t} + \frac{\partial}{\partial x_k}\left(\bar{\rho}\tilde{u}_k(\omega)\right)\alpha\frac{\omega}{\tilde{k}}\frac{\bar{\rho}P_{kk}}{2} - \beta\bar{\rho}\omega^2 + \frac{\partial}{\partial x_k}\left(\left(\bar{\mu} + \sigma\frac{\bar{\rho}\tilde{k}}{\omega)}\right)\frac{\partial\omega}{\partial x_k}\right) + \sigma_d\frac{\bar{\rho}}{\omega}\max\left(\frac{\partial k}{\partial x_j}\frac{\partial\omega}{\partial x_j}; 0\right) \qquad (2.83)$$

The relation giving the assembly between the SSG and LRR regions is obtained by:

$$\phi = F_1\phi^{(LRR)} + (1 - F_1)\phi^{(SSC)} \qquad (2.84)$$

Where the Menter function is given by

$$F_1 = \tanh(\zeta^4) \qquad (2.85)$$

With

$$c = min\left[\max\left(\frac{\sqrt{\tilde{k}}}{C_\mu\omega d}; \frac{500\bar{\mu}}{\bar{\rho}\omega d^2}\right); \frac{4\sigma^{(SSG)}\bar{\rho}\tilde{k}}{\max\left\{2\sigma^{(SSG)}\frac{\bar{\rho}}{\omega}\frac{\partial\tilde{k}}{\partial x_k}\frac{\partial\omega}{\partial x_k}; 10^{-20}\right\}}\right] \qquad (2.86)$$

The values for the overall limit of the closure coefficients for SSG and LRR are given in Table:

	C_1	C_1*	C2	C_3	C_3*	C_4
SSG	3.4	1.8	4.2	0.8	1.3	1.25
LRR	3.6	0.0	0.0	.08	0.0	2.0
	C_5	$\widehat{D}$	α	β	σ	σ_d
SSG	0.4	2.44	0.44	0.0828	0.856	1.712
LRR	0.11	0.5	0.5556	0.075	0.5	0.0

Table 2.1: SSG/LRR- ω model constants

Boundary conditions

$$\tilde{R}_{ij,f\ \text{arfield}} = \frac{2}{3}\tilde{k}_{\text{farfield}}\,\delta_{ij}\omega_{farfield} = \frac{\bar{\rho}\tilde{k}_{\text{far field}}}{\mu_{t_2\ \text{farfield}}}$$

The initial value is a function of the intensity of the far field turbulence $Tu$with:

$$\tilde{k}_{\text{farfield}} = (3/2)(Tu)^2 U^2_{farfield}$$

Typical values are:

$$Tu = 0.001(= 0.1\%)\frac{\mu_{t,far\ \text{field}}}{\bar{\mu}_{\text{farfield}}} = 0.1$$

For solid surfaces (walls):

$$\tilde{R}_{ij,paroi} = 0 \qquad \omega_{\text{paroi}} = 10\frac{6\bar{v}}{\beta^{(LRR)}(\Delta d_1)^2}$$

Where $(\Delta d_1)^2$ is the distance between the wall and the nearest point

2.8.2.4.RSM omega

the system of equations governed the turbulent compressible gas may be written as:

$$\frac{\partial\bar{\rho}}{\partial t} + \frac{\partial}{\partial x_j}\left(\bar{\rho}\tilde{U}_j\right) = 0 \qquad (2.87)$$

$$\frac{\partial\bar{\rho}\tilde{U}_j}{\partial t} + \frac{\partial}{\partial x_j}\left(\bar{\rho}\tilde{U}_i\tilde{U}_j + \bar{\rho}\widetilde{u_i''u_j''}\right) = \frac{\partial\overline{\sigma_{ij}}}{\partial x_j} - \frac{\partial\bar{p}}{\partial x_i} \qquad (2.88)$$

$$\frac{\partial\bar{\rho}\tilde{E}_l}{\partial t} + \frac{\partial\tilde{U}_i\left(\bar{\rho}\tilde{E}_l + \bar{P}\right)}{\partial x_j} = \frac{\partial}{\partial x_j}\left(\overline{\sigma_{lJ}U_l} - \bar{\rho}\overline{u_l''u_l''}\tilde{U}_l - \frac{1}{2}\bar{\rho}\tilde{u}_l''u_i''u_i''\right) - \frac{\partial}{\partial x_j}\left(\bar{\rho}\gamma c_v\overline{T''u_j''} - \overline{k_c\frac{\partial T}{\partial x_j}}\right) \qquad (2.89)$$

Where -$\bar{\rho}, \tilde{U}_j, \bar{P}$and $\tilde{E}_t$ are the density, velocity, the pressure, and the total energy respectively.

$$\bar{\rho}R_{ij} = -\overline{\rho u_l''u_j''} \qquad (2.90)$$

$$\frac{\partial \bar{\rho} R_{ij}}{\partial l} + \frac{\partial(\bar{\rho} u_k R_{ij})}{\partial x_k} = P_{ij} + \Pi_{ij} - \frac{2}{3}\beta^* f_\beta \cdot \bar{\rho}\omega k \delta_{ij} + \frac{\partial}{\partial x_k}\left[\left(\mu + \frac{\mu_i}{\sigma_k}\right)\frac{\partial R_{ij}}{\partial x_k}\right] \quad (2.91)$$

$$\frac{\partial \bar{\rho}\omega}{\partial t} + \frac{\partial(\bar{\rho} U_k(\omega)}{\partial x_k} = \frac{\alpha \bar{\rho}\omega}{k} R_{ij}\frac{\partial U_i}{\partial x_j} - \bar{\rho}\beta f_\beta \omega^2 + \frac{\partial}{\partial x_k}\left[\left(\mu + \frac{\mu_l}{\omega}\right)\frac{\partial \omega}{\partial x_k}\right] + \sigma_d \frac{\bar{\rho}}{\omega}\frac{\partial k}{\partial x_j}\frac{\partial \omega}{\partial x_j} \quad (2.92)$$

The pressure stain correlation is given by:

$$\Pi_{ij} = \beta^* f_\beta \cdot C_1 \bar{\rho}\omega\left(R_{ij} + \tfrac{2}{3}k\delta_{ij}\right) - \hat{\alpha}\left(P_{ij} - \tfrac{2}{3}P\delta_{ij}\right) - \hat{\beta}\left(D_{ij} - \tfrac{2}{3}P\delta_{ij}\right) - \hat{\gamma}\bar{\rho}k\left(S_{ij} - \tfrac{1}{3}S_{kk}\delta_{ij}\right) \quad (2.93)$$

The production tensor of Reynolds stresses is given by:

$$P_{ij} = -\overline{\rho u_i'' u_k''}\frac{\partial U_j}{\partial x_k} - \overline{\rho u_j'' u_k''}\frac{\partial U_i}{\partial x_k} \quad (2.94)$$

With $k = -R_{il}/2, \mu_l = \bar{\rho}k/\omega$ and $P = P_{kk}/2$the tensor D_{ij} differs in the dot-product indices from the production tensor

$$D_{ij} = -\overline{\rho u_i'' u_k''}\frac{\partial U_k}{\partial x_j} - \overline{\rho u_1'' u_k''}\frac{\partial U_k}{\partial x_i} \quad (2.95)$$

The closure coefficients of the model are:

$$\hat{\alpha} = (8 + C_2)/11, \hat{\beta} = (8C_2 - 2)/11, \hat{\gamma} = (60C_2 - 4)/55, C_1 = 9/5$$
$$, C_2 = 10/19, \alpha = 13/25, \beta = \beta_0 f_\beta, \beta^* = 9/100, \sigma_k = 2, \sigma = 5/3, \beta_0 = 0.0708$$
$$, \sigma_d = 0, \text{ for } \left(\frac{\partial k}{\partial x_j}\frac{\partial \omega}{\partial x_j} \le 0\right) \text{ and } \sigma_d = \frac{1}{8}, \text{ for } \left(\frac{\partial k}{\partial x_j}\frac{\partial \omega}{\partial x_j} > 0\right),$$
$$f_\beta = (1 + 70X_\omega)/(1 + 80X_\omega), X_\omega = \left|W_{ij}W_{jk}S_{ki}/(\beta^*\omega)^3\right|, \hat{S}_{ki} = S_{ki} - \frac{1}{2}\frac{\partial a_{mk}}{\partial x_{mk}}\delta_{ki}$$
$$, S_{ij} = \frac{1}{2}\left(\frac{\partial U_i}{\partial x_j} + \frac{\partial U_j}{\partial x_i}\right), W_{ij} = \frac{1}{2}\left(\frac{\partial u_i}{\partial x_j} - \frac{\partial u_j}{\partial x_i}\right), f_{\beta^*} = 1 \text{ if } x_k \le 0$$
$$\& f_{\beta^*} = (1 + 640x_k^2)/\left(1 + 400x_{k_k}^2\right) \text{ if } x_k > 0$$

In the standard $k-\omega$model, you also have the option of including corrections to improve the accuracy in predicting free shear flows. The Shear Flow Corrections option under the k-omega Options is enabled by default in the Viscous Model dialog box, as these corrections are included in the standard $k-\omega$ model. When this option is enabled, ANSYS FLUENT will calculate $f_{\beta}{}^{*}$using this equation (in the separate Theory Guide) and f_{β} using this equation (in the separate Theory Guide).If this option is disabled, $f_{\beta *}$and f_{β} will be set equal to one.

With equations x-k

$$x_k = \frac{1}{\mathrm{w}^3}\frac{\partial k}{\partial x_j}\frac{\partial \mathrm{w}}{\partial x_j} \qquad (2.96)$$

3.1.Introduction

The aim of this investigation is to provide new insights into the factors that affect heat transfer rates in regenerative cooled nozzles, specifically focusing on three known variables. The first factor considered is the effect of coolant mass flow rate, which has been shown to have a significant impact on how efficiently heat can be transferred from the nozzle walls to the coolant.

Secondly, we examine how using liquid hydrogen as a coolant instead of water affects thermal performance. Liquid hydrogen offers several advantages over conventional coolants like water due to its high heat capacity and low density, making it an attractive option for use in rocket propulsion systems.

Finally, we investigate how decreasing the nozzle wall thickness impacts cooling processes within regenerative-cooled nozzles. This variable is essential since thicker walls can lead to increased surface areas over which heat energy must be dissipated effectively while thinner ones may pose structural integrity challenges under harsh operational conditions.

Our study aims to provide conclusive evidence regarding optimal design principles by investigating these three critical factors' influence independently and together simultaneously. We use computational simulations based on ANSYS Fluent software capable of simulating conjugate convection-conduction problems accurately across gas-liquid-solid regions within one domain distinguished by their specific properties such as turbulence models (RANS).

We believe our findings will contribute significantly towards developing better designs for rocket propulsion systems based on improved understanding of conjugate heat transfer mechanisms present within them when considering different combinations or variations involving any or all these variables mentioned above.

In this study, we focus on analyzing the thermal behavior of JPL (Jet Propulsion Laboratory) nozzle designed by NASA. Figure 3.1 presents the dimensions of the nozzle contour obtained using a MATLAB program capable of generating 2-D axisymmetric models.

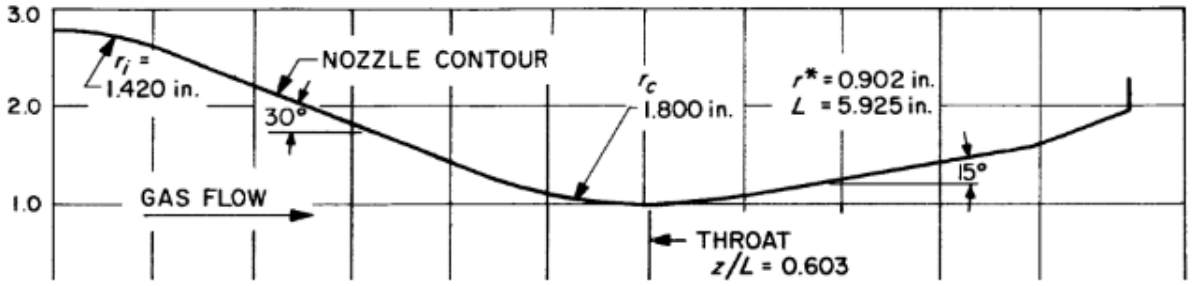

Figure 3.1: Nozzle dimensions diagram

We choose ANSYS Fluent software for our study because it's excellent in simulating fluid dynamics (CFD) and finite volume analysis (FVA). It provides accurate predictions within a short time frame. We found that ANSYS Fluent is an excellent computer-aided engineering tool for simulating the flow of hot gases through the walls of rocket nozzles.

ANSYS Fluent has four essential parts: Workbench, Design Modeler CFD software, ANSYS Meshing, and Solver. These components work together to provide us with reliable results while also adhering to computational constraints.

Nozzle Geometry

To generate a 2-D axisymmetric model of the JPL nozzle, we used MATLAB software to create the contour and uploaded it into ANSYS Design Modeler. **Figure 3.1** shows this contour.

We then added three distinct zones within the model for hot gases, nozzle wall, and coolant using ANSYS Design Modeler CFD software to create the geometry of the conjugate heat transfer processes across gas-liquid-solid regions within one domain. Additionally, we incorporated an inlet length of 18 inches into our model to match the experimental setup of Back et al., which helps us compare our numerical results with previously published data. The final geometry obtained is presented in figure 3.2 with 7 mm thickness wall and in figure 3.3 for 1.6 mm.

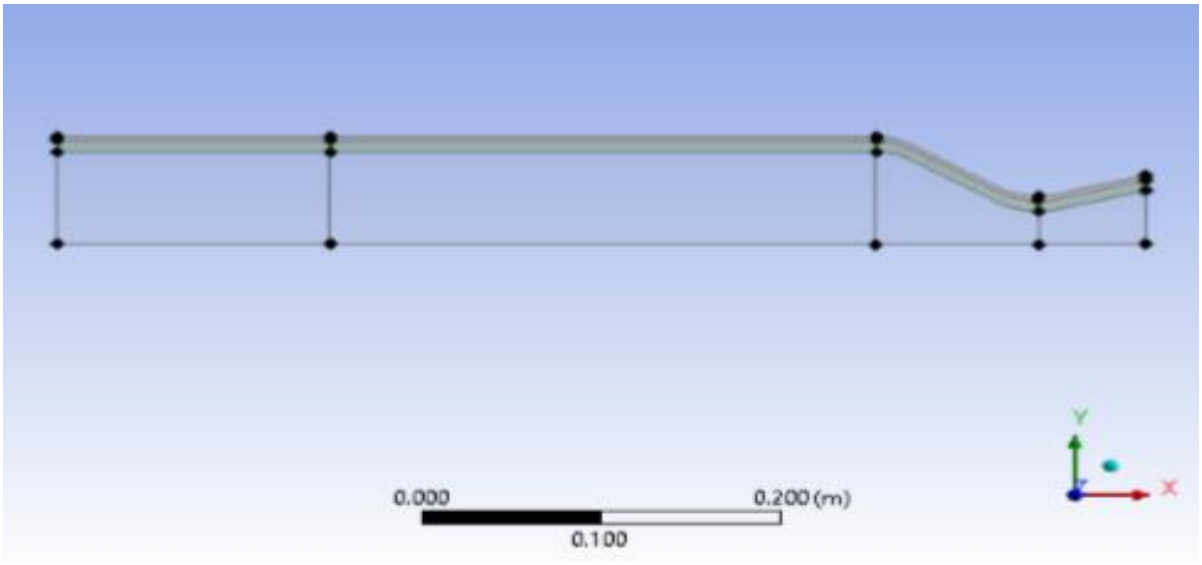

Figure.3.2 : Nozzle geometry **(7-3) mm**

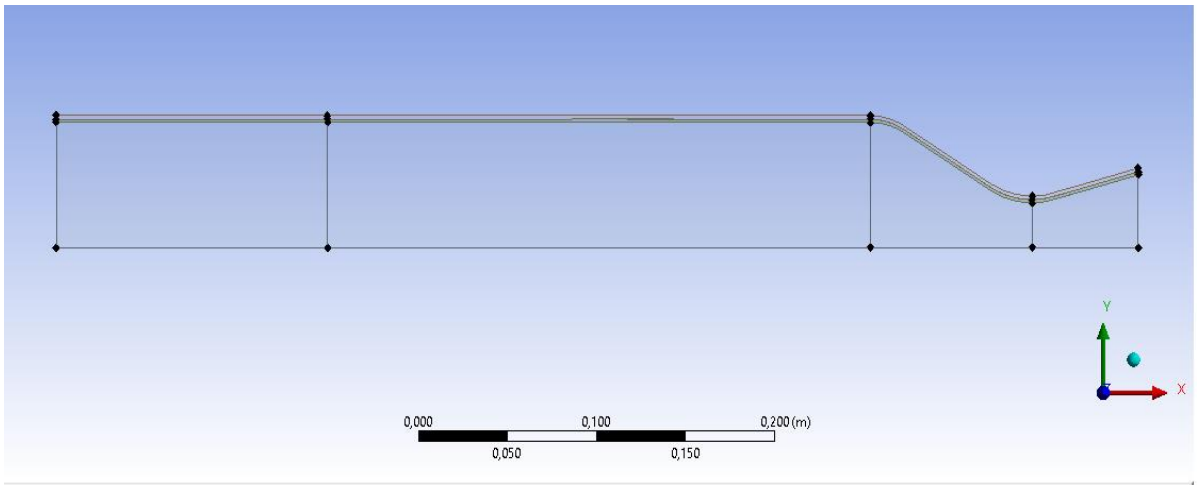

Figure.3.3 : Nozzle geometry **(1.9-1.6) mm**

Grid meshing

The mesh is one of the most crucial factors affecting our simulation's accuracy. We select a suitable turbulence model for the simulation before deciding on the mesh because we need to resolve all boundary layers accurately.

To ensure that our numerical simulations are accurate and mesh-independent, we employed an extended grid refinement strategy for the studied nozzle presented in **Figure 1**. We maintained a fine mesh throughout simulation after ensuring negligible changes between subsequent mesh refinement steps.

We also resolved the laminar viscous sublayer by keeping the maximum non-dimensional wall distance (y+) of the first point near the wall equal to about 0.25, which is sufficiently smaller than 1. This approach allowed us to capture small-scale details within gas-liquid-solid regions accurately.

The resulting model contained approximately 115,000 nodes with grid resolutions. The use of appropriate grid resolution further ensures that all critical features within gas-liquid-solid regions were captured while minimizing computational errors.

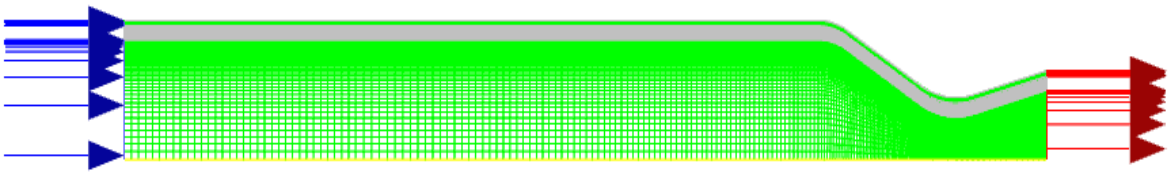

Figure.3.4 : Nozzle mesh **(7-3) mm**

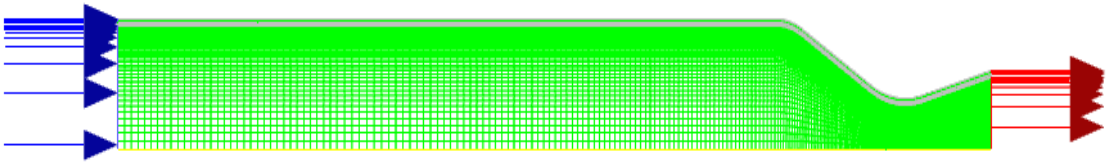

Figure.3.5 : Nozzle mesh **(1.9-1.6) mm**

Numerical method

To solve the axisymmetric flows in this study, we employed a parallel finite volume discretization based on full Favre averaging Naiver-Stokes equations using RSM-ω with Free Shear Corrections (SFC). The simulations were processed using ANSYS Fluent CFD software.

We used second-order upwind schemes with double precision accuracy for convective terms and second-order methods for pressure terms. We solved the steady time-averaged Navier-Stokes equations within fluid zones while achieving pressure-velocity coupling using a SIMPLE pressure correction algorithm.

In solid zones, only Fourier's equation for heat diffusion was solved. At fluid-solid interfaces, an energy balance condition was satisfied at each iteration such that heat fluxes on both sides of the

wall had equal magnitudes but opposite signs. During each iteration, we adjusted the boundary temperature to satisfy this condition.

Our solutions converged to normalized residual mean square values of 10^{-5} or lower during simulations.

3.2. Thermo physical properties

Properties play a crucial role in accurately simulating fluid dynamics and heat transfer within the rocket engine and cooling process. Constant values of physical properties may sometimes lead to erroneous results or deviate from the exact solution. Therefore, it is preferable to use functions that vary based on temperature or another relevant variable to achieve convergence towards the exact solution.

In this research, all properties were obtained from the NASA NIST (National Institute of Standards and Technology) database website: https://webbook.nist.gov/chemistry/fluid/.

The NASA NIST database provides comprehensive and reliable information on the thermos physical properties of various fluids. By using this database, the researchers ensured that the properties used in the simulations were accurate and accounted for any variations based on temperature or other relevant factors. This approach contributes to achieving a more precise and reliable prediction of the fluid dynamics and heat transfer phenomena within the rocket nozzle and cooling channels.

3.2.1-Water properties

The properties of water are given for pressure P = 69 bar, the vaporization temperature for this pressure is Tv = 577.90 K.

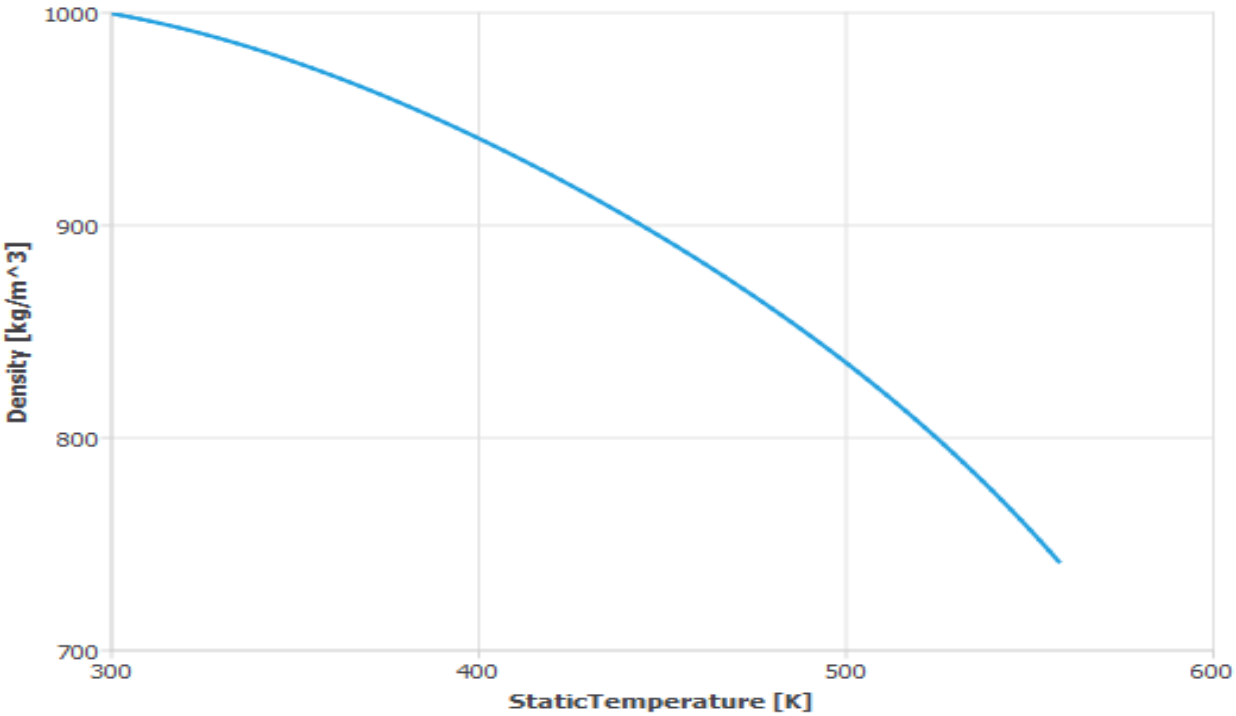

Figure.3.6: water density

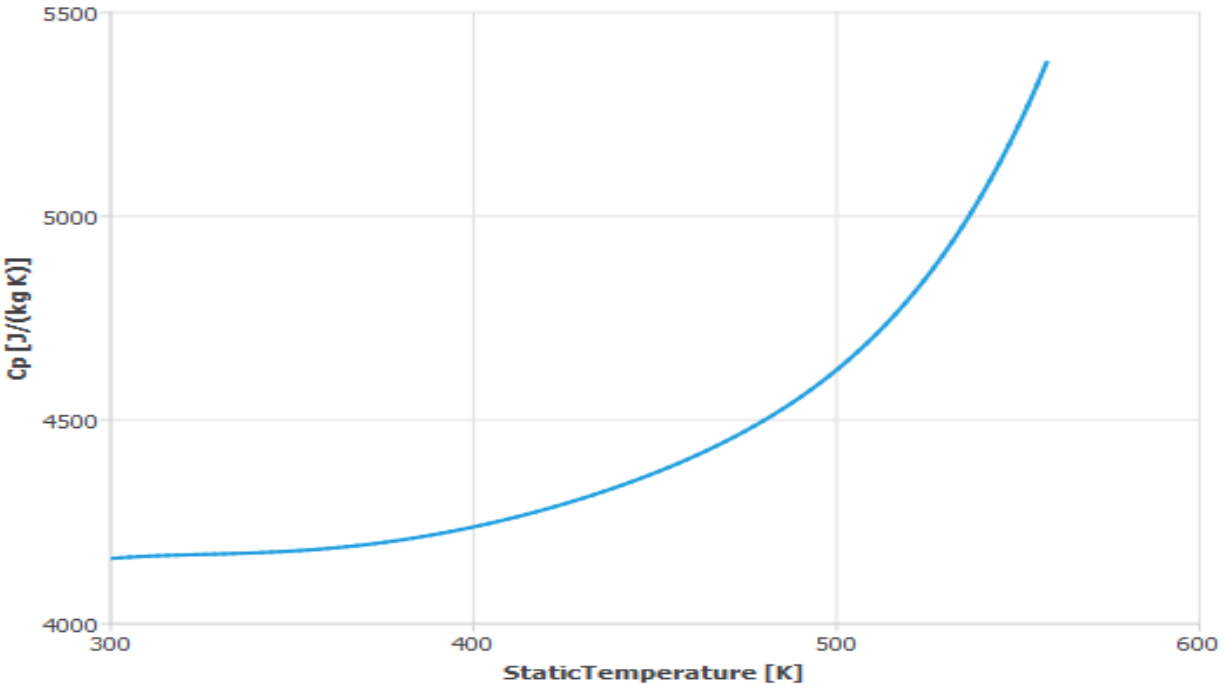

Figure.3.7： water specific heat

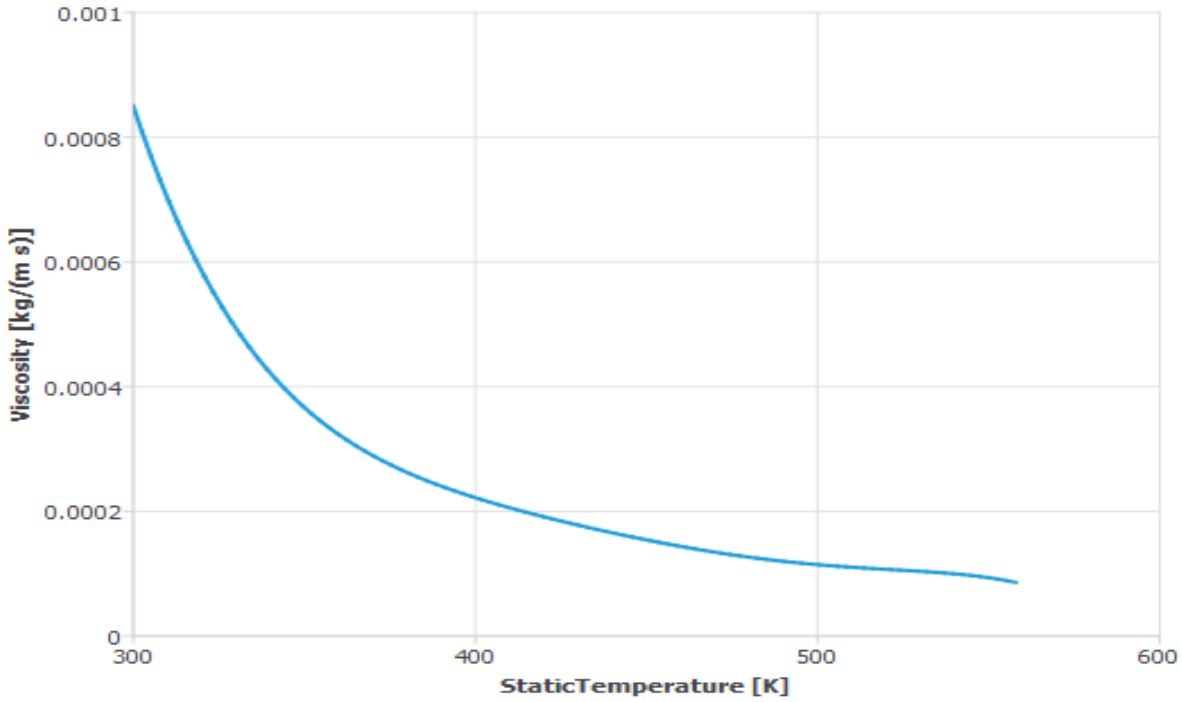

Figure.3.8：water viscosity

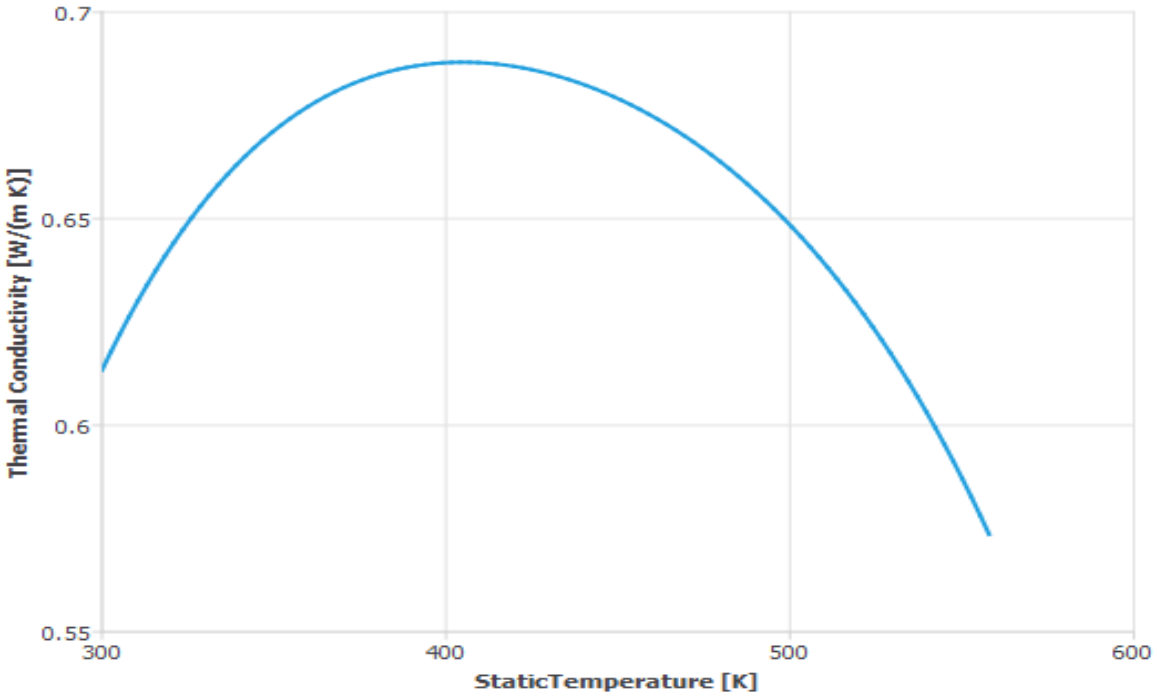

Figure.3.9：water thermal conductivity

3.2.2. Liquid hydrogen properties (LH2)

The coolant used in this simulation is liquid-hydrogen (LH2) that cools the rocket engine by passing through channels attached to the engine structure entering from the chamber at different total pressure and temperature; the properties are given by :

Chemical formula: (h2. l)

Density constant = 70.85 **[Kg/m3]**

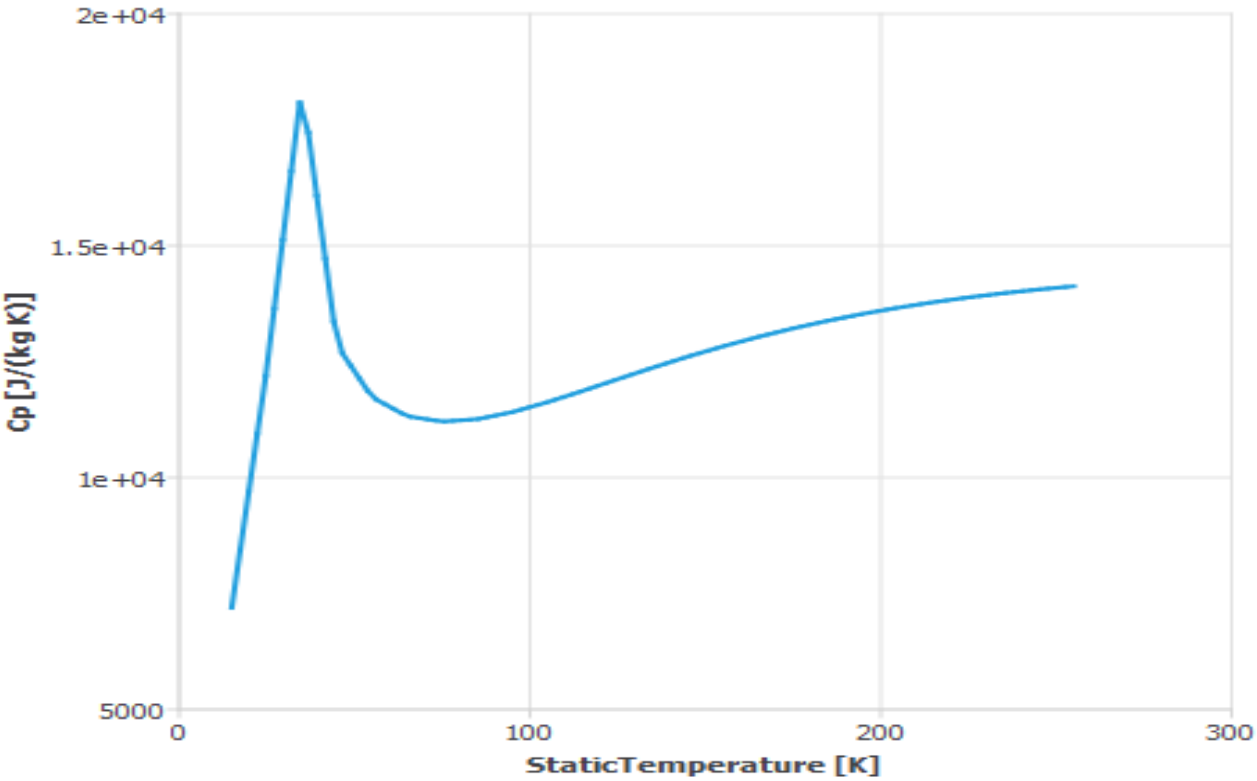

Figure.3.10 : hydrogen specific heat

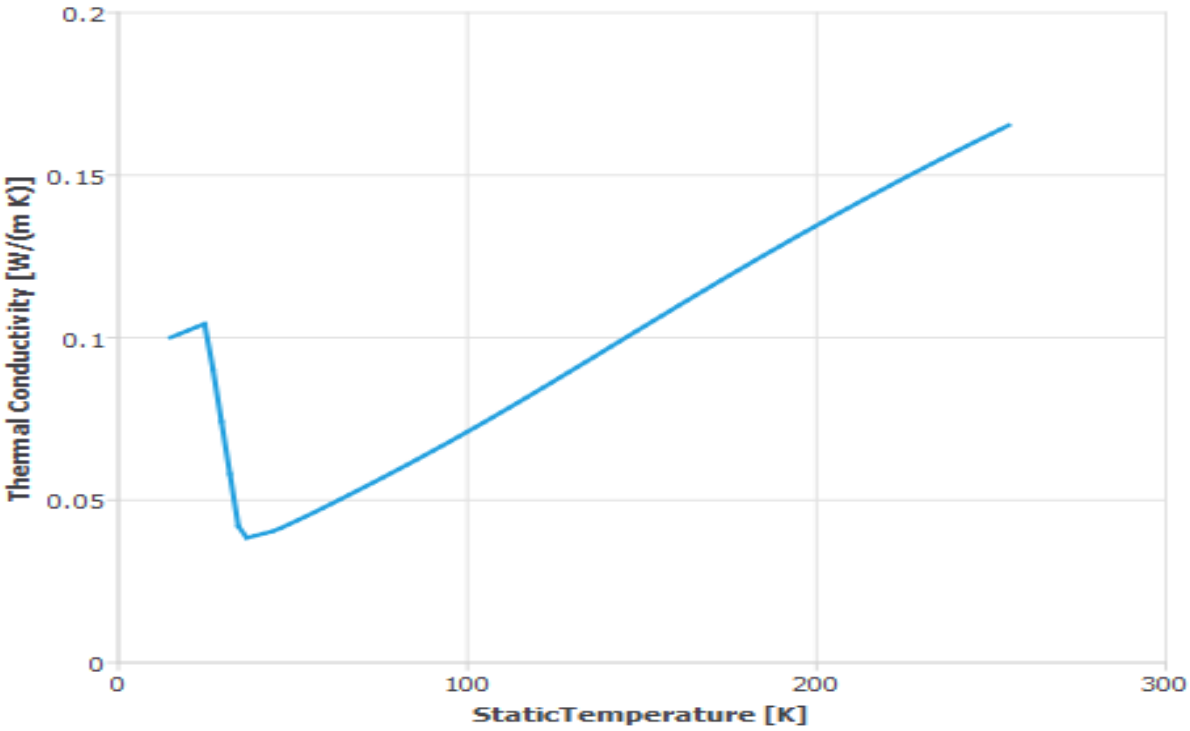

Figure.3.12：hydrogen viscosity

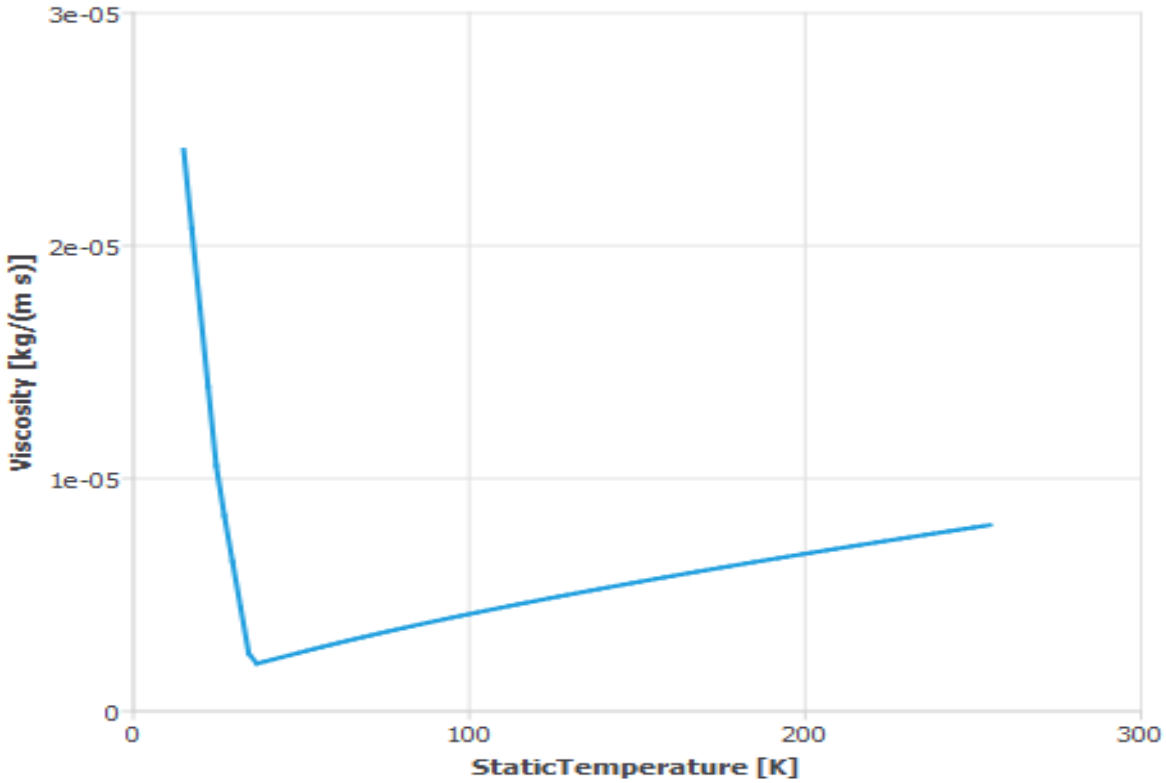

Figure.3.11：hydrogen thermal conductivity

3.2.3. Air properties

In rocket propulsion systems, hot gases (Air in this study) enter the nozzle through the combustion chamber at extremely high temperatures that can reach up to 3500 K. The gas also enters the nozzle under high pressure of approximately 100 bar.

The extreme conditions in which these hot gases flow make designing efficient cooling strategies essential for maintaining structural integrity and preventing burn-through during operation. Regenerative cooling technology is one such example where coolant circulates within the nozzle walls and absorbs heat generated by the combustion process.

Density**[Kg/m3]:** idealgas

Molecular weight M=28.96**[g/mol]**

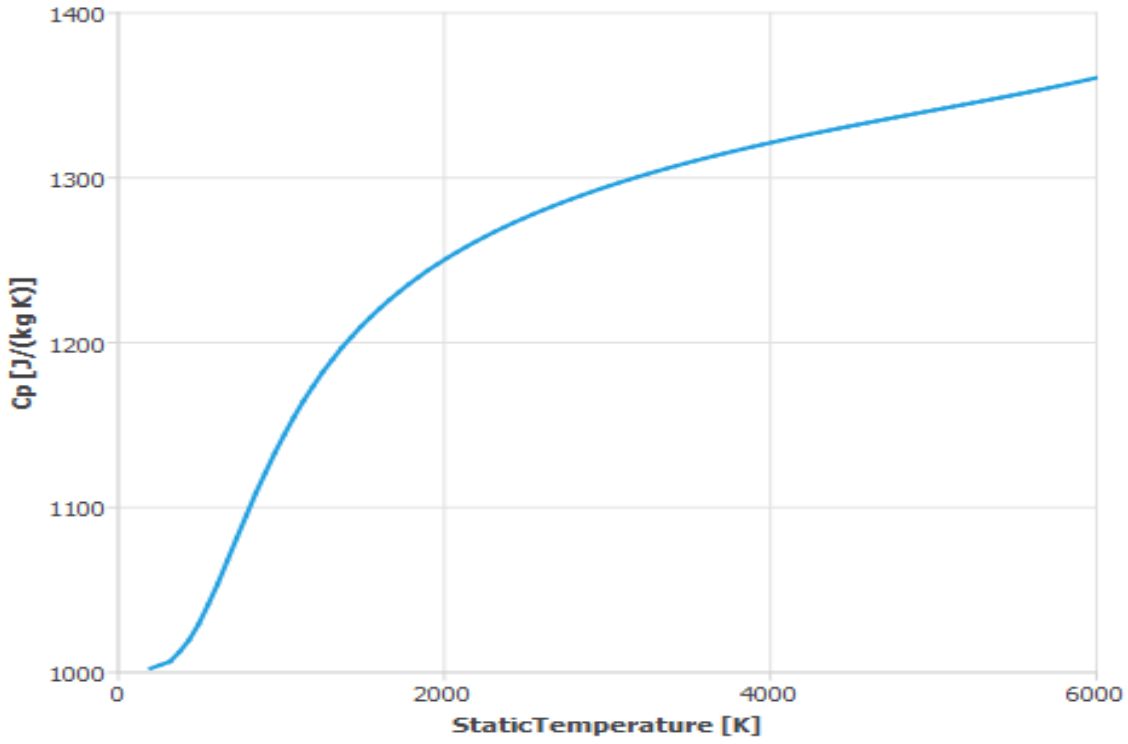

Figure.3.13 : air specific heat

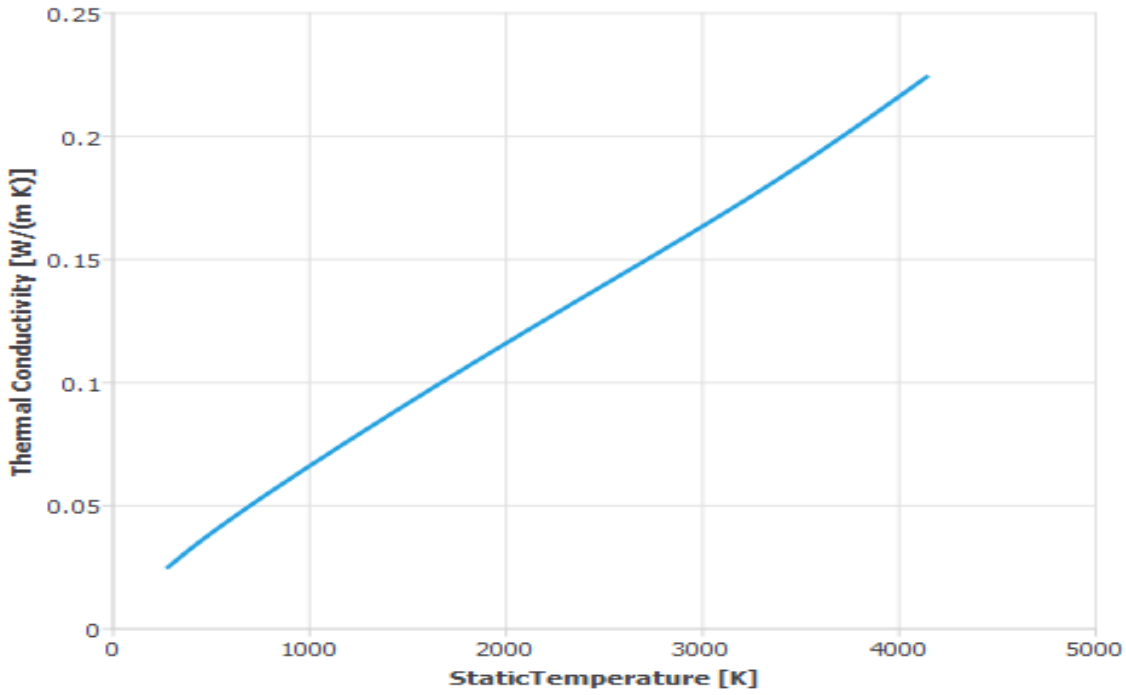

Figure.3.14：air thermal conductivity

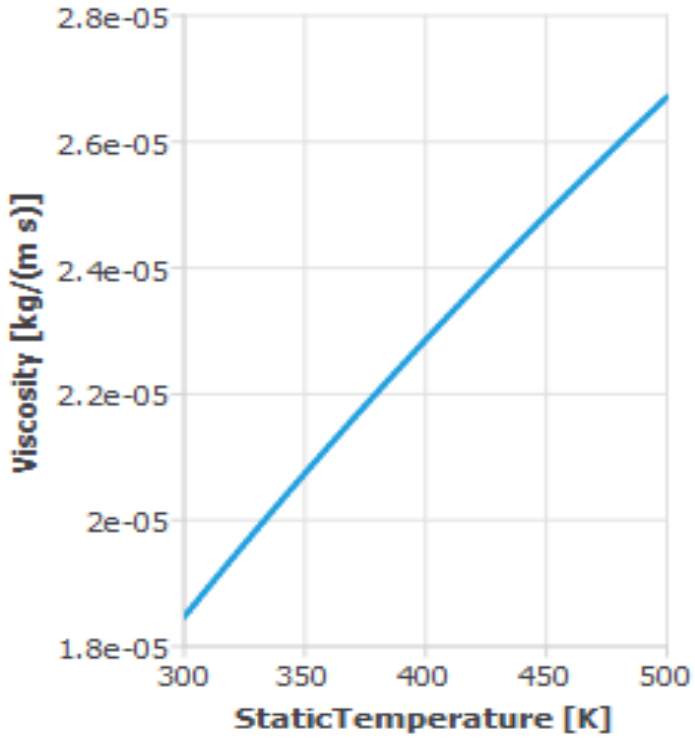

Figure.3.15：air viscosity

3.2.4. Copper Properits

In our study, we chose copper metal for constructing the nozzle and combustion chamber due to its superior thermal conductivity compared to other metals. Copper's high thermal conductivity enables efficient cooling of the rocket engine, preventing it from melting under extreme operational conditions.

By selecting appropriate materials like copper with desirable properties that facilitate heat transfer mechanisms, we can develop better designs for rocket propulsion systems based on improved understanding of conjugate heat transfer mechanisms present within them while optimizing thermal management strategies under varying conditions involving different variables like coolant type, mass flow rate, wall thicknesses etc., as presented earlier in this investigation.

Density ρ= 8978 **[Kg/m3],**

Specific Heat Cp = 381 **[J/Kg.k]**

Melting point temperature= 1358 **K**.

thermal conductivity = 387.6**[w/ (m.k)]**

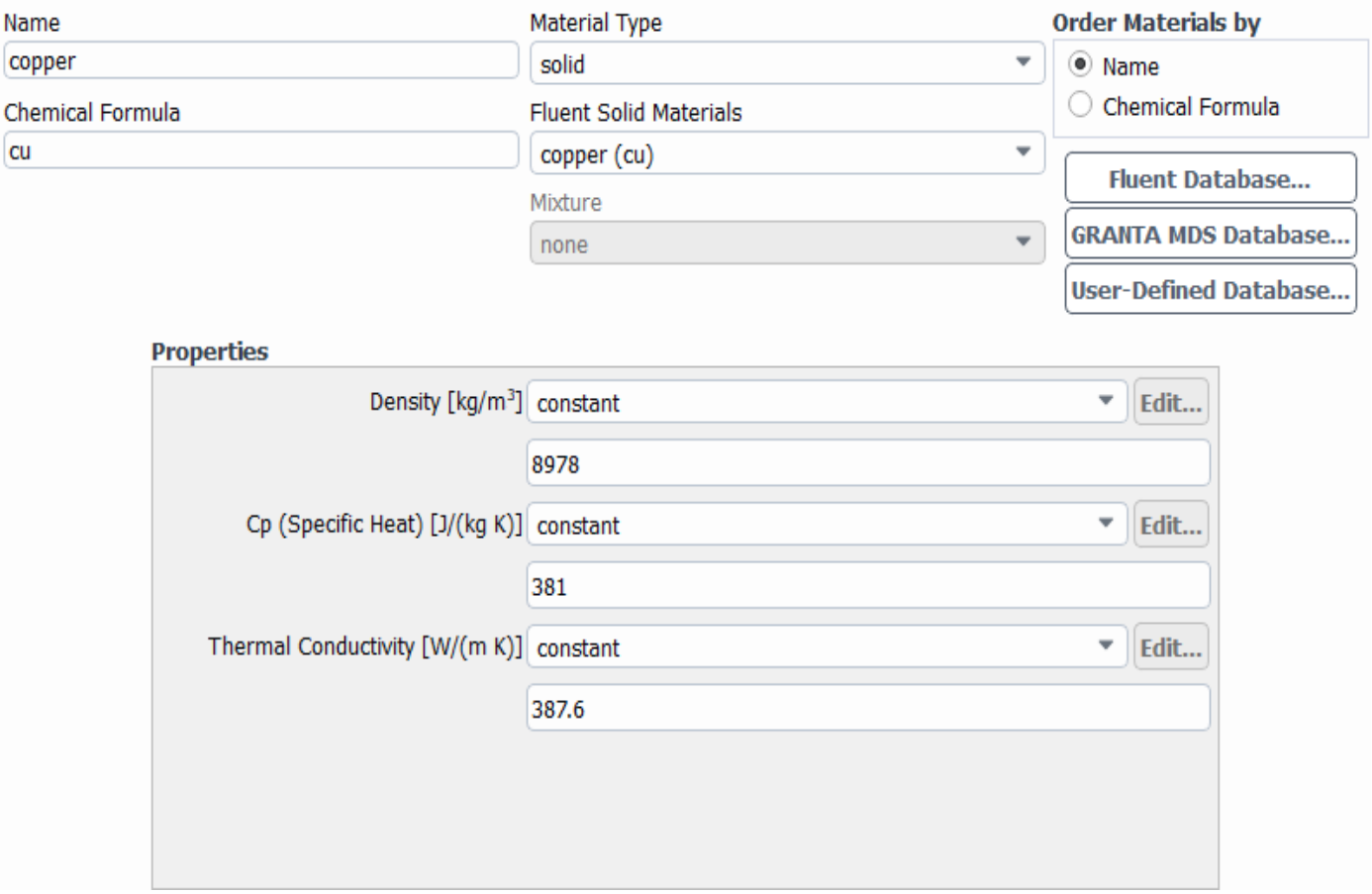

Figure.3.16 : Properits copper

3.3. Cases studied

In our study, we focus on investigating three cases for cooling the rocket engine using regenerative cooling technology. These cases are as follows:

3.3.1. The effect of changing the coolant

To compare the cooling efficiency of different coolants, we chose two types of coolant: liquid hydrogen and water. We studied their effectiveness in cooling a rocket engine under the aforementioned conditions using regenerative cooling technology.

By analyzing how these two coolants perform under varying conditions involving different variables like mass flow rate, wall thicknesses etc., we can provide valuable insights into optimizing thermal management strategies for rocket propulsion systems based on improved understanding of conjugate heat transfer mechanisms present within them while accounting for different factors that affect thermal performance during operation.

The temperature, pressure and mass flow of the inlet of the coolant channel **(hydrogen-liquid)** were specified to be 30 K, 10 bar and 14.234 kg/s respectively.

The temperature, pressure and mass flow of the inlet of the coolant channel **(water)** were specified to be 300 K, 69 bar and 14.234 kg/s respectively

,For the gas**, (air)** 3500k, 100 bar respectively.

Also thickness copper metal **7** (mm) and thickness channels hydrogen and water **3** (mm)

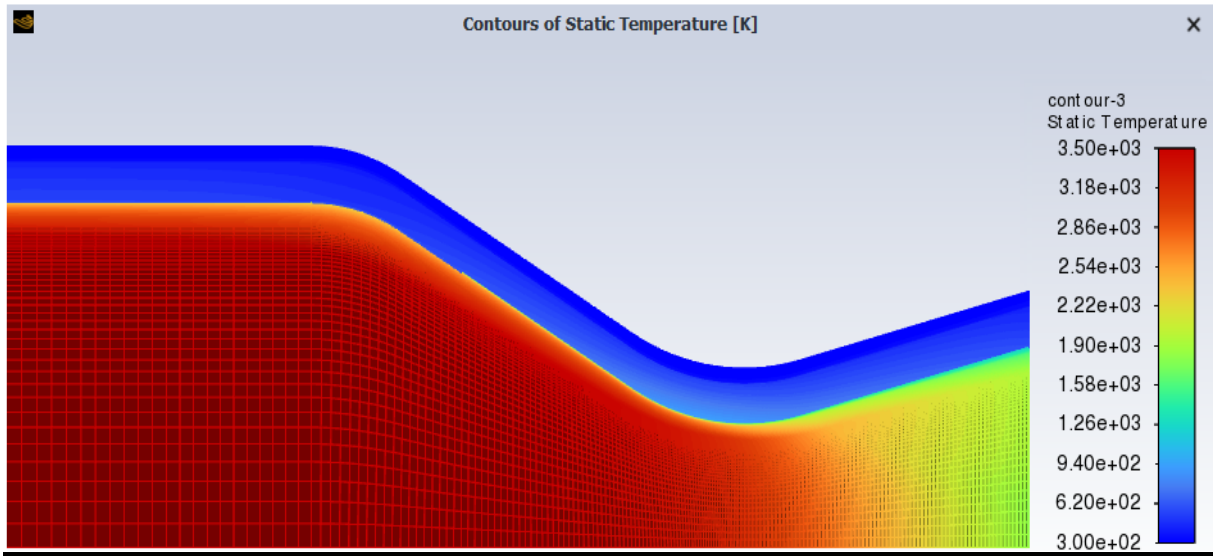

Figure.3.17 :**:** Static temperature contour with water coolant

We recognize that rocket engines operate at high efficiencies, resulting in extremely high temperatures. To better understand the effectiveness of cooling systems under these conditions, we conducted simulations on a rocket engine using two different coolants: water and liquid hydrogen.

Figures 17 and 18 present temperature distributions for water and LH2 respectively within various parts of the nozzle.

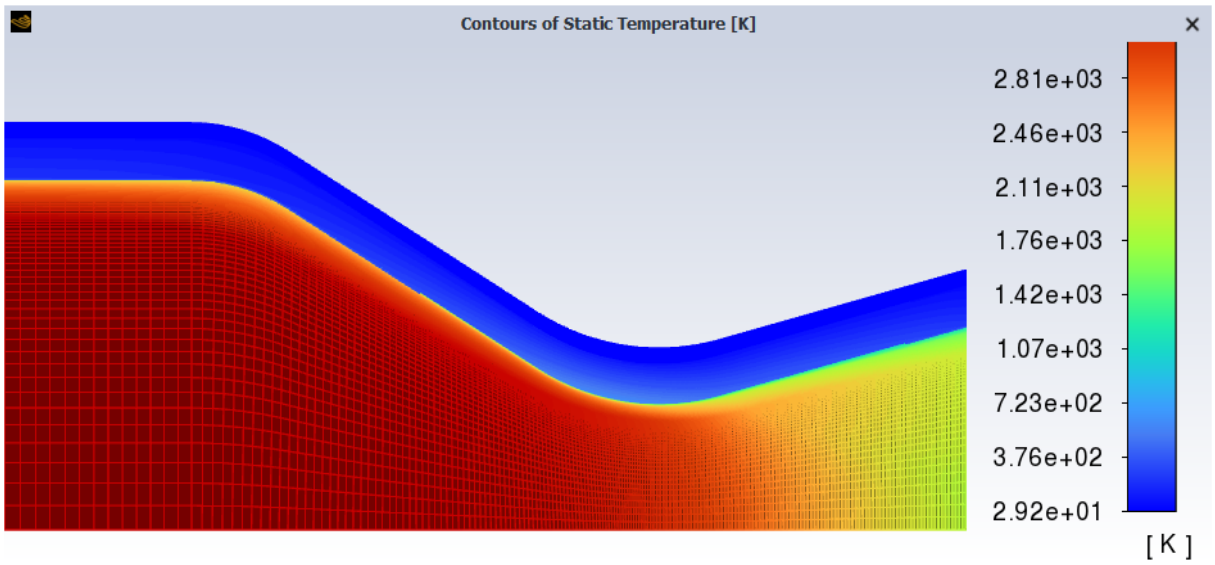

Figure.3.18 **::** Static temperature contour with hydrogen coolant

The simulation results presented in **Figures 17 and 18** show that red and blue colors represent hot and cold zones, respectively. In general, we observe more blue color in the case where LH2 coolant is used compared to water coolant, indicating higher cooling efficiency. Further details of these temperature distributions will be presented later in other figures

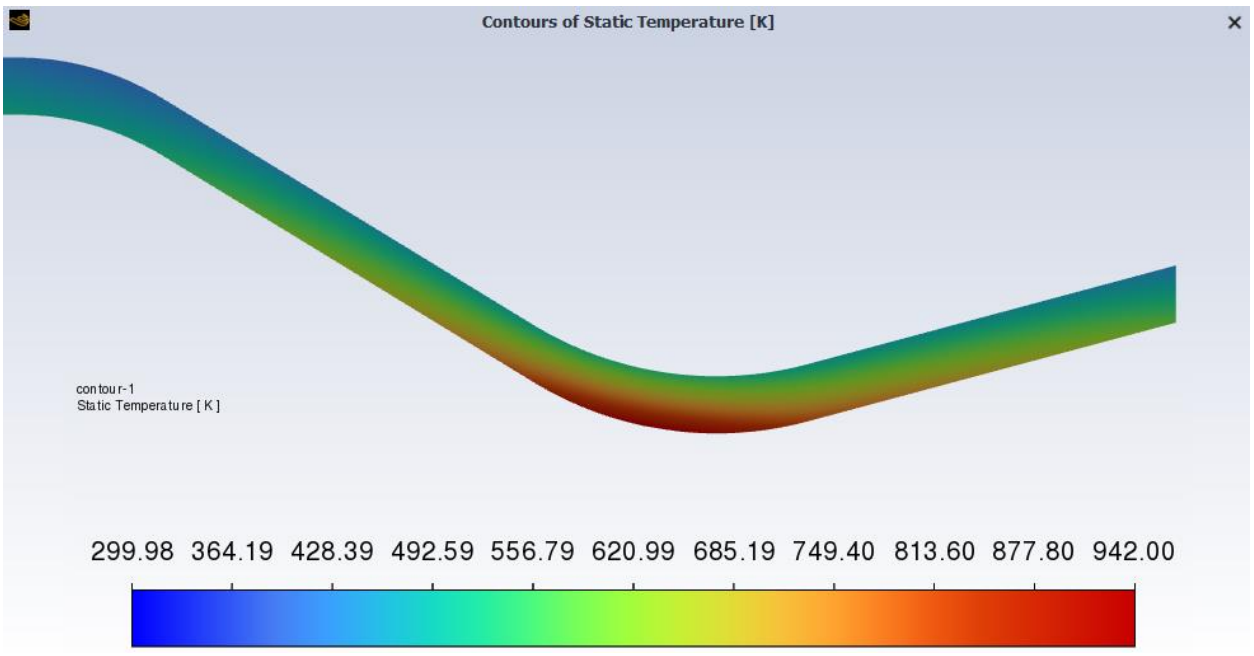

Figure.3.19: Static temperature contour in the of wall of nozzle and water

Despite conducting simulations with equal conditions for the two cases, we noticed the difference in temperature is due to the difference in the coolant and its properties. For hydrogen, its

temperature now it enters the cooling channels is 30 K, which is very cold, unlike water, whose temperature is 300 K, and this is a huge difference.

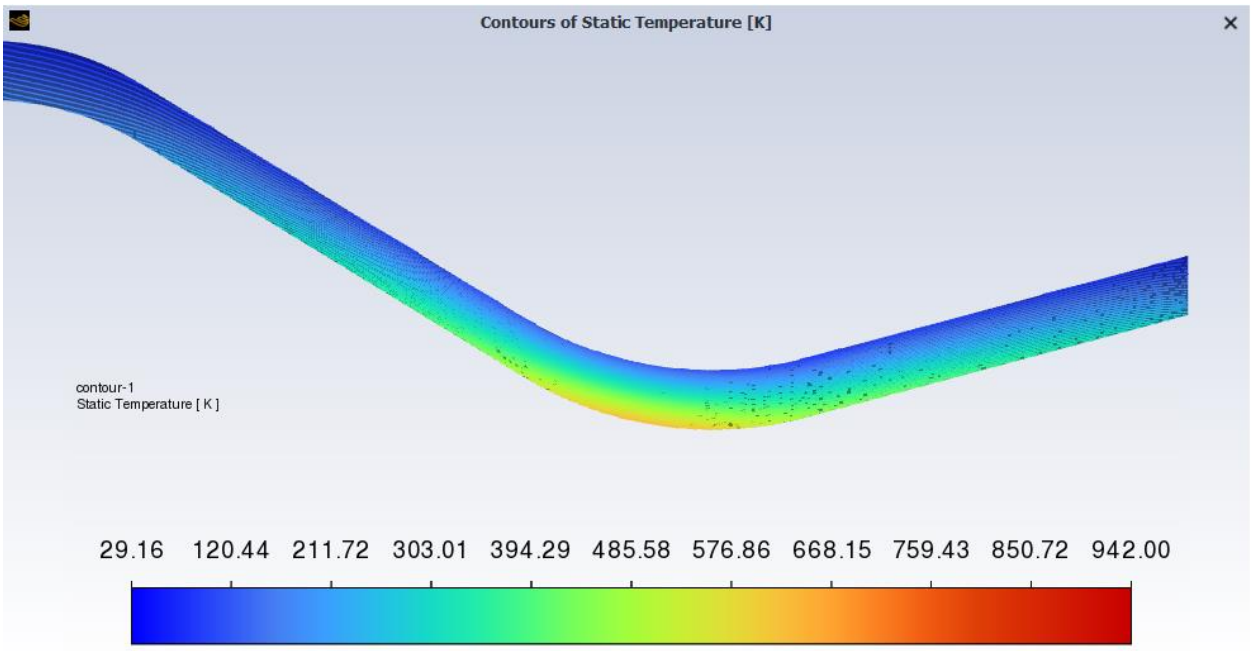

Figure.3.20: Static temperature contour in the of wall of nozzle and hydrogen

The trend of higher cooling efficiency with LH2 coolant is even more evident when comparing the temperature distributions in the solid zone of the wall nozzle. **Figure 19** shows the temperature contour for water coolant, while **Figure 20** shows the temperature contour for LH2 coolant.

By analyzing these figures, we can observe that LH2 provides better cooling efficiency than water. This conclusion aligns with our earlier observations and demonstrates how different variables like coolant type affect thermal balances.

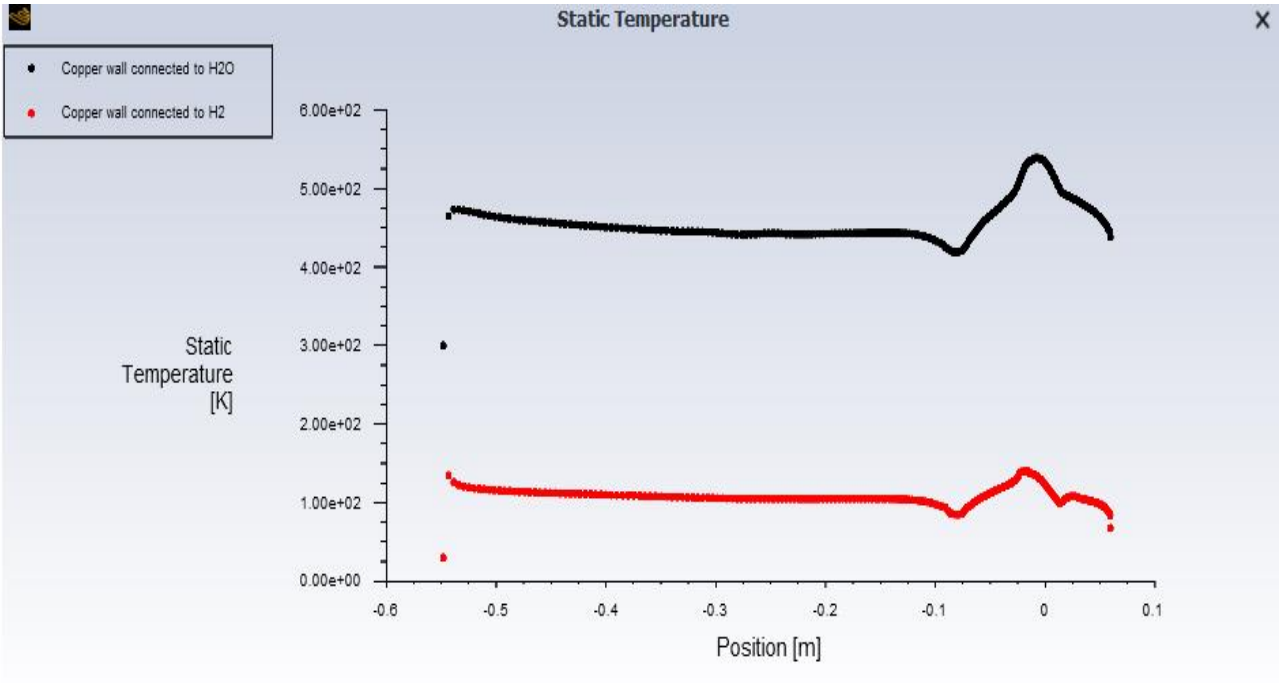

Figure.3.21: Comparison of coolant-side wall temperature of water and hydrogen coolant (H_2O.H_2)

Figure 21 presents an axial distribution of temperature for coolant-side walls that come into direct contact with the coolant, specifically Wall 1. The red curve represents the surface in contact with LH2, whose initial temperature at entry is 30 K.

We observe a significant increase in surface temperature up to a maximum of around 150 K due to heat exchange between the coolant and exhaust gas within copper metal. Copper's high thermal conductivity facilitates efficient heat transfer mechanisms during this process.

On the other hand, the black curve in **Figure 21** represents the surface in contact with water coolant. We observe that the temperature of this surface rises significantly at the entry to around 468 K compared to 300 K of initial water coolant temperature.

This increase can be attributed to heat exchange on copper's surface level, which results in further temperature rise up to a peak value of around 550 K just upstream the throat position (X= 0) before gradually decreasing until reaching approximately 453 K in the supersonic region.

After analysis and study, we discovered a temperature drop of about 73 % between the maximum temperatures in the coolant side.

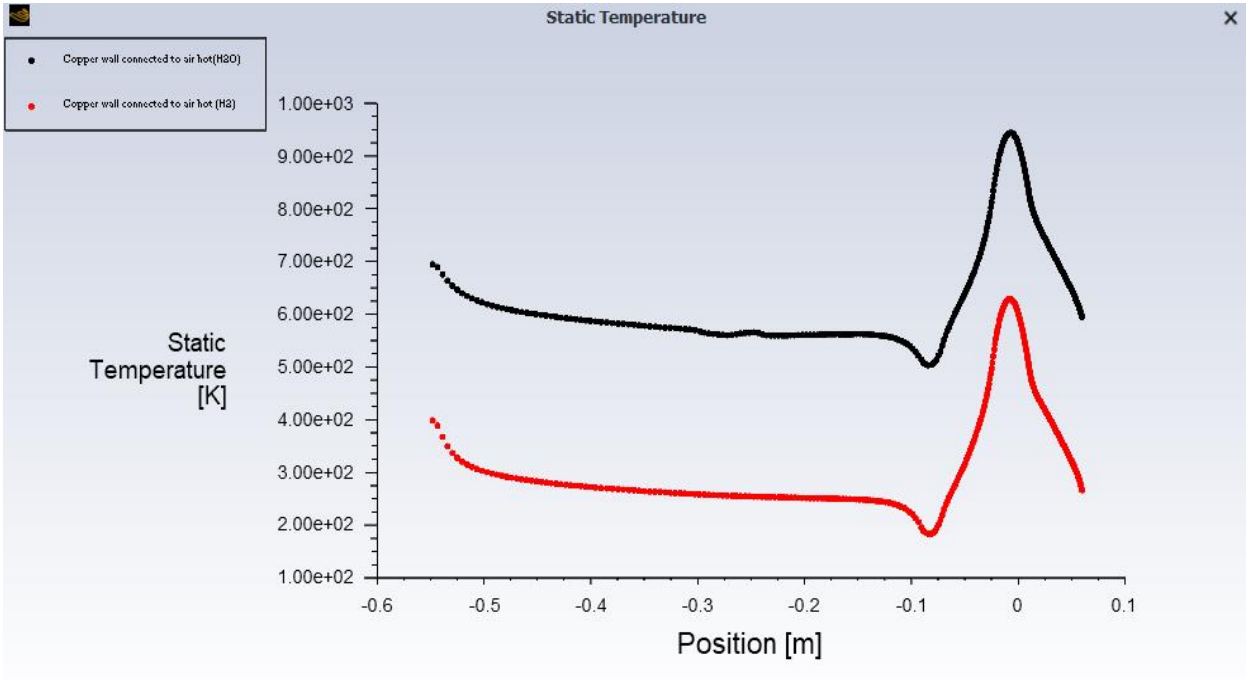

Figure.3.22: Comparison of gas-side wall temperature of water and hydrogen coolant (H_2O.H_2)

Figure 22 represents the axial development of the wall temperature in the gas side of the nozzle. The black curve represents the water coolant, while the red curve corresponds to liquid hydrogen. In fact, this wall-side is considered to be hotter as it is directly connected to the hot gas. Additionally, it is crucial for the maximum temperature on this side to remain low enough so that it does not exceed the melting point of the nozzle wall.

The direct comparison of the two curves reveals that at the nozzle entrance, air is considered as the hot gas with a stagnation temperature of 3500 K and a stagnation pressure of 100 bar. The temperature of the water at the inlet was found to be 700 K, while for liquid hydrogen it is just 400 K. The maximum wall temperature typically occurs just upstream of the throat due to maximum mass flux (ρu). In our findings, this temperature is 947 K for water, which is below the melting point of copper (about 1350 K), and in case with liquid hydrogen coolant, it's observed to be at around 647 K.

The difference in the decrease of wall temperature is approximately 32%, which highlights the efficiency of LH2 compared to water. This increased efficiency can be attributed to the high heat capacity and low density of LH2, resulting in a higher coolant velocity under similar conditions of P0, T0, and mass flow rate.

When using LH2 as a coolant, the heat flux is significantly higher than with water. This elevated heat transfer rate leads to a lower wall temperature for the LH2 case due to its high specific heat

compared to water. Consequently, maximum heat transfer is influenced by both the velocity and specific heat of the coolant.

In summary, liquid hydrogen (LH2) is a more efficient coolant than water due to its high heat capacity and low density, resulting in higher coolant velocities and lower wall temperatures under similar conditions.

3.3.2. The effect of coolant mass flow rate

In this section, we aim to examine the effect of varying the mass flow rate of coolant for both water and LH2. To achieve this, all other conditions will be kept constant except for the mass flow rate of the coolant.

In the case of water coolant, which has an inlet temperature of 300 K and a pressure of 69 bar, alongside the stagnation conditions (P0=100 bar and T0=3500 K), the mass flow rates of water tested for this scenario are 14.234 kg/s and 3 kg/s.

The thickness of copper metal is **7** (mm) and thickness of coolant channel is **3** (mm)

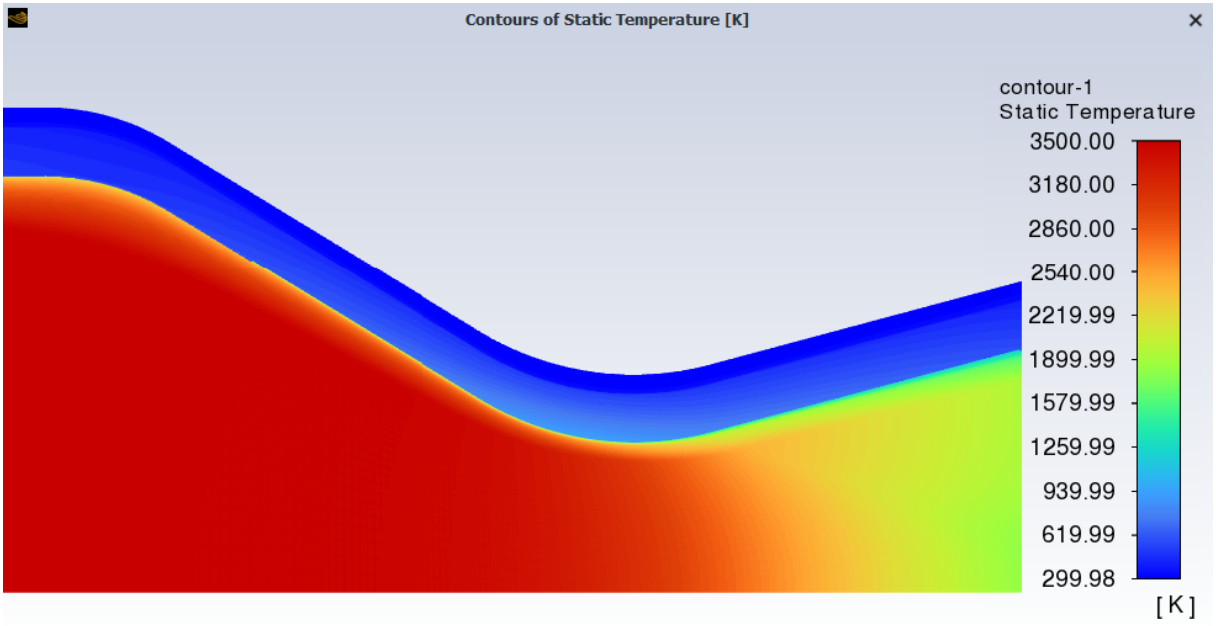

Figure.3.23: temperature contour of water and air exhaust. **14.234kg/s**

The contour of temperature is shown in **Figure 23**. The gas-side temperature ranges from 3500 K to 941 K, and the coolant-side temperature vary from 300 K to 524 K

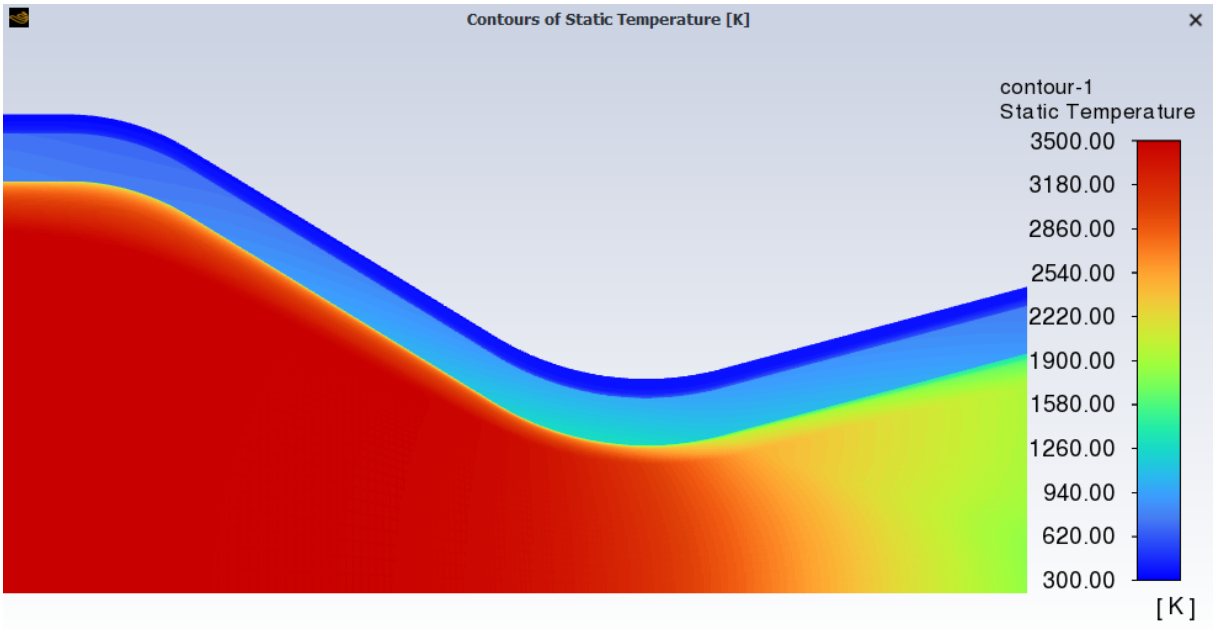

Figure.3.24: temperature contour with water coolant and m = **3 kg/s**

Figure 3.24 represents the temperature contour in the case with a water coolant mass flow rate of approximately 3 kg/s. In this scenario, the maximum temperature is located just upstream of the throat at around 1298 K, which is close to the melting point of copper metal. The coolant side temperature increases to 986 K, leading to vaporization of water and rendering it unable to cool the process efficiently. Under these conditions, nozzle survival becomes uncertain.

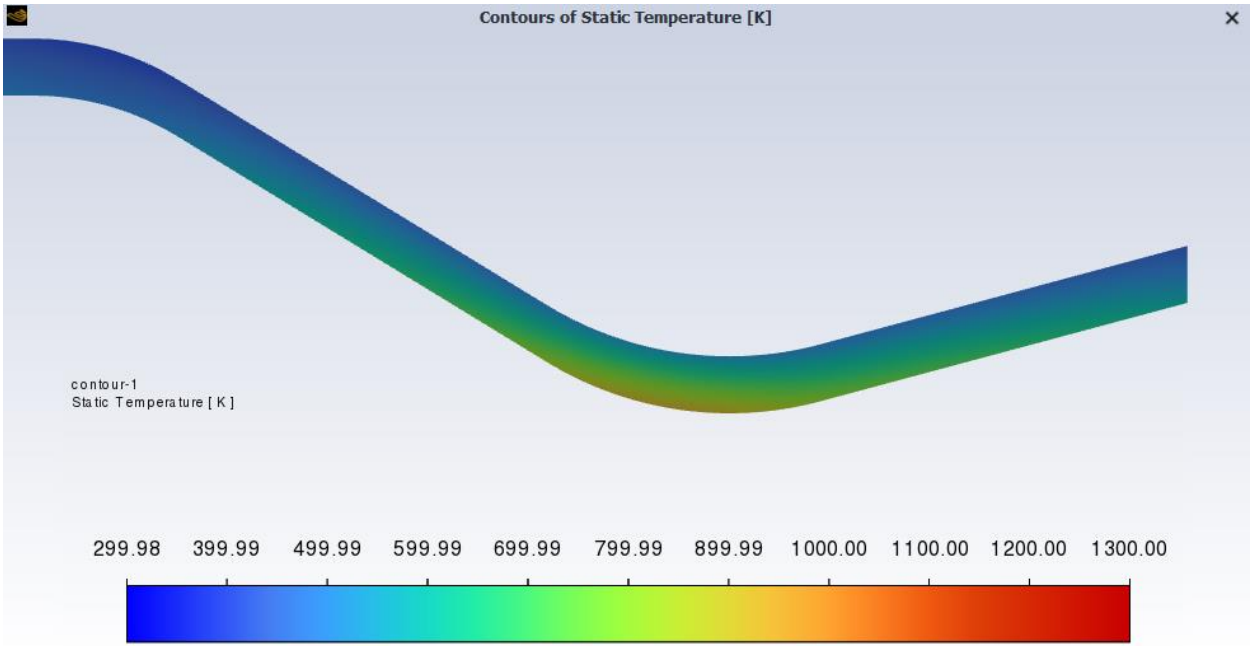

Figure.3.25: Static temperature contour in the of wall nozzle and water coolant .**14.234 kg/s**

Thus, we can conclude that determining an appropriate mass flow rate for coolant is a crucial factor requiring careful consideration. Each cooling configuration has a minimum coolant mass flow rate necessary for efficient operation and preventing damage to components such as nozzles.

This result is best illustrated in **Figures 25 and 26**, which display the temperature contour solely on the nozzle wall for each case. We can observe that in Figure 26, with a mass flow rate of 3 kg/s, the cooler appears more red compared to Figure 25 (m =14.2 kg/s) when using the same scale. This indicates higher temperatures at lower coolant mass flow rates, emphasizing the importance of selecting an appropriate mass flow rate for efficient cooling performance.

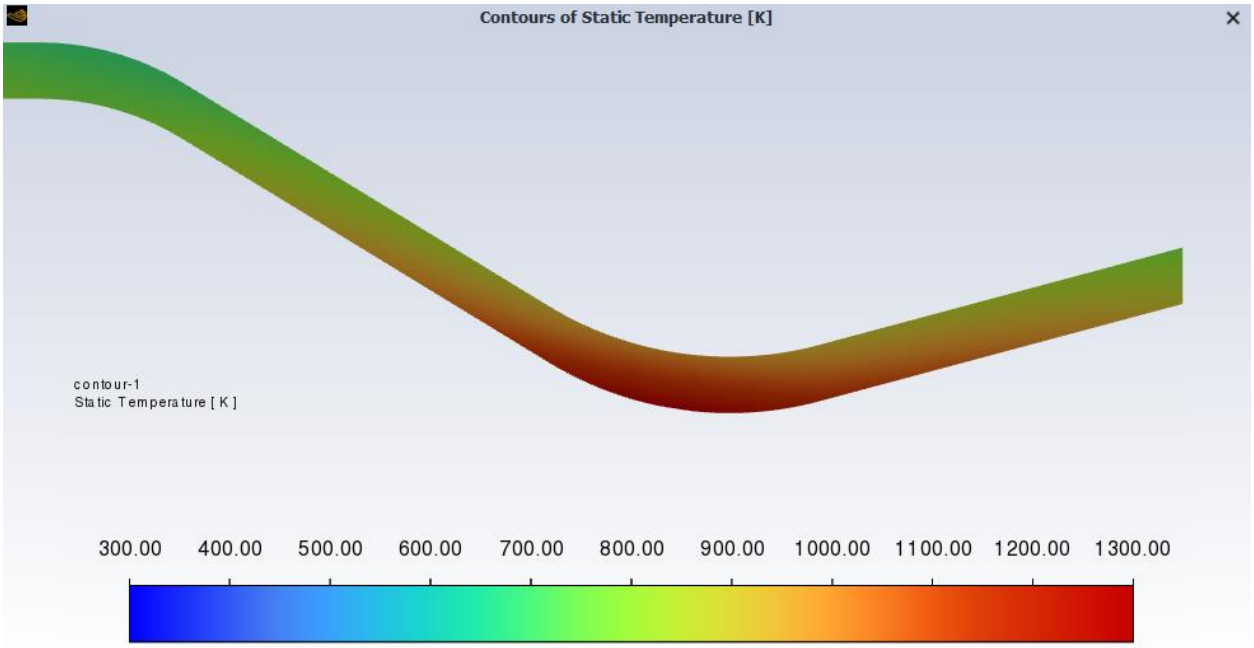

Figure.3.26: Static temperature contour in the of wall of nozzle and water .**3 kg/s**

We will go into the study by analyzing the curves and the conclusion :

Figure 3.27 compares the axial distribution of wall temperature on the coolant side, where water is used as the coolant with two mass flow rates - 3 kg/s and 14.234 kg/s. The maximum temperature, which is consistently located just upstream of the throat, was found to be 986 K for a mass flow rate of 3 kg/s and 525 K for a mass flow rate of 14.234 kg/s.

The temperature value at 986 K exceeds the vaporization temperature (557 K) of water under pressure conditions of up to 69 bar, leading to reduced efficiency in cooling processes due to loss or reduction in coolant performance. These results demonstrate that increasing the mass flow rate leads to a decrease in coolant temperatures while simultaneously promoting efficient heat transfer within cooled-nozzle systems. The percentage of temperature reduction in the coolant side between 3 and 14.234 kg/s is approximately 46.81%.

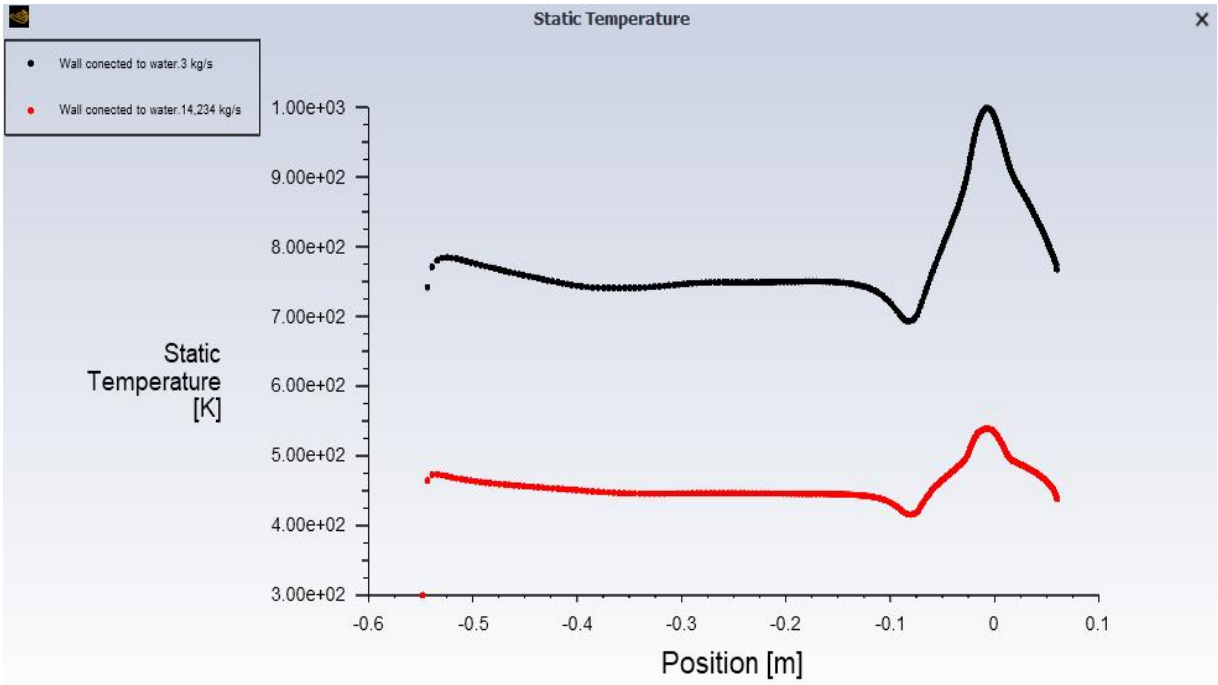

Figure.3.27: Comparison of water coolant-side wall temperature with different mass flow rate (H_2O.H2O) (3, 14.234) kg/s

Figure 3.28 illustrates the axial wall temperature distribution on the gas-side with water as a coolant at two different mass flow rates - 3 kg/s and 14.234 kg/s. In this scenario, we found that the maximum temperature consistently occurred just upstream of the throat, reaching up to about 1300 K for a lower mass flow rate (m=3 Kg/s) and only around 947 K when using higher mass flow rates (m=14.234 Kg/s).

It is important to note that such high temperatures close to copper's melting point can lead to nozzle failure due to material meltdown in cases where insufficient coolant is supplied (lower mass flow rate). This not only indicates poor cooling efficiency but also makes it unsuitable or non-applicable in practical applications due to system failure.

These results highlight the significance of increasing coolant mass flow rates for efficient heat transfer within cooled-nozzle systems while maintaining safe operating conditions.

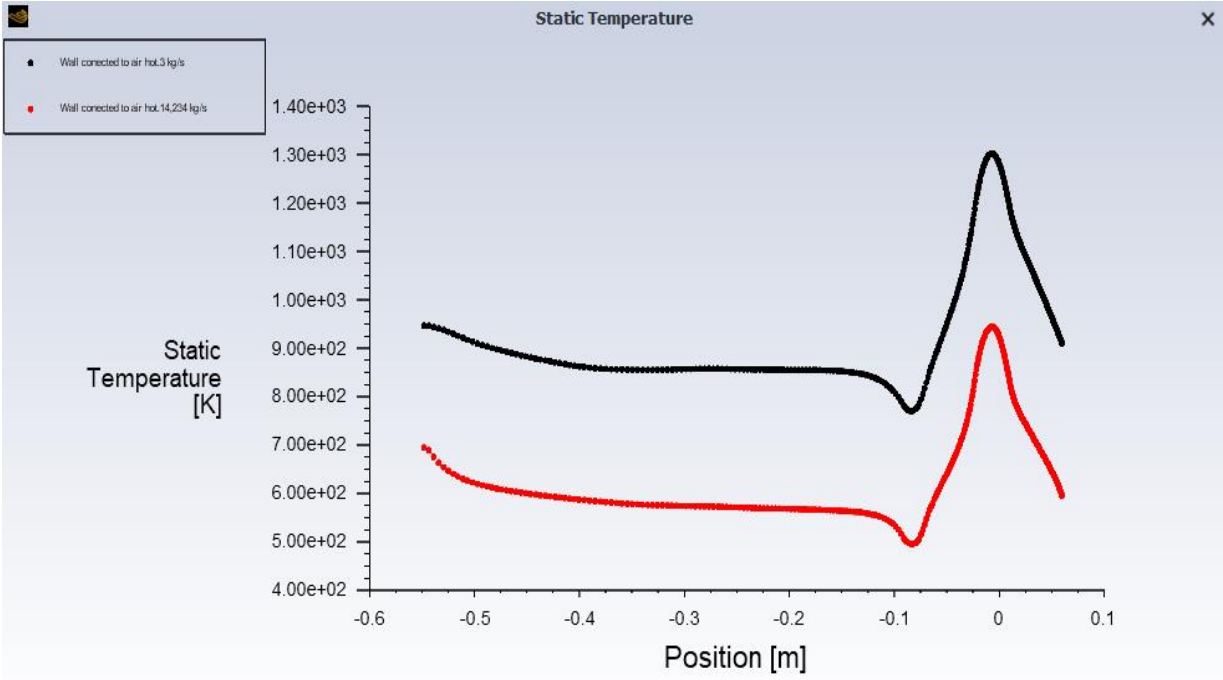

Figure.3.28: Comparison of gas-side wall temperature of water and hydrogen coolant (H_2O.H2O) **(3.14, 234) kg/s**

3.3.3. The effect of reducing the wall thickness.

The concept behind reducing the wall thickness is to reduce thermal resistance. Thus, it's expected that heat flow through a thinner nozzle wall will be much greater than when using a thicker wall.

For this particular case, the wall thickness was reduced from 7 mm to 1.6 mm. The notation (7-3 mm) denotes a wall thickness of 7 mm and coolant passage section height of 3 mm.

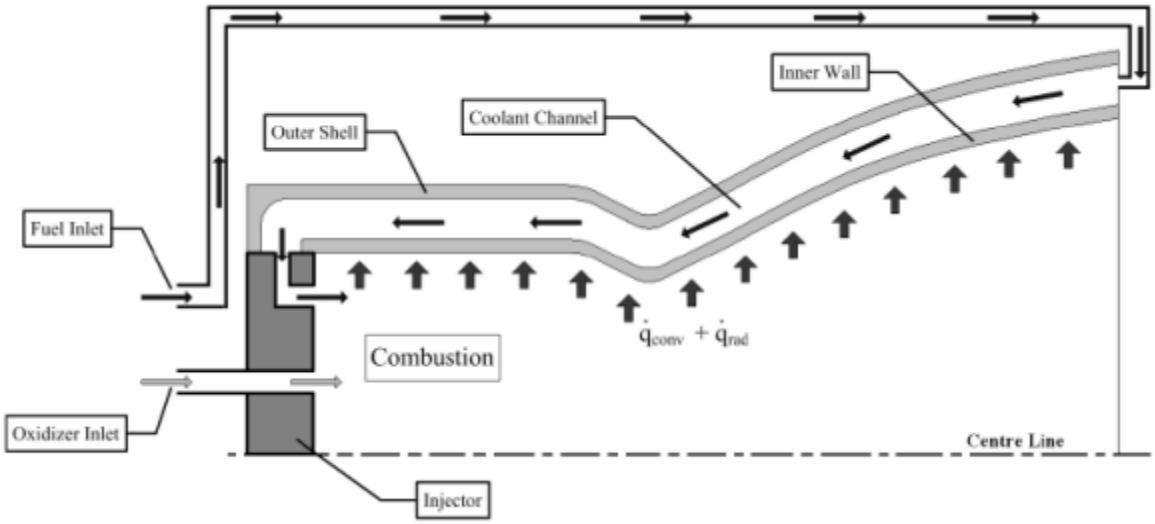

Figure.3.29: An illustrative picture of the structure of a rocket engine and the channels through which the coolant passes

Figure 3.29 illustrates the cooling process typically employed in space applications for liquid rocket motors. This type of cooling is regenerated, and the nozzle walls are cooled by passing liquid hydrogen fuel from the nozzle outlet to inlet before mixing with liquid oxygen for combustion.

For this particular case, a comparison was made at stagnation conditions of pressure and temperature (P0=100 bar, T0=2500 K). The air is compressed and heated before entering the nozzle. In this scenario, water was used as the coolant with an adequate mass flow rate of around 14.234 kg/s.

Figure 3.30 displays the temperature contour in three zones - nozzle section, wall nozzle, and coolant section. Upon analysis of these results, we can estimate that there is an acceleration occurring within the nozzle while simultaneously cooling takes place on the wall to remove heat generated by hot gas expansion and velocity friction near the wall.

Figure 3.31 displays the same temperature contour under identical conditions but with a reduced wall thickness (1.6-1.9 mm). Comparing this to the 7-3 case in Figure 3.30, we can observe that the wall zone is more effectively cooled in this scenario.

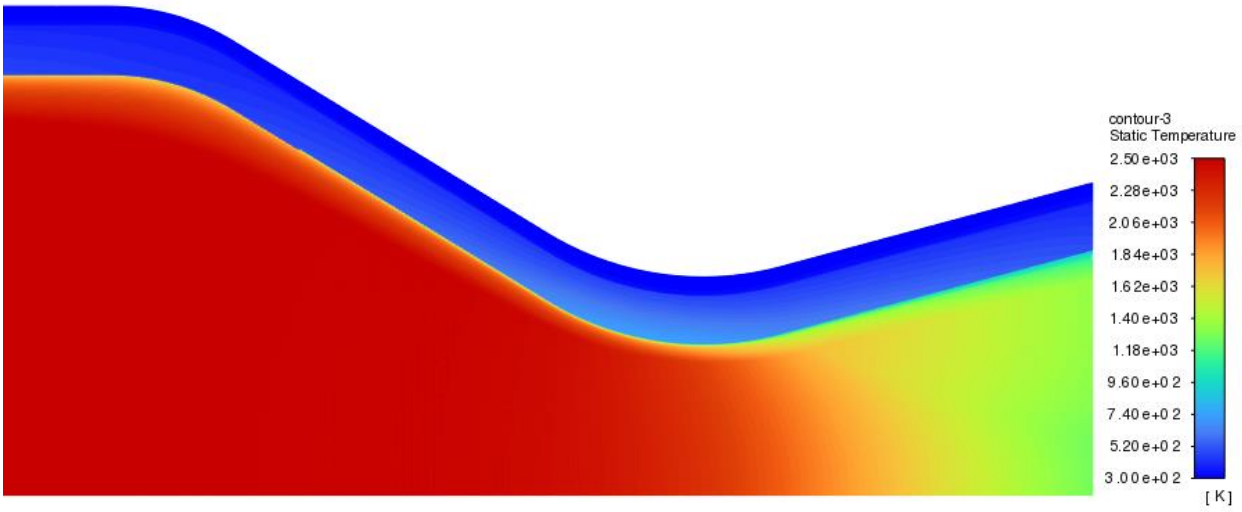

Figure.3.30 : temperature contour of with **(7-3) mm** thickness case

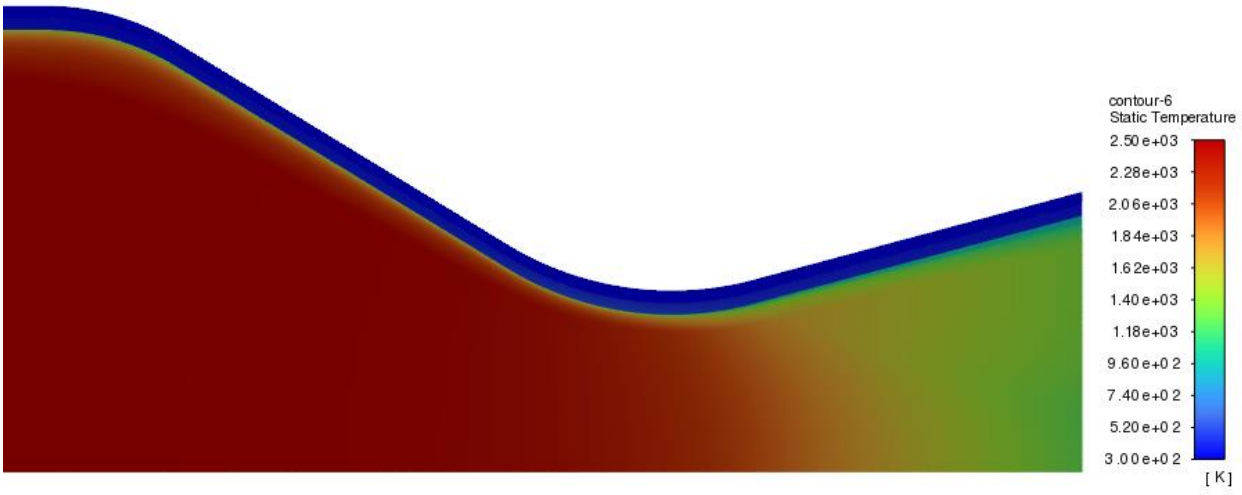

Figure.3.31 : temperature contour of with **(1.6-1.9) mm**

Figures 3.32 and 3.33 illustrate the temperature contour on the nozzle wall, making it easier to identify areas exposed to high temperatures and those that are not. As expected, we can observe that the region just upstream of the nozzle throat is consistently subjected to higher temperatures due to several factors discussed earlier in this study.

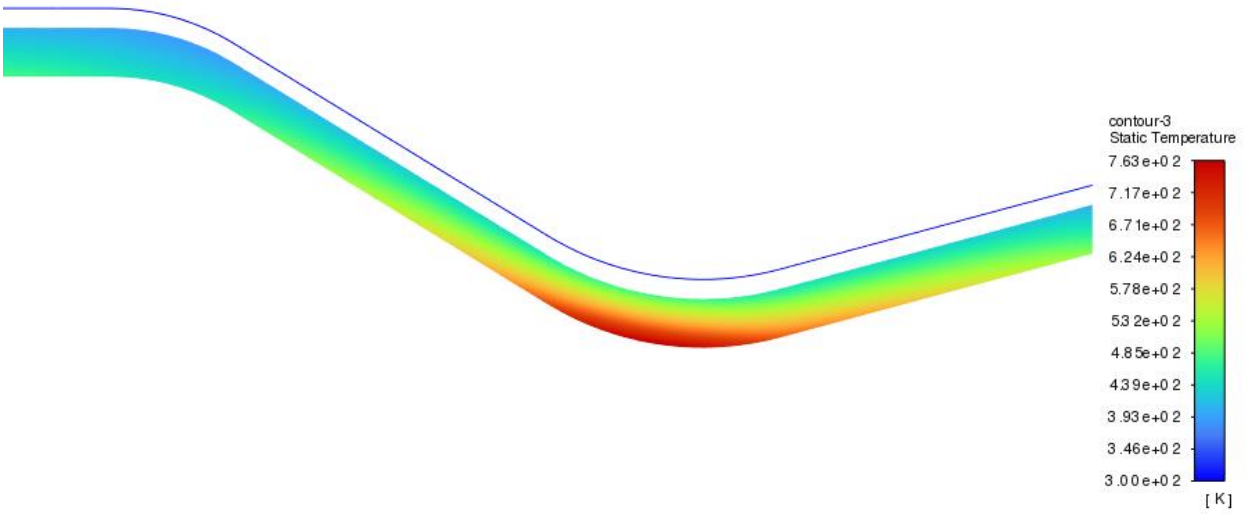

Figure.3.32: Static temperature contour of wall and hydrogen **(7-3) mm**

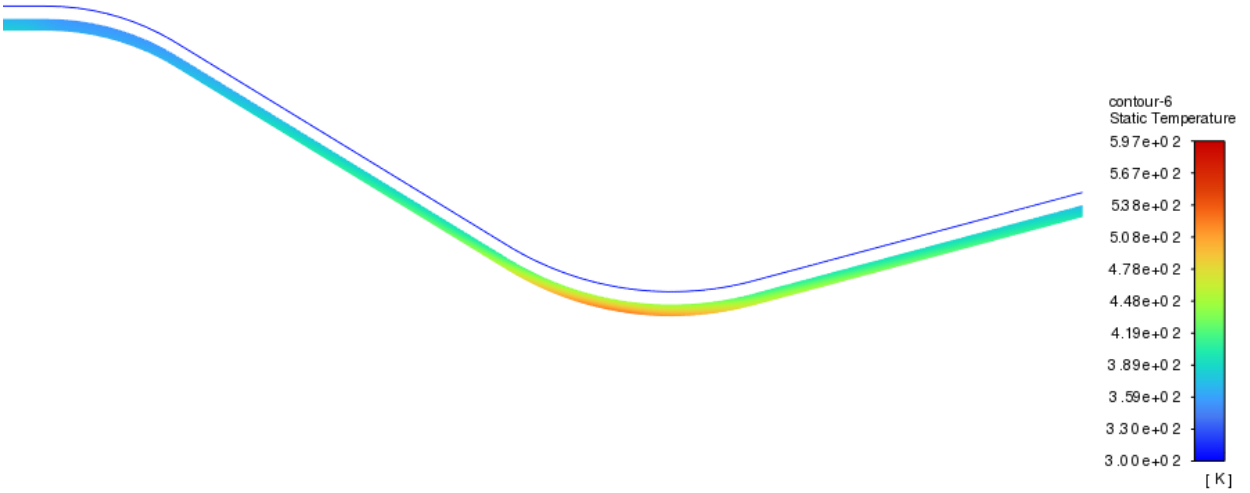

Figure.3.33: Static temperature contour of wall and hydrogen **(1.9-1.6) mm**

Figure 3.34 illustrates the axial wall temperature trend on the coolant side, where we can observe that the maximum temperature for a thickness of 1.6 mm is around 438 K, which is lower than that of a thicker wall (7 mm) at around 473 K. This indicates an approximate reduction in cooler temperatures by about 8% in the hottest region.

On the other hand, **Figure 3.35** shows that when reducing wall thickness from 7mm to just above half (1.6-1.9mm), it leads to a significant reduction in maximum temperature values from approximately 765 K down to only about 521 K. indicating a percentage difference of roughly 32 %.

These results suggest that reducing nozzle wall thickness effectively reduces heat transfer resistance and therefore promotes more efficient cooling within cooled-nozzle systems.

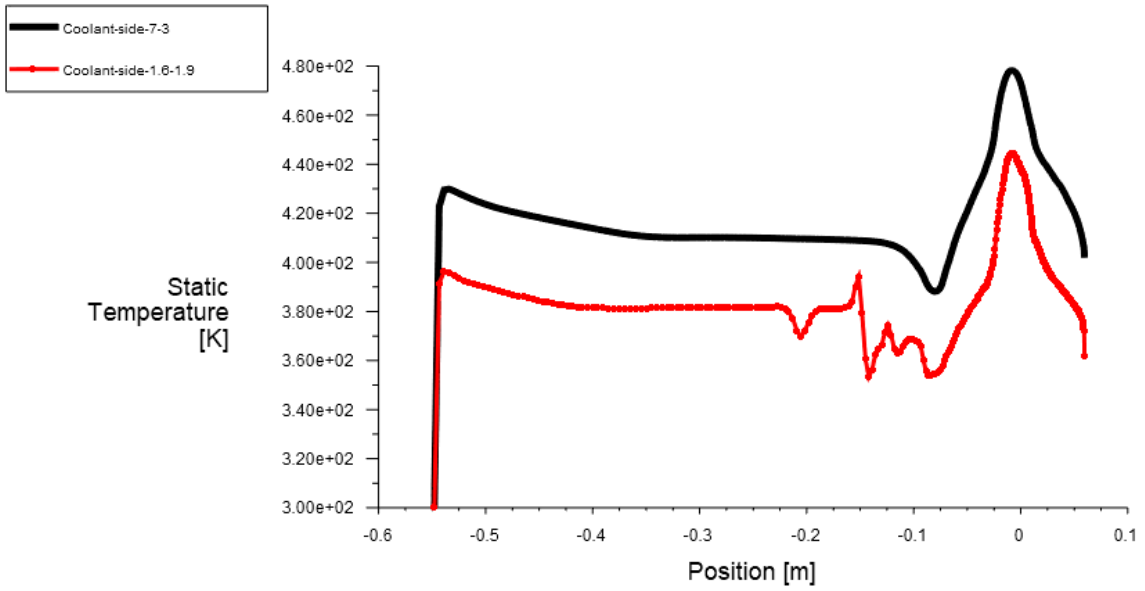

Figure.3.34: Axial distribution of coolant side temperature for two thickness.

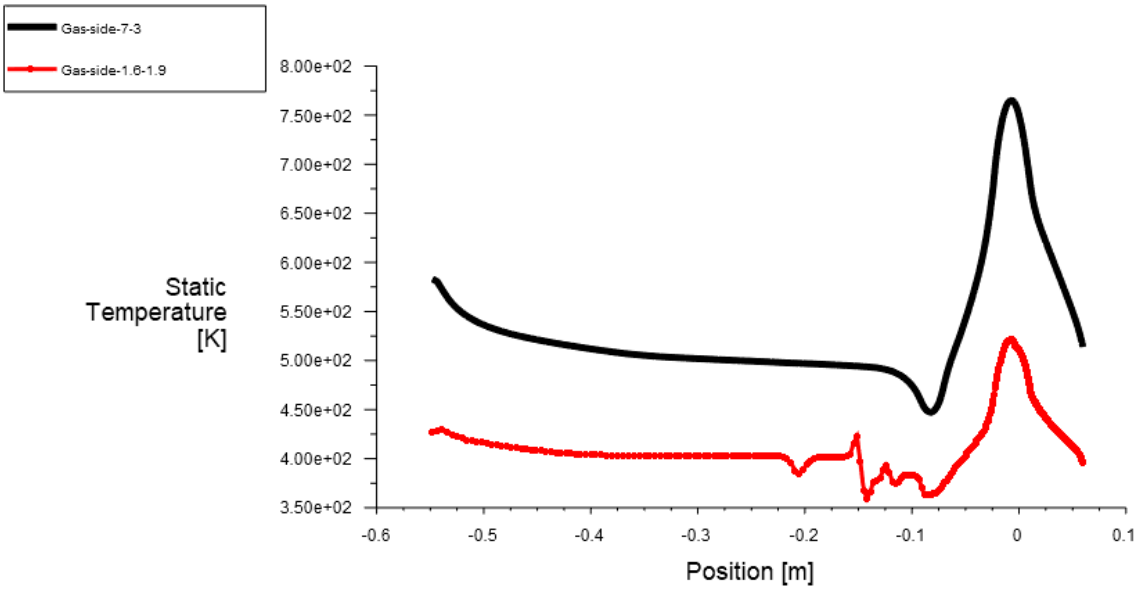

Figure.3.35: Axial distribution of gas side temperature for two thickness.

4. CONCLUSION

In this work, we presented studies of three cases that included the importance of coolant properties and type, the role of a large mass flow rate in coolant systems, and how reducing the wall nozzle thickness can improve cooling efficiency. Our analysis focused on gas flowing through convergent and divergent nozzles cooled with either water or hydrogen to demonstrate the significance of these three factors in maintaining engine integrity while undergoing thermal stress.

As illustrated in this article, several cooling techniques have been deployed to cool the combustion chambers and nozzle walls and prevent them from melting. Sometimes, using one method will suffice; however, more often than not, multiple methods are used together to prevent extreme temperatures from destroying engine components.

Our fluid flow study employed the finite volume method with a second-order Roe scheme to capture the discontinuities in the RANS turbulence. The RSM-Omega turbulence model has proven to be highly effective when incorporating shear flow correction because of the excellent agreement between the numerical predictions and experimental data.

Based on our previous transient study (not presented here), we concluded that initiating the cooling process prior to introducing hot gases into the nozzle is crucial because hot gases rapidly transition from their initial state to stationary within 10-20 microseconds while cooling typically takes approximately 40-60 seconds. In all the cases analysed, the gas-side wall temperature behaviour closely mirrored the wall heat flux behaviour, with peaks occurring slightly upstream from the throat regions.

One critical problem facing rocket engines is thermal failure as combustor gases can reach temperatures up to 3500 K - higher than metal melting points - leading weight reduction concerns. Regenerative and ablative cooling are two commonly used methods to prevent thermal failure in rockets.

The solid materials chosen for constructing rocket engines must meet specific requirements based on initial design specifications, such as task performance needs, as well as structural integrity considerations at various locations throughout each unit. Certain metals/alloys, such as copper, were accepted during our study because they exhibit the high conductivity/heat transfer capabilities required in rocket engine design.

Our results showed that liquid hydrogen is more efficient than liquid water for cooling. This was the first case study, where every increase in mass flow rate proportionally increased the coolant entering channels, leading to better cooling performance and component protection. The second case study highlighted how the structure thickness/diameter of the coolant channels plays a critical role in improving the overall cooling efficiency with larger heat exchange areas, promoting effective heat transfer between the components and coolants.

In summary, our study showed that optimizing thermal management systems by carefully selecting coolant types/properties, controlling mass flow rates, and reducing wall nozzle thickness can significantly improve rocket engine performance by preventing thermal failures and ensuring long-term structural integrity.

Bibliographie

[1] J. G. ST VENANT, C.R.A.S, 17(1843)

[2] G. DEDEBANT et Ph. WEHRLE, sur les équations aux valeurs probables d'un uide turbulent, C.R.A.S. T. 206, pp. 1790-1791(1938)

[3] VAN MIEGHEN et L. DUFOUR, Thermodynamique de l'atmosphère, Mem. Inst. Roy. Meteor. De Belgium, 30(1948)

[4] A. K. BLACKADAR, The transformation of energy by the large scaleeddy stress in the atmosphere, Meteor. Papers vol. 1, n^0 4, New York University (1950)

[5] A. FAVRE, Equations statistiques des gaz turbulents, C.R.A.S 246, pp. 2576-2579, 2723-2725, pp. 2839-2842, 3216-3219 (1958)

[6] A FAVRE, Equations des gaz turbulents compressibles, Journal de Mécanique, vol. 4, n^0 3(1965)

[7] D. VONDROMME, Modèle de turbulence à deux équations pour écoulement plan cisaillé à masse volumique variable, Thèse de Docteur-Ingénieur Lille (1980)

[8] P. CHASSAING et H. HA MINH, Physique et Mécanique des fluides réels, Cours de l'E.N.S.A. E (1982)

[9] H. HA MINH, The impact of turbulence modelling on the numerical predictions of flows, Rome 6-10 July (1992)

[10] D. VONDROMME, Turbulence modelling for compressible flows and implementation in Naiver-Stokes solvers, V.K.I lecture series, March (1991)

[11] M.W. RUBESIN, A one-equation model of turbulence for use with compressible Naiver-Stokes equations, NASA TM X-73-128, (1976)

[12] J.R. VIEGAS, T.J. COAKLEY, Numerical investigation of turbulence

Models for shock speared boundary layer. ows, AIAA paper, No.77-44, (1977)

[13] G.O. FRESKOS, Etude physique et simulation numérique des écoulements dans les entrées d'air supersonique, Thèse, Institut National Polytechnique de Toulouse, (1992)

[14] J. BOUSSINESQ, Théorie de l'écoulement tourbillonnant et tumultueux des liquides dans les lits rectilignes à grande section, volume I-II. Gauthier-Villars, (1897).

[15] R.S. AMANO and P. GOEL, Investigation of third-order closure model of turbulence for the computation of incompressible flows in a channel with a backward facing step. J. Fluids Eng., 109:424-428, (1987)

[16] R. FRIEDRICH. Compressible turbulence. In Space Course, Munich, October (1993)

[17] K.HANJALIC, B.E. LAUNDER, A Reynolds stress model of turbulence and its application to thin shear ows. J.F.M (1972)

[18] H. TENNEKES, J.L. LUMLEY, A First course in turbulence. M.I.T. Press. Cambridge, Massachusetts (1972)

[19] D. VONDROMME, Contribution à la modélisation et à la prédiction d'écoulements turbulents à masse volumique variable. These d'états de l'Université de Lille (1983)

[20] W.P. JAUNES, B.E. LAUNDER, The prediction of linearization with a two-equation model of turbulence. J. of Heat and Mass Transfer, Vol.15, PP.301-314 (1972)

[21] J. BOUSSINESQ, Théorie des écoulements tourbillonnaires, CRAS T23, (1887)

[22] T. VON KARMAN, Mechanise anlichkeit und turbulent, NACA TM. 611 (1930)

[23] P.S. KLéBANOFF, Characteristics of turbulence in a boundary layer with zero pressure gradient, NACA TN. 3178 (1956)

[24] R. MICHEL, C. QUEMARD & R. DURANT, Application d'un schéma longueur de mélange à l'étude de couches limites d'équilibre, Note Technique ONERA. No1. 154 (1969)

[25] E.R. VAN DRIEST, Turbulent boundary layer in compressible. uids. J. Aeronaut. Sci. vol 18, pp. 145-162 (1951)

[26] T. CEBECI, A.M.O. SMITH & S.G. MOSINSKI, Calculations of compressible adiabatic turbulent boundary layer, AIAA Journal. No 8, pp. 1974-1982 (1970)

[27] I.E. ALBER, Similar solutions for a family of separated turbulent boundary layers. AIAA Paper. 71-203 (1971)

[28] B.S. BALDWIN & H. LOMAX, Thin layer approximation and algebraic model for separated turbulent ows. AIAA Paper. 78-0257 (1978)